CAR-Immunotherapies for

the treatment of metastatic rhabdomyosarcomas

Dissertation

zur Erlangung des Doktorgrades

der Naturwissenschaften

(Dr.rer.nat)

vorgelegt beim Fachbereich 14

der Johann Wolfgang Goethe-Universität

in Frankfurt am Main

von

Catrin Birgit Heim

aus Miltenberg

Frankfurt 2023

(D 30)

Vom Fachbereich 14 der

Johann Wolfgang Goethe - Universität als Dissertation angenommen.

Dekan: Prof. Dr. Clemens Glaubitz

Gutachter: Prof. Dr. Rolf Marschalek

PD Dr. Eva Rettinger

Datum der Disputation: 22.04.2024

Abstract

Metastatic rhabdomyosarcoma (RMS) is one of the most challenging tumor entities in pediatric oncology caused by treatment resistances and immune escape. Novel chimeric antigen receptor (CAR) immunotherapies as specific, effective and safe treatment provide antitumor cytotoxicity by soluble factors and ligands/receptor signals. Besides its intrinsic potential as innate immune cell the ErbB2-sprecific CAR-engineered natural killer (NK)-92 cell line NK-92/5.28.z also provides CAR-mediated cytotoxicity, resulting in a high lytic capacity against 2D and 3D RMS cell structures *in vitro.* Also in a xenograft model using immune deficient NOD/Scid/IL2Rγ$^{-/-}$ (NSG) mice inhibited NK-92/5.28.z the tumor growth as long as the cells were administered and therefore prolonged the survival of the animals. The NK-92/5.28.z were distributed by the blood circulation and subsequently infiltrated the tumor tissue. Due to the malignant origin of the NK-92 cell line the cells must be irradiated prior to the use in patients. While the irradiation hampered the proliferation of NK-92/5.28.z cells, the cytotoxicity against RMS cells *in vitro* is retained for at least 24 hours. In the xenograft model irradiated NK-92/5.28.z cells inhibited the tumor growth but to a lower extent than untreated cells, as irradiated cells have only a limited life span *in vivo* no durable persistence and remission was achieved. Therefore, combinatorial approaches were focused and while blocking of the PD-1/PD-L1 axis did not resulted in a significantly enhanced tumor cell lysis, the combinatorial treatment with proteasome inhibitor bortezomib exhibited a significant enhanced cytotoxicity against RMS cells at least *in vitro*. Bortezomib itself induces caspase mediated apoptosis and also the upregulates the expression of TRAIL receptor DR5. The corresponding ligand TRAIL is expressed on the surface of the NK-92/5.28.z and pursuing experiments with purified TRAIL and bortezomib revealed a synergism. NK-92/5.28.z as an off-the-shelf product is therefore feasible for the therapy of metastatic RMS, but it might be necessary to support the cytotoxicity by additive agents like proteasome inhibitor bortezomib to archive durable remission.

Another cell population suitable for RMS CAR-immunotherapy are cytokine induced killer (CIK) cells, a heterogenous cell population generated from autologous PBMCs consisting of T, NK and T-NK cells. Lentivirally transduced ErbB2-specific CAR-CIK cells were previously shown to inhibit the tumor engraftment in a RMS xenograft model. However, lentiviral transduced adoptive immunotherapies bear risks for the transfer in patients, therefore the *Sleeping Beauty Transposon System* (SBTS) as a non-viral method, which integrates the CAR coding DNA by a cut-and-paste mechanism from a minicircle (MC) into the CIK cells genome is more feasible for the generation of CAR-CIK cells. The Sleeping beauty transposase mRNA and the MC were transferred in the cell by nucleofection, different factors influence the transfection efficiency and viability of the CIK cells in this harsh procedure. In preliminary experiments with MC Venus, a MC encoding eGFP, the highest transfection efficiency with

the best proliferative capacity was achieved with cells on day 3 of CIK culture and without the addition of autologous monocytes as feeder cells. For the CAR construct the protocol was further improved by adjusting crucial factors, for this construct the best results were achieved on day 0, without irradiated PBMCs as feeder cells and cultivation in X-Vivo10 medium supplemented with human fresh frozen plasma. The X-Vivo10 medium enhanced the percentage of NK- and T-NK cells significantly compared to CAR-CIK cells cultured in RPMI. Since the gene transfer by SBTS resulted in CAR-CIK cells stably expressing a CAR in all subpopulations, resulting in a significantly enhanced cytotoxicity against RMS cells *in vitro*, these cells were compared to lentiviral transduced CAR-CIK cells *in vitro* and *in vivo*. While the SBTS CAR-CIK cells were superior to viral CAR-CIK cells in 2D short-term assays, the viral cells showed higher lytic capacity in 3D spheroid long-term assays. In a RMS xenograft model lentiviral CAR-CIK cells significantly prolonged the survival of mice and persisted, whereas SBTS CAR-CIKs did not favor the overall survival compared to untreated controls and also did not persist. Phenotypic analysis revealed a highly cytotoxic CD8+ and late effector memory dominant phenotype for SBTS CAR-CIK cells supporting short-term cytotoxicity but also more prone for exhaustion, while viral CAR-CIK cells showed a more balanced phenotype for memory and cytotoxicity. Therefore, the SBTS is feasible for the ErbB2-CAR gene transfer in CAR-CIK resulting in a stable CAR-expression with high short-term cytotoxicity, but these cells are also more prone to exhaustion and the protocol might be adapted further to prevent this limitation for *in vivo* application.

This work underlines the hard-to-treat characteristics of metastatic RMS, but also shows some approaches for further evaluation like the combination of NK-92/5.28.z cells with bortezomib and the feasibility of the generation of CAR-CIK cells via SBTS.

Zusammenfassung

Das Rhabdomyosarkom (RMS) ist der häufigste Weichteiltumor im Kindesalter. Während Patienten mit lokalisierter Erkrankung mittlerweile gute Heilungschancen haben, gab es für ca.15% der Patienten mit metastasiertem RMS (Stadium IV, disseminiertes Tumorstadium mit Knochen- oder Knochenmarkmetastasierung) in den letzten 15 Jahren keine nennenswerte Verbesserung der Behandlung. Somit ist für die Erkrankung für diese Patienten noch immer unheilbar und sie versterben innerhalb von zwei Jahren nach Diagnosestellung. CAR-Immuntherapien als effektive, hochspezifische und wenig toxische Behandlung könnten diese Situation jedoch verbessern. Hierbei kann ErbB2 als Zielstruktur auf Rhabdomyosarkomen von entsprechenden, mit einem chimären Antigen-Rezeptoren (CAR) versehenen Immunzellen erkannt und attackiert werden. Mögliche Trägerzellen für einen solchen CAR sind neben T-Zellen die Natürlich Killer (NK)-Zelllinie NK-92 und Zytokin-induzierte Killerzellen (CIK-Zellen).

Die NK-92-Zelllinie weist bereits per se eine gewisse Toxizität gegen RMS-Zellen auf und in *in vitro* Experimenten konnte gezeigt werden, dass diese intrinsische Toxizität durch eine CAR-Modifikation noch steigerbar ist. Klinisch interessant ist auch, dass sich die CAR-NK-92 (NK-92/5.28.z) Zellen als immortale Zelllinie leicht kultivieren lassen und diese aufgrund ihres NK-Phänotyps allen Patienten mit ErbB2-positivem RMS als allogenes Zelltherapeutikum zur Verfügung gestellt werden könnten. Somit sind Kosten und Personalaufwand für die Herstellung, verglichen mit patientenspezifischen CAR-Zellprodukten überschaubar. Außerdem sind NK-92/5.28.z Zellen bereits als Arzneimittel (ATMP) für die Behandlung von Glioblastomen zugelassen und werden bereits in einer klinischen Phase I Studie für diese Indikation erprobt (NCT03383978). Da die parentalen NK-92 Zellen und damit auch alle Derivate einen malignen Ursprung haben, müssen die NK-92/5.28.z Zellen vor der Verabreichung bestrahlt werden, um ein unkontrolliertes Wachstum im Patienten zu verhindern.

In umfassenden *in vitro* Versuchen konnte gezeigt werden, dass NK-92/5.28.z Zellen eine spezifische und hocheffektive Zytotoxizität gegen RMS Zelllinien, aber auch gegen ErbB2-positive Tumororganoide aus Patientenmaterial in 2D Assays aufweisen. Da 2D Zytotoxizitätsassay die dreidimensionale Struktur von soliden Tumoren nicht nachempfinden können, wurden in einem nächsten Schritt dreidimensionale RH30-Tumorspähroide verwendet. Im Gegensatz zu parentalen NK-92 Zellen, die lediglich das Wachstum von RMS-Tumorsphäroiden inhibieren, lysieren NK-92/5.28.z Zellen etablierte Tumorsphäroide. Durch eine Bestrahlung von 10Gy mittels einer ^{137}Cs-Quelle wird das Wachstum von NK-92/5.28.z Zellen zwar verhindert, jedoch bleibt die Toxizität der Zellen gegen RMS Zellen für mindestens 24 Stunden erhalten.

Aufbauend auf diese vielversprechenden *in vitro* Daten, folgte eine Testung der Effektivität der NK-92/5.28.z im Tiermodell in immundefizienten NOD/Scid/IL2Rγ$^{-/-}$ (NSG) Mäusen. Um die klinische Situation der meist vorab bestrahlten Patienten bestmöglich nachzustellen, wurden die Tiere am Tag vor der Tumorzellapplikation (Tag -1) subletal mit 2,5 Gy bestrahlt. Die Injektion von 1x10^5 RH30$^{luc/GFP+}$ Tumorzellen erfolgte dann intravenös (i.v.) über die Schwanzvene, was einer Metastasierung gleichkommt (Tag 0). Am Tag nach der Tumorzellinjektion (Tag 1) wurden die Tiere in vier verschiedene (Therapie-) Gruppen eingeteilt: Unbehandelte Kontrollen, Behandlung mit konventionellen NK-92 Zellen, mit NK-92/5.28.z Zellen oder mit NK-92/5.28.z Zellen, die direkt vor der Applikation mit 10Gy bestrahlt wurden. Bei den Tieren der Behandlungsgruppen wurden wiederholt sechsmal über einen Zeitraum von vier Wochen jeweils 1x10^7 Immunzellen - ebenso wie die Tumorzellen - über die Schwanzvene injiziert. Tieren in der unbehandelten Kontrollgruppe wurde X-Vivo10, das Medium in dem die Therapiezellen verabreicht wurden, injiziert. Das Tumorwachstum der Tiere wurde mittels wöchentlicher Biolumineszenz-Bildgebung (BLI) nicht-invasiv nachverfolgt. Nach 35 Tagen, zu einem Zeitpunkt an dem sich die Tumore manifestiert hatten, wurden aus der NK-92/5.28.z Gruppen drei Tiere mit etabliertem Tumor zufällig ausgewählt. Diese Tiere erhielten beginnend an Tag 42 drei weitere Immunzellbehandlungen über einen Zeitraum von drei Wochen (NK-92/5.28.z 2.Behandlungszyklus). Tiere mit krankheitsbedingten Auffälligkeiten, Anzeichen von Unwohlsein oder physischen Einschränkungen wurden schmerzlos erlöst. Spätestens am Versuchsende (Tag 105) wurden Leber, Lunge, Milz, Blut und Darm für weiter Analysen entnommen.

Anhand der BLI-Daten wurde ermittelt, dass die Tiere der NK-92/5.28.z Behandlungsgruppe eine signifikant geringere Tumorlast als Tiere aus Kontroll- und NK-92-Gruppe aufwiesen, während zwischen NK-92 und Kontrolltieren kein signifikanter Unterschied ausgemacht werden konnte. In einzelnen Tieren konnte die Behandlung mit NK-92/5.28.z das Tumorwachstum sogar komplett inhibieren. Tiere mit NK-92/5.28.z Behandlung (81,0 ± 8,8 Tage) zeigten ein signifikant verlängertes Überleben im Vergleich zu unbehandelten (66,0 ± 13,4 Tage) oder NK-92 behandelten Tieren (72,5 ± 6,1 Tage), auch hier zeigte sich kein signifikanter Unterscheid zwischen unbehandelten und NK-92 behandelten Tieren. Drei zusätzliche NK-92/5.28.z Zellinjektionen ab Tag 42 verzögerten das Wachstum etablierter Tumore erneut, allerdings nur so lange die NK-92/5.28.z-Zellen verabreicht wurden. Auch bestrahlte NK-92/5.28.z konnten das Tumorwachstum verlangsamen, allerdings nicht so stark wie nicht bestrahlte Zellen. Makroskopisch waren vor allem in der Leber und der Lunge der Kontrolltiere große Tumormanifestationen erkennbar, wohingegen bei den Behandlungsgruppen kleinere Tumorläsionen sichtbar waren. Die Integrität der RH30 Zellen blieb auch im Tiermodell erhalten und typische RMS Marker wie Desmin, MyoD1 und Myogenin konnten nach Versuchende mit Immunhistochemie in den Zellen nachgewiesen werden. Die Milzen der mit Immuntherapie behandelten Tiere waren aufgrund von Immunzellinfiltrationen signifikant vergrößert, die Bestrahlung

der NK-92/5.28.z Zellen führte dazu, dass diese nicht langfristig in den Tieren persistierten, was sich auch durch eine geringere Größe der Milzen zeigte. Durch Immunofluoreszenzmikroskopie konnten die Immuneffektorzellen überwiegend in den Milzen, aber auch in der direkten Tumorumgebung in Leber und Lunge nachgewiesen werden. Weitere mikroskopische Analysen zeigten eine Verteilung der Immunzellen über die Blutbahnen und von dort eine Einwanderung in das Tumorgewebe. Auch in den Chimärismusanalysen wurden die meisten Immunzellen in den Milzen detektiert, jedoch auch im Knochenmark der Tiere. Auch hier konnten keine persistierenden Immunzellen in der Behandlungsgruppe mit bestrahlten NK-92/5.28.z Zellen gefunden werden.

Die vorliegenden Daten zeigen, dass NK-92/5.28.z Zellen das Wachsen von RMS-Tumoren verlangsamen und damit einen Überlebensvorteil gegenüber der unbehandelten Kontrollgruppe oder der NK-92 behandelten Gruppe mit sich bringt. Somit ist die Tumortoxizität der NK-92/5.28.z Zellen auch *in vivo* CAR-spezifisch und hocheffektiv.

Die Daten zeigen allerdings auch, dass die Verminderung des Tumorwachstums in den meisten Fällen nur anhalten kann, wenn die NK-92/5.8.z Zellen dauerhaft appliziert werden. Deshalb und insbesondere aufgrund der Verwendung bestrahlter NK-92/5.28.z Zellen im Patienten, könnte es hilfreich sein, die CAR-Zelltherapie mit anderen Wirkstoffen zu kombinieren. Im klinischen Einsatz von zugelassenen CAR-Therapien werden hierfür häufig Immuncheckpoint Inhibitoren verwendet, oft wird hierbei PD-1 als Target verwendet. Der Ligand PD-L1 ist auf RH30 Zellen hoch exprimiert und auch auf Tumororganoiden aus Patientenmaterial detektierbar. Allerdings zeigte die Blockade von PD-1 auf den NK-92/5.28.z Zellen mit entsprechenden Antikörpern in *in vitro* Versuchen keine signifikant bessere Lyse der RH30 Zellen. Jedoch könnte diese Achse *in vivo* an Bedeutung gewinnen, da PD-1 vor allem auf T-Zellen stark exprimiert wird und diese als adaptive Immunantwort durch die Tumorlyse der NK-92/5.28.z Zellen hinzugezogen werden.

Eine andere Strategie für eine Kombinationstherapie könnte die Verstärkung der Lysemechanismen der NK-92/5.28.z Zellen sein. Neben der primären Degranulation von mit Granzyme B and Perforin gefüllten Vesikeln, ist die rezeptorvermittelte Apoptose über TRAIL ein weiterer nachgeschalteter Killingmechanismus der NK-92/5.28.z Zellen. Ein möglicher Kandidat RMS Zellen anfälliger für TRAIL-vermittelte Apoptose zu machen, ist der Proteasom-Inhibitor Bortezomib, welcher bereits für die Behandlung des Multiplen Myeloms zugelassen ist. Das Proteasom ist ein Zellorganell, in dem nicht mehr benötigte oder fehlgefaltete Proteine abgebaut werden. Ist dieser Prozess beispielsweise durch Bortezomib inhibiert, führt das zu Zellstress. Dieser äußert sich zum einen in Apoptose, aber auch darin, dass die Tumorzellen TRAIL-Rezeptoren in einem erhöhten Maß auf ihrer Oberfläche exprimieren, die dann wiederum von den NK-92/5.28.z Zellen genutzt werden können, die Tumorzellen zu lysieren. In der ersten *in vitro* Studie dieser Art konnten in dieser Arbeit zum einen

gezeigt werden, dass Bortezomib an sich zelltoxisch für RMS Zelllinen und Tumorzellen aus Patientenproben ist. Aber auch, dass die Kombination von Bortezomib und NK-92/5.28.z Therapie zu einer signifikanten Steigerung der Tumorzelllyse führt. Versuche mit aufgereinigtem TRAIL-Protein zeigten, dass Bortezomib und TRAIL sich synergistisch auf die Zelllyse auswirken. Durch Westernblot und quantitiative PCR (qPCR) Analysen des NFκB Stoffwechselwegs, der mit vielen Prozessen innerhalb der Zelle zusammenwirkt und durch Bortezomib gestört werden kann, wurde eine Inhibition des nicht-kanonischen NFκB Stoffwechselwegs festgestellt. Somit könnte die Kombination mit Bortezomib die NK-92/5.28.z Therapie zusätzlich verstärken und so zu einer langfristigen Inhibition des Tumorwachstums und einem damit verknüpften Überlebensvorteil führen. Allerdings ist die Behandlung mit Bortezomib auch für die NK-92/5.28.z bei längerer Ko-Inkubation toxisch und somit muss die Applikation von Bortezomib und anschließender NK-92/5.28.z Behandlung zeitlich gut abgestimmt sein, um zu hohe Bortezomib-Plasmalevel zu vermeiden. Für die Behandlung des Nierenkarzinoms wurde die erfolgreiche Kombination von Bortezomib und CAR-NK-92 Zellen in einem Mausmodell bereits berichtet und andere Arbeitsgruppen konnten *in vivo* einen positiven immunmodulatorischen Effekt auf T-Zellen zeigen, der auch für infiltrierende T-Zellen nach der Tumorlyse durch die NK-92/5.28.z Zellen relevant sein könnte.

Neben den NK-92/5.28.z Zellen können auch ErbB2-spezifische CAR-CIK-Zellen für die Therapie des RMS in Betracht gezogen werden. Für die Generierung von CIK-Zellen werden periphere mononukleäre Blutzellen (PBMCs) nach einem definierten Protokoll mit Interferon (INF)-γ, Interleukin (IL)-2, anti-CD3 (OKT3) und IL-15 stimuliert und entwickeln dadurch einen heterogenen Phänotyp mit einem hohen Anteil an CD3+/56+ doppelpositiven T-NK-Zellen. T-NK-Zellen kommen zu einem geringen Anteil (< 5%) im peripheren Blut vor und zeichnen sich durch T- und NK- Zellcharakteristiken aus. In CIK-Zellen wird der Anteil der T-NK-Zellen auf bis zu 40% erhöht. CAR-CIK-Zellen haben dadurch einen Vorteil gegenüber CAR-T-Zellen, da T-NK-Zellen nicht MHC abhängig sind und somit eine allogene Verwendung, möglich ist. ErbB2-spezifische CAR-CIK-Zellen, die das gleiche CAR-Konstrukt wie die NK-92/5.28.z Zellen tragen, wurden bereits erfolgreich im gleichen Xenograftmodell, das für die Evaluierung der NK-92/5.28.z Zellen verwendet wurde, getestet. Hier konnte durch die CAR-CIK-Zellen, jedoch nicht durch parentale CIK-Zellen eine komplette Remission in allen behandelten Tieren erreicht werden. Die hierfür verwendeten CAR-CIK-Zellen wurden mittels lentiviraler Transduktion hergestellt. Die genetische Modifikation mittels viraler Partikel birgt allerdings einige Gefahren, wie die Integration in krebsassoziierte Gene oder aber Onkogenese durch die Insertation. Deshalb werden zunehmend nicht-virale Methoden wie beispielsweise Transposonsysteme für die Generierung von CAR-Zellen verwendet. In dieser Arbeit sollte die genetische Modifizierung von CIK-Zellen mittels des *Sleeping Beauty Transposon System* (SBTS) etabliert werden, um so nicht-virale CAR-CIK-Zellen herzustellen und somit eine schnelle Translation der Therapie in die Klinik zu ermöglichen. Für die genetische

Modifikation mittels SBTS sind neben der Transposase, die zumeist in Form von mRNA codierend für eine hyperaktive Form dieses Enzyms (SB100x) in die Zelle eingebracht wird, das gene of interest flankiert von Erkennungssequenzen für die Transposase (ITRs) notwendig. Anstelle eines Plasmids wird hierfür häufig ein Minicircle (MC), ohne bakterielle Komponenten, verwendet, da dies zu einer höheren Patientensicherheit beiträgt und eine geringere Toxizität für die Zellen während der Herstellung hat. Beide Komponenten, SB100x mRNA und MC werden durch Nukleofektion in die Zelle eingebracht.

Mittels MC Venus, von dem eGFP durch das SBTS transferiert werden kann, wurde gezeigt, dass die genetische Modifikation von CIK-Zellen durch das SBTS möglich ist. Da für T-Zellen bekannt ist, dass diese sich am besten im aktivierten Zustand mittels SBTS modifizieren lassen, wurde für die CIK-Zellen der beste Zeitpunkt für die Transfektion ermittelt. Während die Transfektion an Tag 0 zu einer geringeren Effizienz führte, konnte bei der Transduktion an Tag 4 und Tag 7 der CIK Kultur Effizienzen über 60% erreicht werden. Allerdings waren CIK-Zellen, die an Tag 7 transfiziert wurden deutlich in ihrer Proliferation gehemmt, wohingegen CIK-Zellen, die an Tag 0 oder Tag 4 transfiziert wurden ein ähnlich gutes Proliferationsverhalten zeigten. Da die Entwicklung von CIK-Zellen aus PBMCs gerade zu Beginn der CIK-Zellkultur stark von den beinhalteten Monozyten abhängig ist, wurde in einem nächsten Schritt untersucht, ob die transfizierten CIK-Zellen durch die Zugabe autologer Monozyten in ihrer Transfektion und/oder Proliferation unterstütz werden können. Allerdings konnte kein Effekt auf die CIK-Zellen durch die Zugabe von autologen Monozyten beobachtet werden.

Da die vorangegangenen Experimente mit MC Venus zeigten, dass eine genetische Modifizierung von CIK-Zellen mittels SBTS möglich ist, wurde ein Plasmid kloniert, das das ErbB2-spezifische 5.28.z-CAR Konstrukt auf beiden Seiten flankiert von Erkennungssequenzen für die Transposase kodiert. Nachdem sichergestellt war, dass von diesem Plasmid die CAR-Sequenz stabil in das CIK-Zellgenom integriert werden kann, wurde auf Grundlage dieses Plasmids von PlasmidFactory ein MC hergestellt. Da an die CAR-Sequenz abgetrennt durch eine IRES-Sequenz ein GFP als Reporterprotein angehängt worden war und die GFP-Expression der CAR-Expression entsprach, konnte die Transfektionseffizienz über die GFP-Expression bestimmt werden. Für den größeren MC ErbB2-CAR wurde erneut der beste Zeitpunkt für die Nukleofektion bestimmt. Hierbei wurde die Nukleofektion der Zellen an Tag 0, Tag 3 und Tag 7 der CIK-Kultur verglichen. Während die Nukleofektion an Tag 0 oder Tag 3 zu ähnlichen Ergebnissen in Effizienz, Viabilität und Proliferatoinskapazität führte, zeigte sich bei einer Nukleofektion an Tag 7 eine deutlich verminderte Proliferation. Basierend auf diesen Ergebnissen wurde Tag 0 für die Nukleofektion festgelegt, da dies zum einen den Vorteil einer möglichst geringen Kultivierungszeit bis zum fertigen CAR-Produkt hat und andererseits aufgrund des frühen Zeitpunkts wenige Zellen transfiziert werden müssen, um die gleiche Endzellzahl am Tag der Ernte (Tag 10) zu erreichen, was ein geringerer Verbrauch an Ressourcen ermöglicht und somit ein möglichst kostengünstiges Produkt

entsteht. In den Protokollen anderer Gruppen wurde die Zugabe bestrahlter, autologer PBMCs als Feeder cells nach der Elektroporation an Tag 0 beschrieben, um die Proliferation und Erholung der CIK-Zellen zu unterstützen. Allerdings zeigte sich durch die Zugabe solcher Feeder cells kein positiver Effekt auf Transfektionseffizienz, Proliferation oder Viabilität im Falle der ErbB2-CAR-CIK-Zellen. Ein wichtiger Faktor für die Viabilität und Proliferation von Zellen im Allgemeinen ist das Kulturmedium. Die Kultivierung der SBTS CAR-CIK-Zellen in X-Vivo10 Medium, einem NK-Zellmedium, supplementiert mit humanem Plasma zeigte ein signifikant besseres Überleben der CAR-CIK-Zellen und eine damit verbundene bessere Proliferation im Gegensatz zu CAR-CIK-Zellen, die im Standardmedium RPMI supplementiert mit fetalem Rinderserum kultiviert wurden. Außerdem wirkte sich das X-Vivo10 Medium durch seine auf NK-Zellen abgestimmte Formulierung auf den Phänotyp der CAR-CIK-Zellen zu Gunsten der NK- und T-NK-Zellen aus. Der Anteil dieser beiden Zellpopulationen war bei der Kultivierung der CAR-CIK-Zellen in X-Vivo10 im Vergleich zur Kultivierung in RPMI signifikant erhöht. Aufgrund der höheren Viabilität der CAR-CIK-Zellen im X-Vivo10-Medium konnte mehr Nukleinsäure bei der Nukleofektion der CAR-CIK-Zellen eingesetzt werden, ohne einen zu großen Zelltod, resultierend in einer stark verminderten Proliferation, zu verursachen. Dadurch war der Einsatz von SB100x mRNA und MC ErbB2-CAR in einem Verhältnis von 4:2 anstelle von 4:1 möglich, was in einer signifikant höheren CAR-Expression bei gleicher Viabilität und ähnlicher Proliferation resultierte. Nachdem ein Protokoll für die Herstellung nicht-viraler SBTS CAR-CIK-Zellen etabliert war, wurden diese Zellen mit konventionellen lentiviral transduzierten (LV) CAR-CIK-Zellen verglichen. Die LVCAR-CIK-Zellen hatten mit durchschnittlich 39,3% einen deutlich höheren CAR-Zell-Anteil als die SBTS CAR-CIK-Zellen mit 9,7%. Allerdings waren die SBTS CAR-CIK-Zellen deutlich viabler als die LV CAR-CIK-Zellen. Der Anteil der T-NK-Zellen in den SBTS CAR-CIK-Zellen war im Vergleich zu unbehandelten CIK- und LV CAR-CIK-Zellen deutlich erhöht und sowohl die T-NK- als auch die T-Zellen der SBTS CAR-CIK zeigten einen deutlich ausgeprägten zytotoxischen Phänotyp aus nahezu ausschließlich CD8+ späten Effektor-Gedächtnis-Zellen (CD45RO- CD62L-). Dieser Phänotyp zeigt sich auch in einer signifikant gesteigerten Zytotoxizität in dreistündigen Toxizitätsassays gegen RH30 Zellen. Diese gesteigerte lytische Aktivität konnte allerdings nicht in Langzeitstudien über sieben Tage in einem 3D Sphäroid Assay bestätigt werden. Hierbei erreichten die SBTS CAR-CIK-Zellen ähnlich wie die parentalen CIK-Zellen auch bei höhen Effektorzellzahlen lediglich eine Inhibition des Sphäroidwachstums, wohingegen die LV CAR-CIK-Zellen eine Lyse der Sphäroide erreichen konnten. Auch im Xenograftmodell in immundefizienten NSG Mäusen konnten die SBTS CAR-CIK-Zellen keinen Überlebensvorteil im Vergleich zu unbehandelten Vergleichstieren vermitteln, wohingegen die LV CAR-CIK das Leben der Tiere signifikant verlängern konnte. Auffällig war hierbei, dass sowohl LV CAR-CIK- als auch parentale CIK-Zellen in den Tieren persistierten, wohingegen keine persistierenden SBTS CAR-CIK-Zellen in den Tieren nachgewiesen werden konnten. Somit ist die nicht-virale Herstellung von ErbB2-CAR-CIK-Zellen

möglich, das Protokoll für die Herstellung bedarf aber noch weiterer Optimierung, damit die SBTS CAR-CIK auch langfristig *in vivo* das Tumorwachstum eindämmen können.

Diese Arbeit zeigt, wie anspruchsvoll die Behandlung des metastasierten RMS ist. Es wurden verschiedene Ansätze für Behandlungsmöglichkeiten verfolgt, die wirksam sind, jedoch eine weitere Verbesserung für den Einsatz im klinischen Setting bedürfen. Neben der Kombination von ErbB2-spezifischen NK-92/52.8.z Zellen mit dem Proteasom-Inhibitor Bortezomib, könnten auch CAR-CIK-Zellen eine wirksame Therapie sein. Hierfür ist jedoch eine weitere Verbesserung des Protokolls für die nicht-virale Herstellung dieser Zellen mittels SBTS notwendig, um einen rapiden Transfer in die Klinik zu ermöglichen.

Table of contents

1 Introduction

1.1 Rhabdomyosarcoma

Soft tissue sarcomas account for nearly 6% of all cancers in children and adolescents and are therefore one of the most common types of solid tumors in this group of patients. Within the soft tissue sarcomas, rhabdomyosarcoma (RMS) accounting for 61% [1] is the most prevalent soft tissue sarcoma with an annual incidence of 4.5 cases per million children and adolescents [2]. RMS tumors, which originate from striated muscle, are identified by expression of Desmin, Myogenin, and MyoD via histological examination [3]. They are further divided into embryonal (eRMS) and alveolar (aRMS) subtypes based on tumor cell morphology [4].

aRMS is frequently associated with PAX fusion genes. The most prevalent fusion is FOXO1-PAX3 (59%) followed by fusion-negative (22%) and FOXO1/PAX7 fusion (19%) [5]. PAX3 (chromosome 1) or PAX7 (chromosome 2) are rearranged with FOXO1 on chromosome 13 [6, 7]. This in-frame fusion combines the DNA binding domain of PAX3 with the transactivation domain of FOXO1. Since both genes encode for transcription factors, the rearrangement results in an additional transcription factor that acts as an oncogenic driver contributing to cell proliferation and survival [8, 9]. For fusion-negative aRMS and eRMS a similar overall survival (Figure 1A) as well as metastasis occurrence (Figure 1B) was observed, whereas fusion-positive aRMS is correlated with a higher tumorigenicity and worse prognosis [8, 10]. Oberlin et al. identified additional prognostic factors besides fusion status (FOXO1-PAX3/7) [11]. Primary tumor sites in the extremities or an unidentifiable primary tumor, more than two metastatic sites at the time of diagnosis, and bone marrow (BM) involvement were also associated with a worse prognosis [11]. These factors determine the Oberlin score for each patient. Higher Oberlin score is associated with worse outcome (Figure 1C) [11, 12].

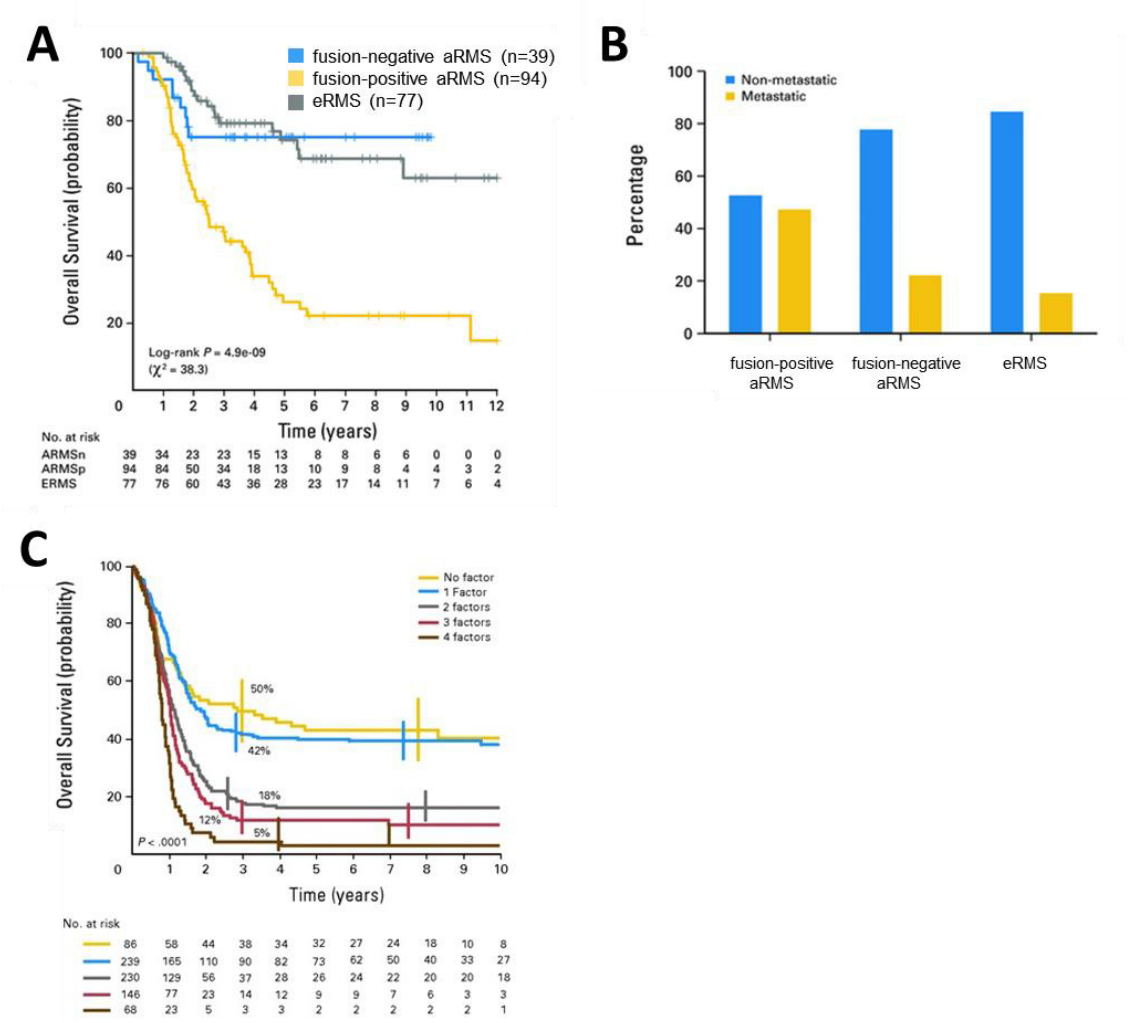

Figure 1: Differences in survival and metastasis in subgroups of RMS. (A) Kaplan-Meier curves show no significant differences for the overall survival of patients with eRMS and fusion-negative aRMS, but patients with fusion-positive aRMS have a significantly worse prognosis. (B) The frequency of metastases is also increased in patients with fusion-positive aRMS compared to patients with eRMS and fusion-negative aRMS. Adapted from Williamson et al. [10]. (C) A high Oberlin score correlates with a poorer prognosis. Adapted fromOberlin et al. [11].

While local RMS manifestation can be cured via surgical excision, patients with Oberlin 4, characterized by advanced metastatic, refractory or relapsed (r/r) RMS, are not cured with standard treatment options such as surgery, radiotherapy and chemotherapy, despite treatment modifications over the last three decades [12, 13]. Early diagnosis is essential for a better outcome of this cohort. In addition, suitable disease markers, such as circulating tumor DNA recently described by Ruhen et al. [14] allow for both an early and improved cancer diagnosis and treatment. But still, there is a high unmet need for novel treatment options.

Besides inhibition of receptor tyrosine kinases, cell cycle regulators, DNA damage response and apoptosis pathways, immunotherapy is an emerging field for the treatment of RMS [15–17].

1.2 ErbB2

ErbB2 also known as human epidermal growth factor receptor-2 (Her2/neu) is one of four membrane tyrosine kinases. Already decades ago, ErbB2 was found to be an oncogene in breast cancer, supporting the pathogenesis and progression of this cancer type [18]. Beside breast cancer ErbB2 is overexpressed in a multitude of other cancers including gastric, esophageal, lung, ovarian cancer, but also RMS [19, 20]. ErbB2 overexpression in general is correlated with increased metastatic potential and also therapeutic resistance, resulting in a poor clinical outcome [21]. It is expressed as a monomer on the cell surface, which undergoes dimerization upon ligand binding [19]. This homo- or heterodimerization with other members of the HER family as EGFR, Her3 or Her4 results in a autophosphorylation and subsequent activation of various cell signaling pathways including mitogen-activated protein kinase (MAPK), phosphatidylinositol-4,5-bisphosphate 3-kinase (PI3K)/AKT and protein kinase C (PKC). The activation of these pathways results in the recruitment of transcription factors mediating cell-cycle progression, proliferation and survival of the tumor cells [19]. Tyrosine kinase inhibitors such as lapatinib, neratinib and afatinib are used to inhibit ErbB2 signaling, but ErbB2 itself as tumor associated antigen (TAA) is also used for immunotherapy [22]. Therapeutic antibodies targeting ErbB2 namely trastuzumab and pertuzumab are clinically used for the treatment of ErbB2 positive breast cancers [23, 24]. Since ErbB2 is expressed only at low levels on the cell surface of most RMS tumors [20, 25, 26] targeting by therapeutic antibodies is not feasible, but ErbB2 can be used as a target for chimeric antigen receptor (CAR)-cell therapy in RMS [26, 27].

1.3 Immunotherapy

Immunotherapy is a rapidly emerging field within cancer therapy with remarkable success and therefore cancer immunotherapy was awarded as the breakthrough of the year in 2013 by the journal Science [28, 29]. The history of this success story began already in the 1891 when William B. Coley injected bacteria into tumors to treat bone and soft-tissue sarcomas to trigger an immune response[30]. Almost 100 years later in 1989, the first chimeric antigen receptors (CARs) were generated by the group of Zelig Eshhar, an Israeli immunologist [31]. After the Food and Drug Administration (FDA) approved the first therapeutic antibodies targeting cytotoxic T-lymphocyte-associated protein 4 (CTLA-4) (2011) [32] and programmed cell death protein 1 (PD-1) (2014) [33, 34] for melanoma patients, the first CAR-T cell therapies against acute lymphoblastic leukaemia were approved by the FDA in 2017 with Kymriah [35]. Since then, several CAR-cell therapies have been approved or have at least entered in clinical trials [36].

1.3.1 Chimeric antigen receptor (CAR)

The success of targeting tumor cells with monoclonal or bispecific antibodies is limited, especially when targeting a low expressed TAA. The combination of the immune cell, mainly T cells, and the antibody in the form of a CAR construct is able to overcome this limitation by CAR cell persistence and enhanced T cell activation via costimulatory domains [37]. To achieve a sufficient CAR-cell activation the assembly of the CAR is critical. The single chain variable fragment (scFv), which is derived from a monoclonal antibody, as the TAA recognizing feature must be carefully selected by appropriate affinity, specificity, immunogenicity and structure [38]. The structures and generations of CAR constructs are shown in Figure 2. The scFv is linked to the signaling domain by a hinge and transmembrane domain, commonly CD8α or CD28 are used. In 1st generation CARs the signaling domain consists only of a CD3ζ chain. CARs were further improved by including costimulatory domains such as CD28, 4-1BB, CD27, CD40, OX40 or ICOS in the signaling domain [39], one domain in the 2nd generation and two domains in the 3rd generation CARs [40]. This basic structure is continuously modified and adapted to the challenges of different cancers. CAR-T cells are already successfully used for the treatment of CD19-positive hematopoietic malignancies [41, 42]. The lack of suitable TAAs and especially the immunosuppressive tumor microenvironment (TME) of solid tumors makes CAR-cell therapy for solid malignancies challenging [43]. 4th generation CARs face the TME by delivering cytokines or disrupting the TME inhibition by the expression of ligands and provide protection for CAR-T cells. These cells are also known as T cells redirected for antigen-unrestricted cytokine initiating killing (TRUCKs) or armoured CAR-T cells [44–47]. Domains leading to the expression of proteins involving transcription factors such as JAK and STAT3/5 and thus initiating memory formation are the latest developments with regard to the classical CAR design (5th generation CAR) [48].

Since TAAs are not solely expressed on tumor tissue but also on normal tissue, the highly potent CAR cells are also redirected to normal cells and therefore toxicity by on-target off-tumor effects [49]. Switchable CARs and CAR cells with suicide mechanisms were developed to archive an control mechanism when unexpected off-tumor toxicities occur [49]. Beside the careful selection of suitable TAAs, two scFv directed against two different antigens are used in case of low TAA selectivity to reduce off-target effects. For tandem CARs the scFvs are linked to one shared signaling domain, whereas for dual CARs each scFv is linked to an own signaling domain[50, 51]. Both CAR constructs may also overcome the loss of TAA in case of immune evasion [52].

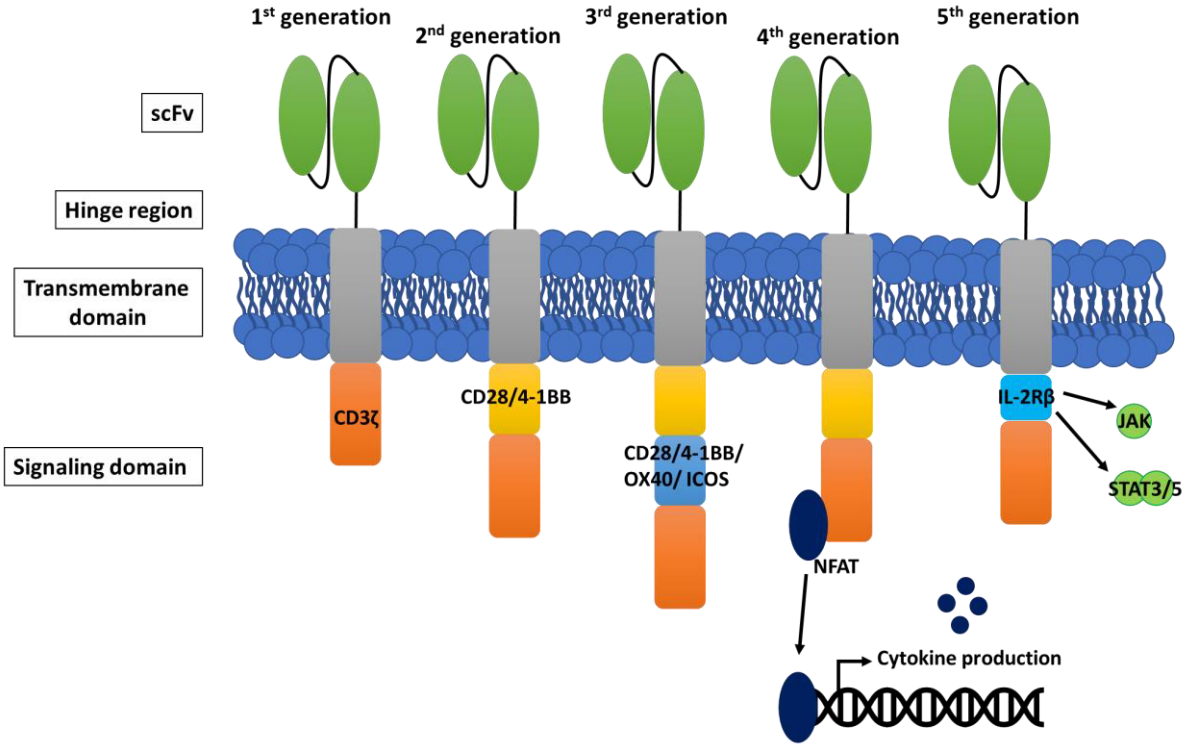

Figure 2: Structure and generations of chimeric antigen receptors (CARs). CARs are generated by fusing the single-chain variable fragment (scFv, green) of monoclonal antibodies to intracellular costimulatory (yellow and blue) and/or signaling (orange) domains. 4th generation CARs can additionally induce the expression of cytokines and 5th generation CARs directly induce cellular memory by activating the transcription factors JAK or STAT3/5.

1.3.2 The 5.28.z CAR

In this study, the 2nd generation ErbB2-specific CAR, designated 5.28.z, was used. The scFv for the 5.28.z CAR was derived from the ErbB2-specific FRP5 antibody. This antibody was generated by immunizing BALB/c mice with the ErbB2-positive human breast tumor cell line SKBR3. The mice were sacrificed and the spleen cells were fused to the murine myeloma cell line PAI. The hybridoma cells were screened for ErbB2-specific antibody-producing clones, and an isolated antibody was designated FRP5 [53]. Subsequently, the scFv of FRP5 was excised and recloned into a pFLAG-1 vector [54]. This FRP5 scFv was used to generate various CAR constructs. The antibody fragment was linked through a CD8α hinge region to human CD3ζ or composite CD137-CD3ζ or CD28-CD3ζ. The activity of the codon optimized CAR constructs after engineering of the NK-92 cell line was then analyzed against highly positive ErbB2 MDA-MB453 breast cancer cells. The 2nd generation CARs with an additional costimulatory domain were superior to the 1st generation CAR, which had only a CD3ζ signaling domain. Furthermore, the CD28-CD3ζ construct led to higher expression rates compared to the CD137-CD3ζ construct [55]. Hence, the 5.28.z construct was cloned into a pSIEW vector. The vector included the enhanced green fluorescent protein (eGFP) separated by an internal ribosome entry site (IRES) sequence, which in case of lentiviral transduction can be used as detection for the CAR construct. For

clinical use the eGFP recognition protein and internal ribosome entry site (IRES) as well as Woodchuck Hepatitis virus posttranscriptional regulatory element (WPRE) in the periphery were deleted (Figure 3).

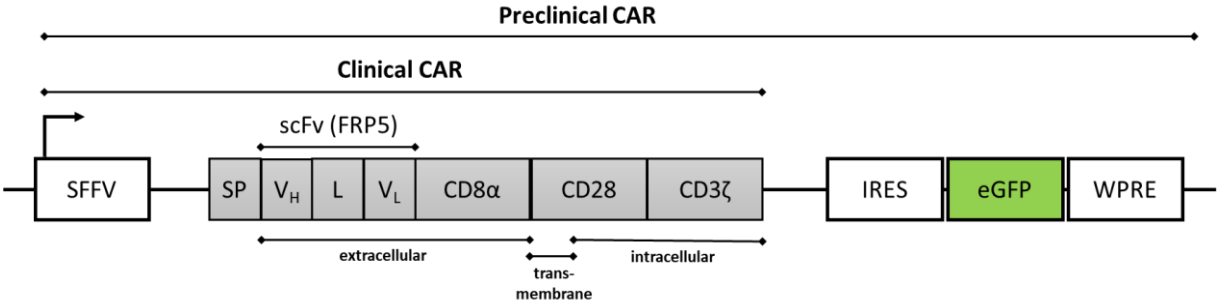

Figure 3: Structure of the 5.28.z CAR. The second generation 5.28.z CAR is driven by a SFFV promoter and consists of a scFv derived from ErbB2-specific FRP5 antibody, a CD8α hinge and a signaling domain composed of the CD28 costimulatory and CD3ζ signaling domain. In the preclinical CAR construct, an additional eGFP for detection is attached to the CAR sequence trough an IRES sequence.

1.3.3 Immune cells as carrier for CAR

Within the immune system, the different immune cells are adapted to their specific tasks by their receptosomes (Figure 4). CAR-T cells were the first CAR-cell products and are still the most commonly used. However, natural killer (NK) cells, the NK-92 cell line and cytokine-induced killer (CIK) cells can also be used as "CAR-carries" [56]. All immune effector cells provide cytotoxicity by the release of granzyme and perforin, as well as through surface ligands, such as TNF-related apoptosis-inducing ligand (TRAIL) and Fas ligand (FasL), which induce apoptosis trough receptors on the surface of the target cells [57]. Recently, macrophages have also been considered as CAR-carrier cells [58], however this cell type will not be discussed here.

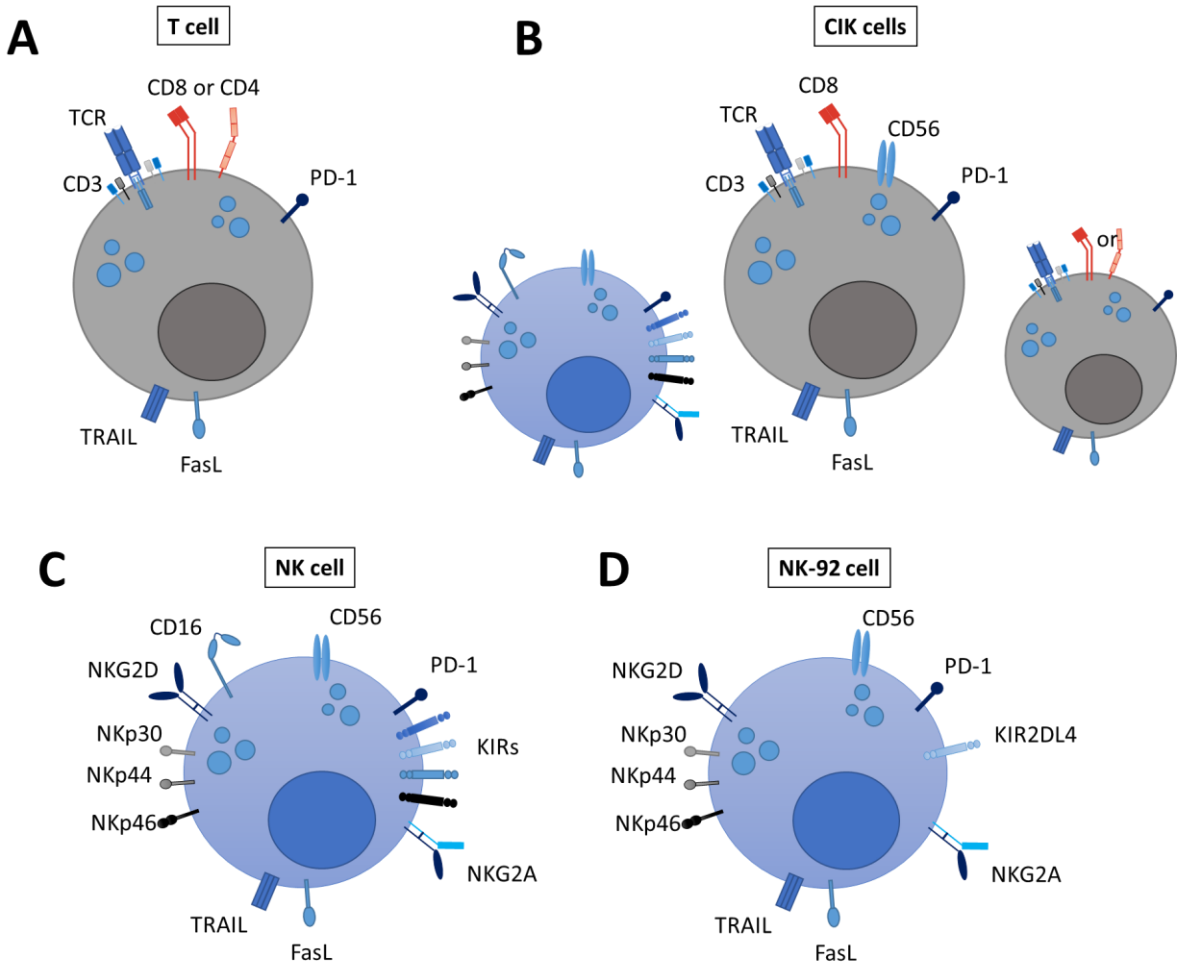

Figure 4: Carrier cells for CAR constructs. (A) T cells are characterized by T cell receptor (TCR), CD3 and CD4 or CD8 as activating components. They also express the cytotoxicity inducing ligands TNF-related apoptosis inducing ligand (TRAIL) and Fas ligand (FasL) as well as programmed cell death protein 1 (PD-1), an immune checkpoint protein. (B) Cytokine-induced killer (CIK) cells are a heterogeneous cell population consisting of CD4+ and CD8+ T cells, natural killer (NK) cells and T-NK cells, cytotoxic CD8+ T cells that also express the NK cell marker CD56. (C) NK cells are characterized by the NK cell marker CD56 and express activating (CD16, NKG2D, NKp30, NKp44 and NKp46) and inhibitory receptors (KIRs and NKG2A). NK cells also express PD-1, TRAIL and FasL. (D) The NK cell line NK-92 is derived from a patient with non-Hodgkin´s lymphoma and is characterized by the NK cell marker CD56 and also the activating receptors of primary NK cells, but NK-92 lacks most of the inhibitory receptors except for NKG2D and low levels of KIR2DL4. NK-92 cells express PD-1, TRAIL and FasL, but in contrast to primary NK cells, do not express CD16.

1.3.3.1 T cells

T cells represent the main effector cell population of the adaptive immune response. After development in the BM, immature CD4 and CD8 double positive T cells migrate to the thymus for differentiation into CD4+ helper or CD8+ cytotoxic T cells [59, 60]. In the lymph nodes, naïve T cells are primed by antigen-presenting cells, usually dendritic cells (DCs), which display exogenous antigens trough the major histocompatibility complex (MHC). T cells bind to the MHC complex trough the T cell receptor (TCR). In addition, binding of the coreceptor CD4 or CD8, interaction of CD28 with CD80/86 on the cell surface of DCs, and secretion of cytokines (IL-6, IL-12 and TGF-β) is required for T cell activation [59]. Upon activation, IL-2-driven proliferation and effector cell differentiation are initiated.

While CD4+ bind to MHC II complexes and act mainly as regulators within the immune system, CD8+ cytotoxic T lymphocytes (CTLs) bind to MHC I complexes leading to the recognition and destruction of infected cells [59]. Initially, the idea behind CAR-based immunotherapy was to kill cancer cells with T cells by mimicking the natural T cell activation upon antigen engagement. Thus, CAR constructs imitate TCR signaling and co-stimulation of CD28 upon binding of the specific TAA [31, 61, 62]. T cells represent the majority of lymphocytes in the peripheral blood, and can be easily isolated by leukapheresis with tolerable side effects [63, 64]. T cells can be genetically engineered by (lenti-)viral transduction and by non-viral technologies such as the *Sleeping Beauty Transposon System* (SBTS) [61, 65]. Despite these advantages, CAR-T cell therapies face some serious challenges. For CAR-T cell therapy, after allogeneic stem cell transplantation, autologous T cells are usually used to reduce alloreactivity and therefore graft versus host disease (GvHD) [66]. However, because the T cells are collected from the individual, the CD4/CD8 ratio varies between the CAR-T cell products. There is increasing evidence that a balanced ratio of CD4/CD8 T cell subtypes results in a superior anti-tumor and an increased proliferative capacity [67, 68]. By separating CD4+ and CD8+ T cells prior to the genetic modification and equally combining both prior to application, disbalances can be solved [69]. Cytotoxic CD8+ CAR-T cells are important for the initial destruction of the tumor, but in a second phase CD4+ CAR-T cells are crucial to maintain a memory phenotype and thus enable long-term remission [70, 71]. However, CD4+ CAR-T cells have been involved in the development of side effects such as the cytokine release syndrome (CRS) and immune effector cell-associated neurotoxicity syndrome (ICANS) [72, 73]. CRS, the most common side effect of CAR-T cell therapy, is induced by the secretion of the cytokines interferon γ (INF-γ) and tumor necrosis factor α (TNF-α) by the T cells upon tumor cell lysis. This activates a cascade of immune cell activation and increased levels of several cytokines, including IL-6, Il-10 and INF-γ, leading to an inflammatory response with organ toxicities [74]. Due to these severe side effects of CAR-T cell therapy, the innovation of switchable CARs has become a new field within the CAR technology [50, 51, 75]. Cells carrying these switchable CAR constructs can be modulated in their activity or eliminated when severe side effects occur [51].

1.3.3.2 Natural killer (NK) cells

NK cells as part of the innate immune system are able to recognize and lyse malignant and virally infected cells and account for 5-20% of human circulating lymphocytes. CD56 surface expression distinguishes between immature ($CD56^{bright}$) and mature ($CD56^{dim}$) NK cells. Immature NK cells have low cytotoxic activity, but secrete cytokines upon activation, mainly INF-γ. These $CD56^{bright}$ NK cells are typically found in lymph nodes, where they act as immune modulators [77]. After maturation in the BM $CD56^{dim}$ NK cells are present in the blood circulation as well as at inflammation sites and play a

major role in cytotoxicity [76]. $CD56^{dim}$, mature NK cells do express $CD16^{bright}$, the key receptor for antibody-dependent cell-mediated cytotoxicity (ADCC), thus supporting the antigen-specific cytotoxicity of mature NK cells [57].

Unlike T cells which are activated by TCR signaling, NK cells possess inhibitory and activating receptors on their surface and get activated, when receptor signaling is shifted towards activating signals [78, 79]. NK cells express a variety of receptors to target and/or eliminate malignant cells. However, NK cells are not MHC-restricted and may therefore be manufactured from human leucocyte antigen (HLA)-mismatched, third-party donors as an off-the-shelf-product [80]. The cultivation of primary NK cells is challenging, but can be facilitated by improved NK cell expansion protocols including cytokines or feeder cells and adapted media/sera [81, 82]. Compared to T cells, genetic modification might sometimes be challenging, as (lentiviral) transduction results in low transduction rates, which might be overcome by non-viral transfection methods [83, 84]. Furthermore, CAR-NK cells are less likely to induce adverse events *in vivo*, such as CRS or ICANS [80]. CAR-NK cells have an *in vivo* life span of about 2 weeks, which is an advantage if on-target off-tumor effects occur, but also an disadvantage if long-term effects are not provided and repeated infusions are needed to facilitate persistence [85]. *In vivo* persistence can be prolonged by intravenous (iv) administration of IL-2, but this can increase severe side effects including capillary leak syndrome [86–88].

1.3.3.3 NK-92 cells

The natural killer cell line NK-92 established by Hans G. Klingemann in 1994 is derived from peripheral blood cells of a 50-year-old white, male patient with rapidly progressing non-Hodgkin´s lymphoma [89]. The IL-2 dependent NK-92 cell line lacks the CD16 expression, expresses a large number of activating NK cell receptors (NKp30, NKp46, 2B4, NKGD and CD28) and lacks most of the inhibitory killer inhibitory receptors (KIRs). In addition, high levels of molecules related to the perforin-granzyme cytotoxic pathway are expressed, as well as proteins for alternative killing pathways such as FasL, TRAIL, TWEAK or TNF-α [90]. This unique expression pattern allows for a high cytotoxic capacity against cancer cells.

NK-92 cells can be lentivirally transduced and can be cost-efficiently expanded to clinical doses [91, 92], thus the ErbB2-specific CAR-NK-92 cell line NK-92/5.28.z was generated by lentiviral transduction. After monoclonal expansion, the clone with the best *in vitro* and *in vivo* properties was selected [55]. Respective cells demonstrated an excellent cytotoxic activity against ErbB2-positive malignancies, including aRMS [26, 91].

NK-92/5.28.z cells are tested in a phase I clinical trial against relapsed glioblastoma (NCT03383978) [93] as an ready-to-use, third party product. To avoid uncontrolled outgrowth, the NK-92/5.28.z cell line must be irradiated with 10 Gy prior to clinical use due to regulatory reasons, [91]. Hence, long-term anti-tumor response is only provided by priming of bystander immune cells within the tumor microenvironment [92]. The INF-γ and TNF-α secreted by the NK-92/5.28.z cells upon activation promotes the maturation and tumor antigen uptake of dendritic cells. Afterwards the dendritic cells present the antigens to T and NK cells in the lymph nodes inducing the differentiation of these cells towards tumor antigens [94, 95].

1.3.3.4 Cytokine-induced killer (CIK) cells

Cytokine-induced killer (CIK) cells are a heterogeneous cell population, generated *in vitro* by optimizing the lymphokine-activated killer (LAK) cell protocol [96], and consist of T, NK and a high percentage of T-NK cells. Rosenberg´s group established the LAK protocol in the 1980s; these cells were generated from human lymphocytes and were able to sufficiently lyse various tumor cells, but showed poor expansion capacity [97, 98]. CIK cells are generated from human peripheral blood mononuclear cells (PBMCs) by adding the cytokines INF-γ, IL-2 and anti-CD3 (OKT3) [96]. Later, the protocol was further improved by adding IL-15, as this cytokine supports the survival of NK, T-NK and CD8+ T cells and significantly increases tumor cell lysis [99, 100]. INF-γ activates the monocytes within PBMCs, which then provide CD58 and IL-12, two essential factors for the expansion of CD56+ cells [101]. OKT3 and IL-2 promote T cell activation and proliferation [102], IL-15 signaling enhances the expression of CD56, which is increasingly expressed on NK cells, but also on T-NK cells, a highly cytotoxic cell population that represents up to 40% of CIK cells [99, 103, 104]. These T-NK cells are T cells characterized by the expression of T cell features (CD3 and αβ-TCR) that obtain typical NK cell markers (CD16 and CD56) during culture and are therefore HLA unrestricted [103, 105]. This unique expression pattern allows for the combination of both, adaptive and innate immune responses within this T-NK cell subpopulation [103].

Several phase III and IV trials have recently been conducted to evaluate the efficacy of autologous CIK cells against a variety of solid tumors [106, 107]. CIK cells are also approved as an Advanced Therapy Medical Product (ATMP) for the treatment of relapsed hematologic malignancies [108]. Like T cells, CIK cells can be directed to tumor cells by therapeutic antibodies [109] or CARs [110, 111]. Genetic modification by lentiviral transduction [111] or SBTS [112, 113] leads to efficient CAR expression in CIK cells.

CIK cells kill tumor cells by NKG2D-dependent, but TCR-independent mechanism [114]. This intrinsic cytotoxicity can be enhanced through the 5.28.z CAR targeting ErbB2 [111, 115]. Like CAR-T cells, CAR-CIK cells can induce GvHD in the allogeneic setting, but the risk of GvHD is lower compared to T cells, as T-NK cells exhibit a late effector phenotype with lower proliferative potential and a cytokine profile less likely to induce GvHD [106]. CAR-CIK cells may therefore be more suitable for adoptive transfer than CAR-T cells, at least in an allogeneic setting [116].

1.3.4 Combinational approaches

CAR-cell therapies are well established for CD19-positive hematological malignancies. Hurdles in solid cancers are mainly linked to the composition of solid tumors. The immunosuppressive TME of these multicellular 3D structures as wells as hypoxic conditions, both limit the access for CAR cell therapies [117]. The TME is characterized by a non-cellular extracellular matrix (ECM) composed of proteins, glycans, growth factors and cellular components that through cancer-associated fibroblasts and M2 macrophages support tumor growth [118]. The ECM of RMS tumors consists of XVII collagen alpha 1 [119, 120] infiltrated by cellular components. Different groups reported an infiltration of tumor-supporting fibroblasts, and an absence or very low number of T and B cells [119, 121]. Kather et al. attributed this low infiltration to the absence of CD54+ microvessels in aRMS tumors, which resulted in a poor prognosis for these patients [121]. Recently DeMartino et al. reported single-cell transcriptomic data showing higher numbers of infiltrating T and B cells [122]. In addition, the tumor cells themselves can inhibit access of CAR cells through an increased surface expression of immunosuppressive ligands like PD-L1 and CTL-4 [118, 120]. Taken together, these inhibitory factors make solid tumors a challenging target for CAR cells. Enhancing their efficacy by checkpoint blockade or small molecules/anti-cancer therapies might be beneficial in terms of anticancer activity.

1.3.4.1 Checkpoint blockade

Immune checkpoints are proteins, which regulate immune cells by inhibitory or stimulatory signaling and are therefore the gatekeepers of the immune response, the first one targeted by immunotherapy was PD-L1 [123]. This ligand is expressed at low to intermediate levels on various cancers including RMS [124]. In a phase II trial, single agent treatment with PD-1 blocking antibody nivolumab showed limited efficiency against sarcomas, with only 5% of the patients responding to the treatment. Therefore, a monotherapy did not warrant further investigation [125]. But, combinatorial treatment with nivolumab or PD-1 axis blockade in general and additional agents or immunotherapies was promising. The combination of nivolumab and ipilimumab, an antibody targeting CTL-4, prolonged

survival of sarcoma patients [125]. Moreover, PD-1 or PD-L1 blockade supported CAR cell efficacy by engaging the patient´s immune system and/or harnessed the power of CAR cell therapy [126]. Besides, PD-L1 and CTL-4, TIM-3 and LAG-3 might be considered in this context [127]. PD-1 blockade with pembrolizumab and ErbB2-specific CAR-T cell therapy induced complete remission in a patient with metastatic RMS [128]. Increased levels of PD-1 on CD8+ CAR-T cells seen during remission suggests additional efficacy provided by pembrolizumab [128]. Altogether, PD-1/PD-L1 inhibition is known to rescue T and NK cells from exhaustion and avoiding immune evasion of tumor cells [126, 129].

1.3.4.2 Bortezomib

Another way to overcome immune evasion is the use of agents that target intracellular structures rendering cancer cells more susceptible for immunotherapy. RMS cells are resistant to Fas induced apoptosis, but were found to be highly responsive to TRAIL induced apoptosis [130]. This is of particular interest, as TRAIL-mediated apoptosis is strictly restricted to cancer cells [131]. Both cytotoxic T and NK cells are capable to facilitate TRAIL-mediated apoptosis [132]. The apoptotic elimination of cancer cells by TRAIL can be enhanced by combinatorial treatment with bortezomib. Bortezomib, also known as PS-341 or Velcade, is a dipeptidyl boric acid that selectively and reversibly inhibits the 26S unit of the proteasome [133]. Bortezomib was the first proteasome inhibitor tested in humans and was shown to be safe and efficient in patients with refractory or progressive multiple myeloma (MM) [134]. As a result, bortezomib was approved for the treatment of MM by the FDA in 2003.

The mechanisms of TRAIL-mediated apoptosis and the involvement of bortezomib within the pathways is shown in Figure 5. The agonistic TRAIL-Rs (receptors) involved in this process are death receptor 4 (DR4) and 5 (DR5) [131]. The two decoy receptors DcR1 and DcR2 are unable to transduce an apoptotic signal due to a truncated or missing death domain [135]. Bortezomib is one of the most potent enhancers for TRAIL-mediated apoptosis, as the treatment with bortezomib induces the upregulation of DR4 and DR5 on the surface of the tumor cells [136]. After trimerization of TRAIL-receptors (TRAIL-R) by TRAIL, the trimer interacts with the Fas-associated death domain (FADD). This leads to the aggregation of pro-caspase-8, resulting in caspase-8 autocleavage, which results in apoptosis via the activation of caspase-3 [135, 137]. Bortezomib additionally supports TRAIL-mediated cytotoxicity by preventing the degradation of p53 and pro-apoptotic proteins Bid and Bax [138, 139]. Caspase-8 activates t-Bid, resulting in the release of cytochrome c from mitochondria mediated by Bak und Bax [140]. Cytochrome c activates caspase-9, thereby inducing apoptosis through the caspase cascade [141]. This cascade can be inhibited by anti-apoptotic BcL-x_L. Bortezomib can prevent this inhibition as it stabilizes the tumor suppressor p53, which inhibits the BcL-x_L [135]. Beside these apoptotic pathways, the NFκB pathway can be involved in TRAIL signaling and supports cell survival and

proliferation through the transcription factors c-Rel and p65 in the canonical and p100 in the non-canonical pathway [141]. This pro-survival effect can be inhibited by bortezomib, since the NFκB pathway is dependent on the proteasomal activation of its transcription factors. Notably, bortezomib is not only able to enhance apoptosis in TRAIL-sensitive cells, but also sensitizes initially resistant cells to this cytotoxic mechanism [142–145].

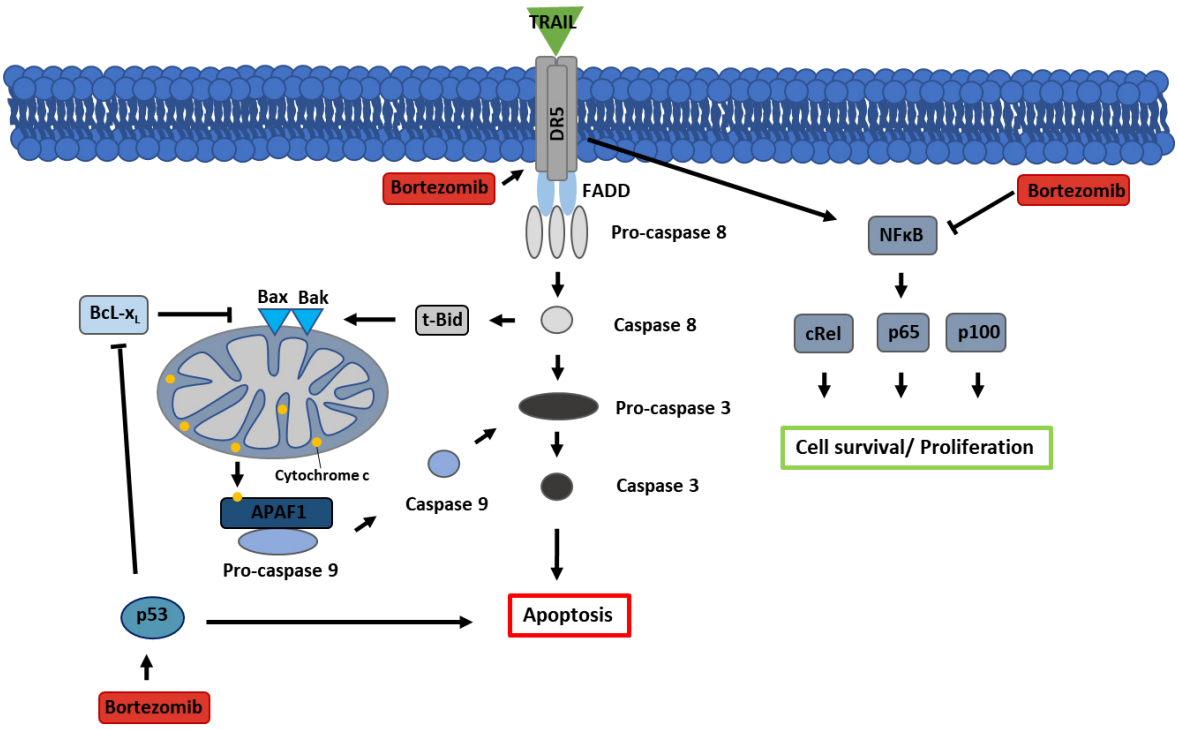

Figure 5: Mechanism of TRAIL-mediated apoptosis and effects of bortezomib treatment. TRAIL protein is bound by trimerized TRAIL-receptor (TRAIL-R), which leads to caspase cascade resulting in apoptosis. In addition, caspase 8 activates apoptosis through t-Bid activation and mitochondrial induced apoptosis. The NF-κB pathway is also triggered by TRAIL binding. Bortezomib supports the cancer cell apoptosis through several interactions: increased TRAIL-R expression, inducing apoptosis through p53 and inhibition of the NF-κB pathway and anti-apoptotic protein BcL-x_L.

In combination with CAR-NK-92 cells, bortezomib significantly reduced tumor growth of renal carcinoma in a xenograft model compared to single agent therapy [146]. The combination of bortezomib and NK cell therapy may be of particular interest, as proteasome inhibition down-regulates the HLA-E and HLA-I surface expression on MM and thus additionally supports NK cell activation [147, 148]. In the context of RMS, bortezomib has already been evaluated as single agent for the treatment of metastatic RMS in a multicentre phase II trial, where it was well tolerated but showed limited efficiency [149]. However, it is unclear whether the combination of bortezomib and CAR-cell immunotherapy is also beneficial in RMS. Since bortezomib inhibits the proteasome of all cells, this could also impair CAR-cell therapy. Therefore, the timing of bortezomib and delayed immunotherapy application is critical in case of clinical use. Nevertheless, CAR-NK-92 cell function was not impaired in a combinatorial treatment with bortezomib in renal carcinoma [146]. Moreover, bortezomib was found to enhance immune responses by enabling cytokine release that promotes CD8+ T cell function,

and by increasing the expression of effector molecules within lymphocytes by stimulating Notch-NFκB crosstalk [150, 151].

1.4 Sleeping beauty transposon system (SBTS)

Adoptive immunotherapy for cancer has become an important treatment option in the recent years [152]. While T cells are easily transducable by lentiviral particles, this is not the case for NK cells [83]. The genetic modification is associated with cell cytotoxicity and is time- and cost-consuming, and requires adequate facilities with appropriate safety levels and specially trained personnel [153]. Furthermore, viral vectors tend to integrate to highly expressed and cancer-related genes and may also induce insertional mutagenesis, leading to serious safety issues [154]. To overcome these limitations, non-viral genetic modifications have become increasingly important, especially since the availability of CRISPR/Cas9 [155]. Recently, transposon-based methods have gained interest, and protocols based on piggyBac and sleeping beauty transposon system (SBTS) have been established for the manufacturing of CAR cells [156, 157].

Class I subclass II transposon systems, including piggybac and SBTS, generally consist of a transposon and a transposase [158]. The transposase recognizes the transposon by flanking inverted terminal repeats (ITRs) consisting of two direct repeats (DR) and subsequently excise the transposable element (TE) and reintegrates it in another genomic location [159]. For genome engineering of cells, the gene of interest, such as the CAR, is used as TE. The SBTS is a synthetic transposon system that was established by Zoltan Ivics in the late 1990s by accumulated mutations of a fish transposon [160]. The activity of the Sleeping Beauty transposase (SB) is restricted to vertebrates, and an improved, hyperactive variant, designated SB100x was developed as the original SB showed limited efficiency [161]. Mechanistically, four SB molecules, two on each side of the transposon, bind the DR repeats within the ITRs by their N-terminal DNA binding domains (Figure 6). A defined sequence of DNA-protein and protein-protein interaction is essential for the formation of a synaptic complex, which ultimately results in the formation of a tetramer and a double-strand break, the excision of the TE from the donor DNA [158, 159]. The excision process leaves a 3bp footprint on the donor DNA sequence. The C-terminal catalytic domain attacks the target DNA through free OH-groups at TA dinucleotides and integrates the TE. As the integration results in single-strand gaps, these gaps are filled by DNA repair machinery [158, 159].

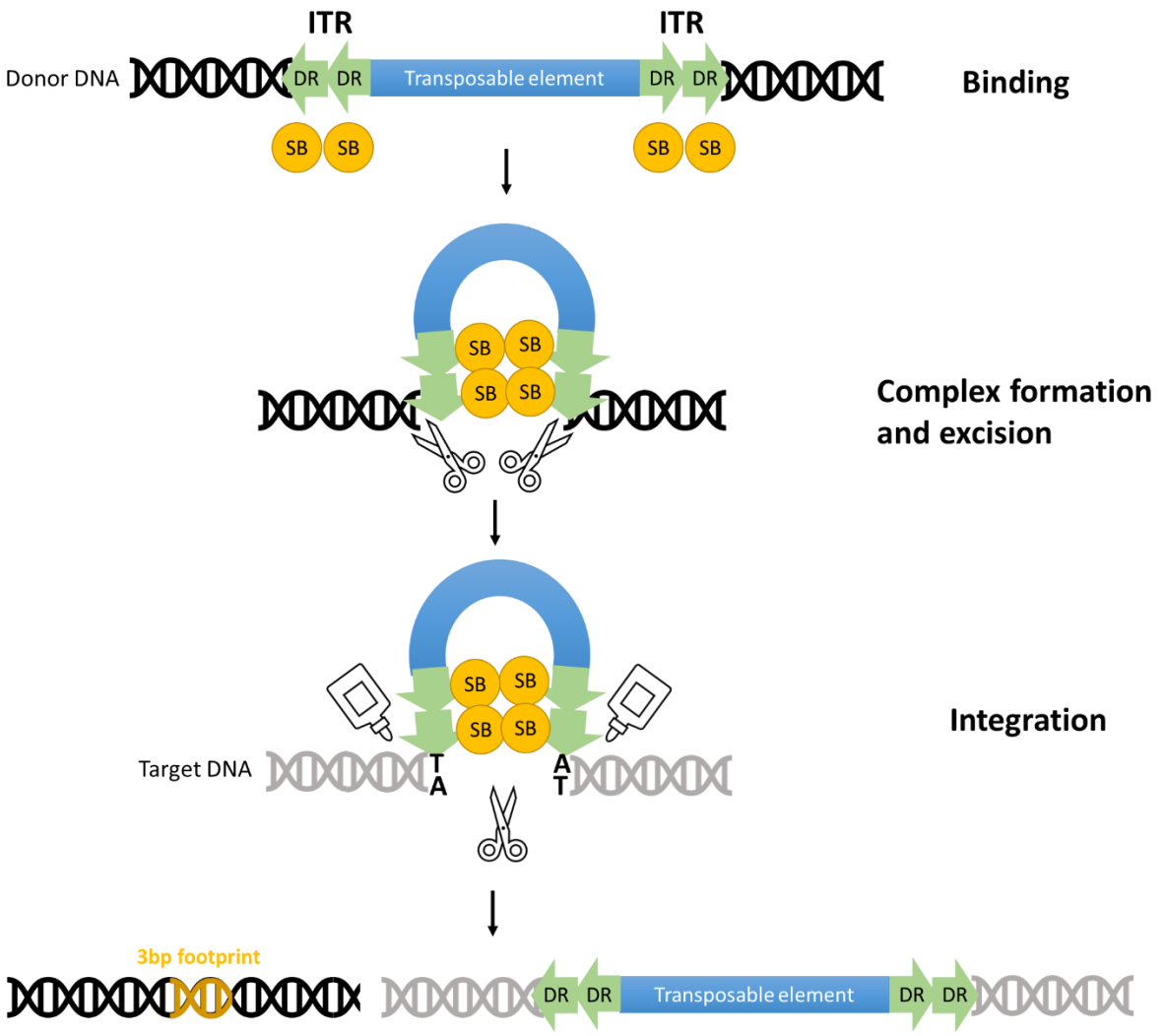

Figure 6: Schematic mechanism of SBTS. Sleeping Beauty transposases (SB) binds the direct repeats (DRs) within the inverted terminal repeats (ITRs) flanking the transposable element (TE). This binding is highly dependent on the interactions occurring in the correct order to form a synaptic complex consisting of a SB tetramer bound to the donor DNA. The transposon is excised from the donor DNA by double-stand breaks leaving a 3bp footprint, and is reintegrated in the target DNA at a TA site.

In contrast to viral transduction, SBST exhibits a nearly random integration pattern in genetic safe harbours, which is advantageous for clinical application by eliminating safety concerns about genotoxic and mutagenic effect after gene integration near proto-oncogenes [162]. For clinical application, cells are transfected with plasmids encoding the transposase and the TE, here the gene of interest (GOI). To make the GOI accessible for SBTS, the sequence has to be transferred between the ITRs in a SB transposon vector. Currently, several vectors with improved ITR versions derived from the original pT vector are available, namely pT2, pT3, pT2B and pT4 [158]. Due to low transfection efficiency and high cell cytotoxicity, the use of SB100x mRNA and GOI on minicircles (MC) are preferred over plasmids [158]. MC are small plasmids without bacterial components. In addition, the reduced size eliminates safety concerns, particularly with respect to antibiotic resistance genes [158]. SBTS is now used as an efficient gene transfer method for CAR-T cells, but since nucleofection and infiltration of large amounts of external nucleic acids is a harsh method, several attempts were made to improve the protocol:

Besides the reduction of nucleic acids by using mRNA encoding hyperactive SB100x and MC instead of plasmids [154, 163], feeder cells have been used to support the expansion of CAR-T cells [164, 165]. Successful implementation of this method resulted in SB CAR-T products targeting CD19 on leukemia [166] and SLAM7 on MM [167]. Of note, the SBTS technology was also successfully applied to NK [84] and CIK cells [113].

1.5 Aim of this work

In this work, novel and specific therapies for the treatment of metastatic RMS are developed and evaluated in both, preclinical *in vitro* and *in vivo* models. Metastatic RMS is resistant to available treatment options such as surgery, chemo- and radiotherapy, therefore specific and effective CAR immunotherapies are considered as novel therapy approaches. Especially since the Houston group reported a durable complete remission in a boy with metastatic RMS after ErbB2-CAR-T cell and combinatorial PD-1 inhibitor treatment [128]. However, the optimal immune effector cell type expressing the CAR and/or the best combinatorial treatment with other anticancer therapeutics remains unclear.

In this work, the ErbB-2 specific CAR-NK-92 cell line NK-92/5.28.z as clinically used product, is assessed against RMS in 2D and 3D *in vitro* assays. Since NK-92/5.28.z cells must be irradiated prior to clinical application, the proliferative and cytotoxic potential of NK-92/5.28.z cells after irradiation is also addressed. In preclinical xenograft models of metastatic RMS the therapeutic potential of NK-92/5.28.z cells and also irradiated NK-92/5.28.z cells is examined using untreated and NK-92-treated animals as reference. The CAR-mediated and the intrinsic cytotoxic potential is assessed in detail in the presence of an immunosuppressive TME. Combinational treatment options to overcome the TME and increase NK-92/5.28.z-mediated efficacy, such as PD-1 immune checkpoint blockade and proteasome inhibition by bortezomib are evaluated.

In addition, ErbB2-specific CAR-CIK cells are generated and evaluated as an alternative immune effector cells source. Establishing a protocol for SBTS-modified enables a rapid translation towards clinical application for metastatic RMS patients with high unmet medical need for novel treatment strategies. Various factors, such as timing, feeder cells and media, potentially impacting the efficient genetic modification of CAR-CIK cells by SBTS are examined. The characteristics and cytotoxicity of the CAR-CIK cells generated by the established protocol are evaluated *in vitro*. Finally, SBTS-engineered CAR-CIK cells are compared to lentivirally transduced CAR-CIK cells *in vitro* and *in vivo*.

2 Material & Methods

2.1 Materials

2.1.1 Animals

NOD/Scid/IL2Rγ$^{-/-}$ mice (NSG mice) with the genotype NOD.Cg-*Prkdc*^{scid} *Il2rg*^{tm1Wjl}/SzJ were used for *in vivo* experiments. Mice were bred by mfd Diagnostics GmbH (Wendelsheim, Germany). Experiments were performed in the animal facility of the Georg-Speyer-Haus (Frankfurt/Main, Germany). Immunodeficient mice were housed in small groups in individually ventilated cages. I*n vivo* experiments were approved by the governmental committee (Regierungspräsidium Darmstadt, Darmstadt, Germany; Gen.-Nr. TVA FK/1070 and FK/2033) and were performed according to the requirements of the German Animal Welfare Act.

2.1.2 Cell lines and cell culture

Table 1: Cell lines and cell culture.

Name	*Supplier/Source*
HEK293T/17 (human embryonal kidney cell line)	Prof. Dr. Winfried Wels, Georg-Speyer-Haus, Frankfurt/Main, Germany
NK-92 (human NK cell line)	Prof. Dr. Hans G. Klingemann, Tufts University School of Medicine, Boston, MA, USA
NK-92/5.28.z (human CAR-NK cell line)	Prof. Dr. Winfried Wels, Georg-Speyer-Haus, Frankfurt/Main, Germany
Primary human PBMCs	Isolated from fresh peripheral blood or buffy coat preparation of healthy donors, DRK-Blutspendedienst, Frankfurt/Main, Germany
RH30 (human aRMS cell line)	DSMZ, Deutsche Sammlung von Mirkoorganismen und Zellkulturen GmbH, Braunschweig, Germany
RH41 (human aRMS cell line)	DSMZ, Deutsche Sammlung von Mirkoorganismen und Zellkulturen GmbH, Braunschweig, Germany
RMS102 (human patient-derived aRMS organoid)	Prof. Dr. Frank C. P. Holstege, Prinses Máxima Center, Utrecht, Netherlands
RMS127 (human patient-derived aRMS organoid)	Prof. Dr. Frank C. P. Holstege, Prinses Máxima Center, Utrecht, Netherlands

RMS335 (human patient-derived aRMS organoid)	Prof. Dr. Frank C. P. Holstege, Prinses Máxima Center, Utrecht, Netherlands
Fluorescent cell lines	
RH30 GFP/luc+ (RH30 cell line stably expressing GFP fluorescence protein and Firefly luciferase)	Prof. Dr. Evelyn Ullrich, University Hospital, Frankfurt/Main, Germany
RH30 mCherry/luc+ (RH30 cell line stably expressing mCherry fluorescence protein and Firefly luciferase)	Dr. Laura Moser, University Hospital Frankfurt/Main, Germany
RMS335 GFP/luc+ (RMS335 cell line stably expressing GFP fluorescence protein and Firefly luciferase)	Parental RMS335 cells transduced with pSL2GW
RH41 GFP/luc+ (RH41 cell line stably expressing GFP fluorescence protein and Firefly luciferase)	Parental RH41 cells transduced with pSL2GW

2.1.3 Viral particles

Table 2: Viruses.

Name	*Description*	*Source*
ErbB2-CAR lentiviral particles	pSIEW derivate coding ErbB2-CAR (5.28.z) with GFP separated by IRES sequence	Dr. Laura Moser, University Hospital Frankfurt/Main, Germany

2.1.4 Plasmids & Minicircles

Table 3: Plasmids and minicircles.

Name	*Description*	*Source*
Plasmids		
pSL2GW	pSEW derivate, GFP was replaced by luciferase-GFP separated by a T2A restriction site	Prof. Dr. Christian Buchholz, Paul-Ehrlich-Institute, Langen, Germany
pLenti-fLuc-P2A-mCherry	pSIEW derivate with firefly luciferase and GFP	Dr. Laura Moser, University Hospital Frankfurt/Main, Germany

pΔ9.8.1	HIV-1 packaging plasmid for gag/pol expression for the generation of lentiviral particles	Prof. Dr. Winfried Wels, Georg-Speyer-House, Frankfurt/Main, Germany
pMD2.G	VSV-G envelope expressing plasmid for the generation of lentiviral particles	Prof. Dr. Winfried Wels, Georg-Speyer-House, Frankfurt/Main, Germany
pT2-5.28.z	pSIEW derivate coding ErbB2-CAR (5.28.z) with GFP separated by IRES sequence flanked with ITRs	Prof. Dr. Winfried Wels, Georg-Speyer-House, Frankfurt/Main, Germany
Minicircles		
MC Venus	Coding eGFP flanked by ITRs	PlasmidFactory GmbH & Co.KG, Bielefeld, Germany
MC ErbB2-CAR	Coding ErbB2-CAR (5.28.z) with GFP separated by IRES sequence flanked by ITRs	PlasmidFactory GmbH & Co.KG, Bielefeld, Germany

2.1.5 mRNA

Table 4: mRNA.

Name	*Description*	*Supplier*
SB100x mRNA	mRNA coding active *Sleeping beauty* 100x	ethris GmbH, Planegg, Germany

2.1.6 Primer

Table 5: Primer.

Target	*Sequence 5´-3´*	*Supplier*
Human DR4 (TNFRSF10A)	TGTTGCATCGGCTCAGGTTG (forward) ACGAAAGTGGACAGCGAGTC (reverse)	Eurofins, Hamburg, Germany
Human DR5 (TNFRSF10B)	CAGGTGTGATTCAGGTGAAGTG CCCACTGTGCTTTGTACCTG	Eurofins, Hamburg, Germany
Human Caspase-3	TGTTTGTGTGCTTCTGAGCC CACGCCATGTCATCATCAAC	Eurofins, Hamburg, Germany

Human NF-kB p65 (RELA)	GCCGAGTGAACCGAAACTCT GCCTGGTCCCGTGAAATACA	Eurofins, Hamburg, Germany
Human NF-kB p100 (NFKB2)	GAGGGCCTTTAGCGGACAG CGGGTCCGCGTATCTTTGTA	Eurofins, Hamburg, Germany
Human JNK (MAPK8)	CTGAAGCAGAAGCTCCACCA TGCACCTAAAGGAGAGGGCT	Eurofins, Hamburg, Germany
Human p53	AGTCTAGAGCCACCGTCCAG CAGTCTGGCTGCCAATCCA	Eurofins, Hamburg, Germany
Human BCL-XL (BCL2L1)	CTGAATCGGAGATGGAGACC TGGGATGTCAGGTCACTGAA	Eurofins, Hamburg, Germany
Human TRAIL (TNFSF10)	ACCAGAGGAAGAAGCAACACA GTTGCTCAGGAATGAATGCCC	Eurofins, Hamburg, Germany
Human 18S	CGCAAATTACCCACTCCCG TTCCAATTACAGGGCCTCGAA	Eurofins, Hamburg, Germany
Human RPII	GCACCACGTCCAATGACAT GTGCGGCTGCTTCCATAA	Eurofins, Hamburg, Germany

2.1.7 Antibodies

Table 6: Antibodies.

Flow Cytometry			
Target	Fluorophore	Clone	Supplier
Human CD3	PerCP	HIT3a	BioLegend, San Diego, CA, USA
Human CD4	PE-Cy7	A161A1	BioLegend, San Diego, CA, USA
Human CD56	PE-Cy7	HCD56	BioLegend, San Diego, CA, USA
Human CD8	APC	SK1	BioLegend, San Diego, CA, USA
Human ErbB2	PE	24D2	BioLegend, San Diego, CA, USA
Human PD-1	PE	EH12.2H7	BioLegend, San Diego, CA, USA

Human PD-L1	PE	MIH2	BioLegend, San Diego, CA, USA
Human CD45	PE-Cy7	HI30	BioLegend, San Diego, CA, USA
Mouse IgG1, κ	PE	MOPC-21	BioLegend, San Diego, CA, USA
Human TruStain FcX™ (Fc Receptor Blocking Solution)	-	-	BioLegend, San Diego, CA, USA
Human IgG Fc	APC	M1310G05	BioLegend, San Diego, CA, USA
Human CD45	PerCP	HI30	BioLegend, San Diego, CA, USA
Human CD16	PE	3G8	BioLegend, San Diego, CA, USA
Human CD56	BV421	NCAM162	BD Biosciences, San Jose, CA; USA
Human TCR α/β-	BUV737	T10B9.1A-31	BD Biosciences, San Jose, CA; USA
Human CD3	BUV395	SK7	BD Biosciences, San Jose, CA; USA
Human CD3	BV786	SK7	BD Biosciences, San Jose, CA; USA
Human CD45RO	BV711	UCHL1	BD Biosciences, San Jose, CA; USA
Human CD62L	BUV737	SK11	BD Biosciences, San Jose, CA; USA
Human CD8	BUV395	RPA-T8	BD Biosciences, San Jose, CA; USA
Immunofluorescence microscopy			
Target	*Fluorophore*	*Clone*	*Supplier*
Human CD45	-	SPM496	abcam, Cambridge, UK
GFP antibody	-	Polyclonal (Rabbit)	Invitrogen, Waltham, MA, USA

Mouse F(ab`)$_2$ fragment	Alexa Fluor™ 647	Polyclonal (Goat)	Jackson ImmunoResearch, Ely, UK
Rabbit IgG	Alexa Fluor™ 488	Polyclonal (Goat)	Invitrogen, Waltham, MA, USA
Mouse Meca32	-	MECA-32 (Rat)	BD Biosciences, San Jose, CA; USA
Rat IgG	Alexa Fluor™ 546	Polyclonal (Goat)	Invitrogen, Waltham, MA, USA

Blocking antibody		
Target	*Clone*	*Supplier*
PD-1	EH12.2H7	BioLegend, San Diego, CA, USA

Western blot			
Target	*Catalog number*	*Host species*	*Supplier*
Human caspase 3	9662	rabbit	Cell Signaling Technology, Danvers, MA, USA
Human phospho-NF-κB p100 (Ser866/870)	4810	rabbit	Cell Signaling Technology, Danvers, MA, USA
Mouse IgG (HRP)	ab6789	goat	abcam, Cambridge, UK
Rabbit IgG (HRP)	ab6721	goat	abcam, Cambridge, UK
Human NF-κB p52	05-361	mouse	Merck KGaA, Darmstadt, Germany
Human p53	554294	mouse	BD Biosciences, San Jose, CA; USA
Human cRel	4727	rabbit	Cell Signaling Technology, Danvers, MA, USA
Human phospho-JNK1/2 (Thr183/Tyr185)	44-682G	rabbit	Thermo Fisher Scientific, Waltham, MA, USA
Human JNK1	44-690G	rabbit	Thermo Fisher Scientific, Waltham, MA, USA
Human phospho-NF-κB p65 (Ser536)	3033	Rabbit	Cell Signaling Technology, Danvers, MA, USA
Human NF-κB p65	sc-8008	mouse	Santa Cruz Biotechnology
Human Bcl-XL	2762	rabbit	Cell Signaling Technology, Danvers, MA, USA

Human GAPDH	5G4cc	mouse	HyTest Ltd, Turku, Finland
Human Vinculin	V9131	mouse	Merck KGaA, Darmstadt, Germany
Human β-actin	A5441	mouse	Merck KGaA, Darmstadt, Germany

2.1.8 Chemicals and Compounds

Table 7: Chemicals and compounds.

Compound	*Supplier*
A83-01	Tocris, Minneapolis, MN, USA
Acrylamide mix (30%)	Carl Roth, Karlsruhe, Germany
Advanced DMEM/F12 medium	Gibco, Waltham, MA, USA
Aqua destillata (A.dest.)	B.Braun, Melsungen, Germany
Aqua-Poly/Mount	Polysciences, Inc., Warrington, PA, USA
B27	Gibco, Waltham, MA, USA
BD FACS Clean solution	BD Biosciences, San Jose, CA, USA
BD FACS Flow solution	BD Biosciences, San Jose, CA, USA
BD FACS Shutdown solution	BD Biosciences, San Jose, CA, USA
BD Quantibrite™ Beads	BD Biosciences, San Jose, CA, USA
Bortezomib	Hölzel Diagnostika Handels GmbH, Cologne, Germany
Caspase-Glo® 3/7 Assay Systems	Promega GmbH, Mannheim, Germany
Collagenase D	ROCHE, Basel, Switzerland
Complete™ EDTA-free Protease Inhibitor Cocktail (PIC)	Roche, Basel, Schweizerland
Cultrex BME	Bio-Techne, Minneapolis, MN, USA
DAPI	Sigma-Aldrich, St. Louis, MO, USA
DDT	Merck KGaA, Darmstadt, Germany
D-Luciferin	Promega GmbH, Walldorf, Germany
DMEM medium, high glucose, GlutaMAX™ Supplement	Gibco, Waltham, MA, USA
DMEM/F12 medium	Gibco, Waltham, MA, USA
DMSO	Sigma-Aldrich, St. Louis, MO, USA

DPBS without calcium and magnesium	Gibco, Waltham, MA, USA
FCS	Sigma-Aldrich, St. Louis, MO, USA
Fresh frozen human plasma	BSD, Frankfurt/Main, Germany
Heparine	Gibco, Waltham, MA, USA
HEPES 1M	Gibco, Waltham, MA, USA
Histopaque®-1077	Sigma-Aldrich, St. Louis, MO, USA
Human anti-CD3 mAB (OKT3, MACS GMP CD3 pure)	Miltenyi Biotec, Bergisch-Gladbach, Germany
Human EGF	Peprotech, Hamburg, Germany
Human FGF-basic	Peprotech, Hamburg, Germany
Human IGF-I	Peprotech, Hamburg, Germany
Human IL-15	Peprotech, Hamburg, Germany
Human IL-2 (Proleukin S)	Novartis Pharma, Nuermberg, Germany
Human INF-γ (Immukin®)	Boehringer Ingelheim, Ingelheim, Germany
Human recombinant Her2/ERBB2 protein with hFc Tag	Sino Biological, Beijing, China
Isoflurane	TEVA, Tel Aviv-Jaffa, Israel
Linear polyethylenimine (PEI)	Sigma-Aldrich, St. Louis, MO, USA
MEM non-essential aminoacids	Gibco, Waltham, MA, USA
Milk powder (blotting grade)	Carl Roth, Karlsruhe, Germany
N-2	Gibco, Waltham, MA, USA
N-Acety-L-cyteine	Sigma-Aldrich, St. Louis, MO, USA
NP-40 IGEPAL™ CA-630	Thermo Fisher Scientific, Waltham, MA, USA
P3 Primary Cell 4D-Nucleofector® Kit S	Lonza, Basel, Swizerland
PageRuler™ Prestained Protein Ladder	Thermo Fisher Scientific, Waltham, MA, USA
Penicillin-Streptavidin	Gibco, Waltham, MA, USA
peqGOLD total RNA isolation kit	VWR, Radnor, PA, USA
Pierce™ BCA protein assay kit	Thermo Fisher Scientific, Waltham, MA, USA
Pierce™ ECL blotting solution	Thermo Fisher Scientific, Waltham, MA, USA
Pierce™ Universal Nuclease	Thermo Fisher Scientific, Waltham, MA, USA
Polybrene	Sigma-Aldrich, St. Louis, MO, USA
RBC Lysis Buffer (10x)	BioLegend, San Diego, CA, USA
Recombinant Human TRAIL (TNFSF10) protein (carrier-free)	BioLegend, San Diego, CA, USA

RevertAid H Minus First Strand Kit	Thermo Fisher Scientific, Waltham, MA, USA
ROENTOROLL HC X-ray developer	TETENAL, Norderstedt, Germany
RPMI 1640 medium, GlutaMAX™ Supplement	Gibco, Waltham, MA, USA
Sodium pyruvate	Gibco, Waltham, MA, USA
Staurosporine	Alomone Labs, Jerusalem, Israel
STR multiplex PCR system Powerplex 16	Promega GmbH, Mannheim, Germany
SUPERFIX MRP X-ray fixer	TETENAL, Norderstedt, Germany
TEMED 99%	Carl Roth, Karlsruhe, Germany
Tris-HCl	Carl Roth, Karlsruhe, Germany
Triton X-100	Sigma-Aldrich, St. Louis, MO, USA
Trypan blue (0,4%)	Gibco, Waltham, MA, USA
TrypLE™ Select with phenolred	Gibco, Waltham, MA, USA
TrypZean solution	Sigma-Aldrich, St. Louis, MO, USA
Tween20	Carl Roth, Karlsruhe, Germany
X-Vivo10 medium	Lonza Group Ltd., Basel, Schweiz
Y-27632	R&D systems, Minneapolis, MN, USA
Zombie Violet Kit	Biolegend, San Diego, CA, USA

2.1.9 Media, Buffers and Gels

Table 8: Media.

Name	*Composition*
BM	DMEM/F12 + 10% FCS + 1% Pen-Strep
BM Washing Medium	DMEM/F12 + 1 mM HEPES + 1% Pen-Strep
BM1*	47,5 ml BM + 500 µl N-2 + 125 µl N-Acetylcysteine (500 mM), 500 µl non-essential amino acids + 5 µl sodium pyruvate (100 mM) + 5 µl hparine (5000 U/ml) + 500 µl hEGF (2 µg/ml) + 50 µl hFGF (40 µg/m) + 10 µl hIGF-I (100 µg/ml) + 5 µl Y-27632 (100 mM) + 50 µl A83-01 (5 mM)
DMEM+	DMEM (high glucose) + GlutaMAX™
DMEM+++	DMEM (high glucose) + GlutaMAX™ + 10% FCS + 1% Pen-Strep
RPMI+	RPMI 1640 + GlutaMAX™
RPMI++	RPMI 1640 + GlutaMAX™ + 10% FCS
X-Vivo+	X-Vivo 10 + 5% FFP(AB)
X-Vivo++	X-Vivo 10 + 5% FFP(AB) + 100 IU/ml IL-2

Table 9: Cell lysis buffer.

Component	*Volume*
RIPA buffer	904 µl
10 % (w/v) SDS	10 µl
100 mM Sodium orthovanadate	10 µl
500 mM Sodium fluoride	10 µl
100 mM β-Glycerophosphate	10 µl
100 mM PMSF	5 µl
Protease inhibitor cocktail (1 tablet per 2ml)	50 µl
Nuclease	1 µl

Table 10: RIPA buffer.

Component	*Volume*
1 M Tris-HCl	2.5 ml
20 % (w/v) NP-40	2.5 ml
5 % (w/v) Natriumdodecyl detergent	5.0 ml
5 M NaCl	1.5 ml
1 M $MgCl_2$	0.1 ml
ddH_2O	38.4 ml

Table 11: SDS-Loading buffer.

Component	*Concentration*
Tris-HCl pH 6.8	350 mM
Glycerine	38 %
SDS	0.1 %
DTT	0.093 %
Bromphenole blue	0.12 %
ddH_2O	fill to 100 %

Table 12:SDS-Gels.

Component	*Volume*
10% Separating gel	
ddH_2O	4.0 ml
30 % (v/v) Acrylamide	3.3 ml
1.5 M Tris-HCl pH 8.8	2.5 ml
10 % (w/v) SDS	0.1 ml
10 % (w/v) Ammoniumpersulfate	0.1 ml
TEMED	6 µl
5% Collecting gel	
ddH_2O	1.4 ml
30 % (v/v) Acrylamide	0.33 ml
1.5 M Tris-HCl pH 8.8	0.25 ml
10 % (w/v) SDS	20 µl
10 % (w/v) Ammoniumpersulfate	20 µl
TEMED	3 µl

2.1.10 Consumables

Table 13: Consumables.

Consumable	*Supplier*
6-well plate	Corning Inc., New York, NY, USA
12-well plate	Corning Inc., New York, NY, USA
24-well plate	Corning Inc., New York, NY, USA
48-well plate	Corning Inc., New York, NY, USA
96-well plate, flat bottom	Corning Inc., New York, NY, USA
96-well, flat bottom, white	BRAND GmbH & Co.KG, Wertheim, Germany
96-well plate, round bottom	Corning Inc., New York, NY, USA
96-well, round bottom, ultralow attachment	Corning Inc., New York, NY, USA
T25 cell culture flask	Greiner Bio-One, Nürtingen, Germany
T75 cell culture flask	Greiner Bio-One, Nürtingen, Germany
T75 cell culture flask	Corning Inc., New York, NY, USA
T175 cell culture flask	Greiner Bio-One, Nürtingen, Germany
15 ml tube	Corning Inc., New York, NY, USA

50 ml tube	Corning Inc., New York, NY, USA
Petri Dish, 10 cm	Corning Inc., New York, NY, USA
Cryovial, 2 ml	Corning Inc., New York, NY, USA
Round bottom tube, 5 ml	Corning Inc., New York, NY, USA
Round bottom tube, 14 ml	Corning Inc., New York, NY, USA
Pipette tips (10µ-1000 µl)l	Biozym Scientific GmbH, Hessisch Oldendorf, Germany
Serological pipetts (5 ml-50 ml)	Corning Inc., New York, NY, USA
U-100 Syringe	BD Biosciences, San Jose, CA, USA
Nitrocellulose Membrane Protran™ 0.2 µm	Amersham, Amersham, UK
X ray film Super RX-N 18x24	Fuji Medical, Minato, Japan
Microscopy slides	Engelbrecht Medizin- & Labortechnik, Edermünde, Germany

2.1.11 Instruments & Devices

Table 14: Instruments and devices.

Instrument/ Device	*Supplier*
Freezing container "Mr. Frosty"	Thermo Fisher Scientific, Waltham, MA, USA
Bioluminscence imaging Instument IVIS Lumina II	PerkinElmer, Waltham, MA, USA
Liquid nitrogen storage tank Biosafe MD	Cryotherm GmbH & Co. KG, Kirchen, Germany
Flow cytometers	
FACS Canto 10c	BD Biosciences, San Jose, CA, USA
FACS Celestar	BD Biosciences, San Jose, CA, USA
Incubators	
BBD 6220	Hereaus, Hanau, Germany
HeraCell 150i	Thermo Fisher Scientific, Waltham, MA, USA
Centrifuges	
Multifuge 3 S-R	Hereaus, Hanau, Germany
Multifuge X3	Hereaus, Hanau, Germany
Rotina 46R	Andreas Hettrich GmbH & Co. KG, Tuttlingen, Germany
Sterile work benches	
HERASafe	Heraeus, Hanau, Germany
Safe 2020	Thermo Fisher Scientific, Waltham, MA, USA

Pipets	
Pipet	Eppendorf SE, Hamburg, Germany
Pipet	Starlab, Hamburg, Germany
Pipet aid	INTEGRA Biosciences GmbH, Biebertal, Germany
Plate Reader	
Victor 3	PerkinElmer, Waaltham, MA, USA
GloMAX Multi+	Promega GmbH, Walldorf, Germany
Microscopes	
Celigo cell cytometer	Nexcelom, Lwarence, MA, USA
ECLIPSE Ts2	Nikon, Minato, Japan
BZ-X810 All-in-One Fluorescence microscope	Keyence, Osaka, Japan
IncuCyte SX5	Sartorius AG, Göttingen, Germany
Nucleofection	
4D-Nucleofecor® CoreUnit	Lonza, Basel, Swizerland
4D-Nucleofecor® X Unit	Lonza, Basel, Swizerland
SDS-PAGE & Western blot	
Mini-Protean® Tetra Cell	Bio-Rad Laboratories, Inc., Hercules, CA, USA
PowerPac HC	Bio-Rad Laboratories, Inc., Hercules, CA, USA
Trans-Blot SD Semi-Dry-Transfer-Cell	Bio-Rad Laboratories, Inc., Hercules, CA, USA
7900GR Fast Real-time PCR system	Applied Biosystems, Darmstadt, Germany

Software

Table 15:Software.

Software	*Supplier*
Living Image (Version 4.5.4)	Perkin Elmer, Waltham, MA, USA
FlowJo (Version 10.8.1)	BD Biosciences, San Jose, CA, USA
BD FACSDiva (Version 8.0.2)	BD Biosciences, San Jose, CA, USA
Microsoft Office 2016	Microsoft Corporation, Redmond, WA, USA
GraphPad Prism (Version 9)	GraphPad Software Inc.
Fiji (Version 2.3.0)	[168]
IncuCyte202B Analysis Software	Sartorius AG, Göttingen, Germany

2.2 Methods

2.2.1 RMS cells

2.2.1.1 RH30 and RH41

Alveolar RMS cell lines RH30 and RH41 were stored in 1 ml aliquots in the vapour phase of liquid nitrogen. To be used in experiments, cell vials were thawed rapidly by gentle swirling in a water bath at 37°C. The DMSO-containing freezing medium was removed by gentle centrifugation at 300xg and cells were then seeded into a flask containing RPMI++. Cells were grown at 37°C in a 5% CO_2 atmosphere to 70-80% confluence.

The medium was removed and the cell layer was washed with Dulbecco´s phosphate buffered saline without calcium and magnesium (DPBS). Then, 1 ml or 2 ml of TrypZean was added and the cell flask was incubated for several minutes at room temperature until cells became detached. Detachment was observed under a microscope and the enzymatic reaction was then stopped by adding 3 to 8 ml of pre-warmed RPMI++ medium. Cell aggregates were dissolved and 7 to 18 ml of fresh pre-warmed RPMI++ were added to 1/20 to 1/10 of cell suspension. Cells were cultured at 37°C in 5% CO_2 and were splitted three times a week, up to passage 30.

For long-term storage the cells were harvested, counted and subsequently centrifuged at 300xg. Cells were resuspended in freezing medium (RPMI++ with 10%DMSO) to a final concentration of 1-3x10^6 cells per millilitre. Cell suspension was aliquoted into in cryovials with 1 ml per vial and the vials were placed in a Mr. Frosty container and subsequently stored in a -80°C freezer. After a minimum of 24 hours, the cryovials were transferred to the liquid phase of a nitrogen tank.

2.2.1.2 Patient-derived RMS tumor organoids

Patient-derived RMS tumor organoids were stored in the vapor phase of liquid nitrogen. The cryovial was thawed in a 37°C warm water bad under gentle swirling. After thawing, the cell suspension was transferred to a tube containing 9 ml BM washing medium and the tube was centrifuged at 300xg. Cell pellets were resuspended in BM1* medium and cell suspensions were seeded into a cell culture flask precoated with BME. Having reached 70-80% of confluence, the medium was removed and the cell monolayer was washed with pre-warmed DPBS. Then 1-2 ml of TrypLE Select was added and the flask was incubated for several minutes until cells became detached. Complete detachment was verified under the microscope. The enzymatic reaction was stopped by adding 4 - 8 ml BM1*. Then 6 - 12 ml BM1* supplemented with 0,1% BME was added to 1/10 – 1/5 of the suspension. Cells were splitted 1 - 2 times a week once reaching 70-80% of confluence. For long-term storage, cells were cryopreserved in BM1* with 40% FCS and 20% DMSO at a density of 1 - 3x10^6 cells per vial. Cells were immediately

placed in a Mr. Frosty container and stored in a -80°C freezer for at least 24h. Thereafter cryovials were stored in the vapor phase of liquid nitrogen.

Table 16 shows an overview of the RMS cell lines and patient-derived RMS tumor oganoids used in this thesis, including origin, clinical information and fusion state.

Table 16: Overwiev of RMS cells used in this thesis. Adapted from [169].

Cell line/ Tumor organoid	***Origin***	***Disease instance of establishment***	***Histology***	***Karyotype/ gene fusion state***	***Reference***
RH30	Bone marrow metastasis of a 16-year-old male	Untreated primary disease	Alveolar	t(2;13) (*PAX3-FOXO1*), *TP53* mutation, amplification of 12q13–15 region including CDK4	[170]
RH41	Lung metastasis of a 7-year old female (xenograft)	Post-chemotherapy (progressive disease)	Alveolar	t(2;13) (*PAX3-FOXO1*), *TP53* mutation	[170]
RMS102	Lymph node metastasis (clavicle) of a 18-year-old male	Second relapse after vincristine, irinotecan, temozolomide treatment and radiotherapy (RT)	Alveolar	t(2;13) (*PAX3-FOXO1*)	[171]
RMS335	Lymph node metastasis (groin) of a 8-year-old female	Second relapse after vincristine, irinotecan, temozolomide treatment	Alveolar	t(1;13) (*PAX7-FOXO1*)	[171]

RMS127	Bone marrow metastasis of a 16-year-old male	Untreated primary disease	Alveolar	t(2;13) (*PAX3-FOXO1*)	[171]

2.2.1.3 ErbB2 surface expression of RMS cells

Since ErbB2 is the target for the CAR construct, the target cells were analyzed for their ErbB2 surface expression by flow cytometry. $5x10^5$ cells were washed in 1 ml DPBS in FACS tubes and were incubated with 5 µl anti-ErbB2 or mouse IgG1, κ isotype antibody conjugated to PE for 20 minutes at 4°C. After a thorough washing in DPBS, the cells were resuspended in 200 µl DPBS and the samples were analyzed using a BD Canto 10c instrument with BD Diva Software. Additionally, the ErbB2 receptor number per cell was determined using the BD Quantibrite Kit according to the manufacturer´s instructions.

2.2.1.4 Lentiviral transduction

Target cells expressing fluorescent proteins such as GFP or luminescent proteins namely firefly (*Photinus pyralis*) luciferase (FLuc) can be used as a readout for viable tumor cells allowing for discrimination of non-fluorescent, inactive effector cells. Furthermore, in *in vivo* experiments tumor growth was monitored by (non-invasive) bioluminescence imaging using the FLuc signal of tumor cells. Genetic modification with GFP and FLuc can be achieved by lentiviral transduction: Viral particles containing the appropriate gene sequences are generated in HEK293T cells using a second-generation system, and these particles are then used to transduce RMS cells by spinfection.

2.2.1.4.1 Generation of lentiviral particles

$4x10^6$ HEK239T/17 cells were seeded into 10cm petri dishes in DMEM+++ culture medium. 24 hours later, cells were washed twice with DPBS and maintained in DMEM+ for another 2 hours. 240 µl DPBS was mixed with 10 µg pSL2GW (transfer plasmid), 3.5 µg pMD2.G (encoding) and 6.5 µg pΔ9.8.1 (encoding gag-pol). All plasmid stocks were concentrated to 1 µg/ µl. In a second tube, 2.7 µl polyethylenimine (PEI) per µg DNA (= 54 µl) was added to 240 µl DPBS. Mixtures from both tubes were combined and incubated for 15 minutes at room temperature. The PEI-Plasmid mixture was then added dropwise to the HEK293T/17 cells while the plate was agitated continuously. After four hours, the medium was changed to DMEM+++ and the cells were incubated for four days. Lentivirus particles

were harvested by filtering supernatants through a 2µm filter. Virus particles were aliquoted and stored at -80°C.

2.2.1.4.2 Transduction of RMS cells

In addition to the aRMS cell line RH41, patient-derived aRMS tumor organoids RMS102, RMS127 and RMS335 were lentivirally transduced with GFP/FLuc genes. For this purpose, $3x10^5$ RMS cells were seeded in a 6-well plate and grown in appropriate media. 24 hours later, the medium was replaced with 2.68 ml RPMI+ or BM1* without BME, 300 µl pSL2GW virus and 24 µl (= 8 µg/ml) polybrene were added. After spinfection at 800xg for 60 minutes at 34°C, cells were incubated overnight. The medium was changed to growth medium and the cells were then cultivated and transferred to larger culture vessels if necessary. Five days after transduction, cells were examined for GFP expression using a Keyence BZ800 microscope. Ten days after transduction, the percentage of GFP-expressing cells in the population was quantified by flow cytometry. Percentage of >96% GFP-expression was achieved and stable over 12 days, therefore sorting was not necessary.

2.2.1.4.3 S1 classification of transduced RMS cells

For a transfer from S2 to S1 safety class, the supernatant of the transduced cells was added to HEK293T/17 cells seeded in 24-well plates at 25,000 cells per well. After two days of incubation, HEK293T/17 cells were harvested and analyzed for GFP expression using flow cytometry as a readout for viral particles in the supernatant. Untreated cells served as reference. When no GFP expression was detected in HEK293T/17 cells co-incubated with the supernatant of transduced RMS cells, the RMS cells were considered as S1.

2.2.2 Functional analysis

The cytotoxic capacity of effector cells against RMS cell lines or primary RMS models was evaluated in functional cytotoxicity assays. In this study, an europium release assay (ERA) and a luciferase based toxicity assay (Luc Tox) were used. The ERA was used in case of wild-type and primary cells. The Luc Tox assay depends on the modification of the target cells with the luciferase gene. The ERA is time-consuming and labour-intensive, whereas the Luc Tox assay is easy to perform and can be considered an 2D *in vitro* counterpart to *in vivo* bioluminescence imaging.

2.2.2.1 Europium Release Assay (ERA)

For the europium release assay (ERA), 1 -2x10^6 RMS cells were incubated in 1 ml of medium containing 5 µl of the fluorescence enhancing ligand Bis(acetomethyl)2,2'':6',2''-terpyridine-6,6''-dicarboxylate (BATDA) for 30 minutes at 37°C. BATDA-loaded cells were washed four times with X-Vivo10 medium containing probenecid as spontaneous release inhibitor. After an additional washing step in X-Vivo++ without probenecid, cells were adjusted to a density of 5x10^4 cells/ml. Supernatants from this last washing step were used as background measurements. 100 µl of the supernatants and 100 µl of fresh medium were transferred as triplicates into three wells onto a 96-well U-bottom plate. The remaining wells were filled with 100 µl medium and 100 µl of target and NK-92/5.28.z cells at effector to target (E:T) ratios ranging from 20:1 to 1.25:1. As controls for either maximal or spontaneous lysis, Triton-X100 and medium were added to target cells. Analyses were performed as triplicates. Culture plates were centrifuged for 3 minutes at 100xg with deceleration set to 0xg and then incubated for three hours at 37°C in a 5% CO_2 atmosphere. Plates were centrifuged again, 20 µl of supernatants were transferred to a 96-well flat bottom plate. 200 µl of Europium solution was added. Plates were covered with aluminium foil, incubated for 15 minutes at room temperature on a shaker. The europium signal was measured using a Victor 3 fluorescence reader. Spontaneous and specific lysis were calculated according to the following formulas:

$$Spontanous\ lysis\ [\%] = \frac{Spontaneous\ release\ (counts) - Background\ (counts)}{Maximum\ release\ (counts) - Background\ (counts)}\ x\ 100\%$$

$$Specific\ lysis\ [\%] = \frac{Experimental\ release\ (counts) - Spontaneous\ release\ (counts)}{Maximum\ release\ (counts) - Spontaneous\ release\ (counts)}\ x\ 100\%$$

2.2.2.2 Luciferase based Cytotoxicity Assay (Luc Tox)

RMS cells stably expressing FLuc were used; the intensity of the luciferase signal correlates with the cell number [172] and is used as readout parameter for this toxicity assay . 5000 or 7500 RMS cells per well were seeded onto a white 96-well flat bottom plate. After adherence of targets cells, the medium was removed and replaced by 100 µl of effector cell suspensions at E:T ratios ranging from 40:1 to 1.25:1. Controls for maximal target cell lysis were obtained after adding 100 µl of 10% Triton X-100 solution. Untreated cells maintained in 100 µl of effector cell medium were used as reference. Analyses were performed in triplicates. Cells were co-incubated for three to 24 hours. 20 µl of a 3 mM D-luciferin solution was added per well. After another 15 minutes of incubation at 37°C, the luminescence signal of the plate was analyzed by a GloMAX Multi+ instrument with an integration time of 1s/well. The specific lysis was calculated using the following formula:

$$Specific\ lysis\ [\%] = 100\% - \frac{Experimental\ signal\ (counts)}{Untreated\ cell\ signal\ (counts)}\ x\ 100\%$$

2.2.2.3 3D Spheroid Assay

5x10^3 RMS cells stably transfected with GFP were seeded in ultra-low attachment 96-well round bottom plates in 200 µl of medium. After centrifugation at 1000xg for 10 minutes, cells were incubated at 37°C for four days 100 µl of medium was removed and 100 µl of either 2x10^5 NK-92 or NK-92/5.28.z cells were added. An untreated control was included in the experiment by adding 100 µl effector cell medium without cells. The size and green fluorescent signal of the spheroids was determined via bright field and fluorescence imaging using a Co-cultures were recorded by a Celigo cell cytometer in bright field and green fluorescence channel. Obtained images were analyzed for particle size in the GFP channel using Fiji software [168].

2.2.3 NK-92/5.28.z as innate CAR-cell line for RMS treatment

2.2.3.1 NK-92 cultivation

NK-92 cells were stored in 1 ml aliquots in the vapor phase of liquid nitrogen. To be used in experiments, the cryovial was rapidly thawed in a water bath at 37°C while being gentle swirled. After thawing, the cell suspension was immediately transferred to a tube containing 9 ml of X-Vivo++ medium and DMSO was washed out by centrifugation at 300xg. Cells were seeded in a T75 cell culture flask at a density of 4x10^5 cells per millilitre and cultured in X-Vivo++ at 37°C in 5% CO_2. After 2 days, 10 ml of fresh medium was added. Another 2 days later, cells were adjusted to a density of 3x10^5 cells per millilitre in fresh X-Vivo10++ medium. Every 5-6 days, cell density was readjusted.

For cryopreservation, cells were counted, pelleted at cell densities of 0.5 – 2x10^6 cells per millilitre in X-Vivo++ containing 10% FCS. Cell suspensions were aliquoted into cryovials and immediately placed in a Mr. Frosty container. Having remained for a minimum of 24 hours in a -80°C freezer, cell vials were transferred to the vapor phase of liquid nitrogen.

NK-92/5.28.z cells were treated accordingly.

2.2.3.2 Verification of CAR expression

The ErbB2-CAR surface expression of the NK-92/5.28.z cells was assessed by flow cytometry. 2x10^6 either NK-92/5.28.z or NK-92 cells were washed once with DPBS in 5 ml FACS tubes. To avoid non-

specific binding, the cells were incubated with Human TruStain FcX™ (Fc Receptor Blocking Solution) for 20 minutes at 4°C. After another washing step in DPBS, the cells were incubated with 10 µg recombinant ErbB2 with human Fc tag for 20 minutes at 4°C. After two additional washing steps, cells were stained with APC antibody directed against the Fc tag. Cells were washed again and resuspended in 300 µl DPBS and analyzed by a BD FACS Canto 10c instrument.

2.2.3.3 Irradiation of NK-92/28.z

Due to their malignant origin NK-92/5.28.z have to be γ-irradiated with 10 Gy prior to clinical use in patients. NK-92/5.28.z cells were irradiated with 10 Gy using a BioBeam Cs^{137} irradiator. Thereafter, the proliferative and cytotoxic capacity of NK-92/5.28.z was assessed against RMS tumors *in vitro*. After a washing step in DPBS, irradiated NK-92/5.28.z cells were resuspended in fresh X-Vivo10 medium supplemented with 5% fresh frozen plasma (FFP) and 100 U/ml IL-2 at a density of $5x10^4$ cells/ml. One, two and three days after irradiation, cell counts were determined and compared to non-irradiated controls. In parallel, the cytotoxic activity of irradiated NK-92/5.28.z cells against RH30 cells was evaluated by Luc Tox assay. Non-irradiated NK-92/5.28.z cells were used as controls.

2.2.3.4 In vivo experiment

In vivo experiments were approved by the governmental committee (Regierungspräsidium Darmstadt, Darmstadt, Germany; Gen.-Nr. TVA FK/1070) and were conducted according to the requirements of the German Animal Welfare Act.

2.2.3.4.1 Treatment

Ten to 12-week-old female non-obese diabetic (NOD)/severe combined immunodeficient (SCID)/Il2 receptor gamma−/− (NSG) mice were sublethally irradiated with 2.5 Gy (Biobeam 2000) (d-1). 24 hours later (d0), $1x10^5$ RH30GFP/luc+ cells resuspended in 100 µl DPBS were intravenously (iv) infused via the tail vein, mimicking minimal residual disease (MRD) status in patients. The cytotoxic capacity of parental NK-92 cells and NK-92/5.28.z cells was assessed by randomly allocating mice to three different groups: Controls injected with medium (X-Vivo+++, n=5), 12 animals injected with parental NK-92 cells ($10x10^6$ cells each, n=12), and 13 animals injected with NK-92/5.28.z cells ($10x10^6$ cells each, n=13). Effector cells were resuspended in X-Vivo+++ and applied six times over a period of four weeks (last injection d+35), starting at d+1.

On day +42, three animals of the NK-92/5.28.z cell treatment group with visible tumors received three additional doses of NK-92/5.28.z cell therapy. Here, doses of $10x10^6$ effector cells were injected weekly from day +42 to day +62.

Altogether, safety and efficacy of NK-92/5.28.z cell therapy was compared to parental NK-92 treatment and untreated controls as follows:

- Control: one course of six infusions of X-Vivo+++, n=5
- NK-92: $10x10^6$ cells, one course of six effector cell infusions, n=12
- NK-92/5.28.z: $10x10^6$ cells, one course of six effector cell infusions, n=10
- NK-92/5.28.z 2^{nd} course: $10x10^6$ cells, one course of six effector cell infusions followed by a second course of three effector cell infusions (2^{nd} course), (>d+42) therapy, n=3

Animals were monitored daily for signs of disease and adverse events until day +105 (end of the study). Mice showing signs of health problems or physical abnormalities were painlessly sacrificed by isoflurane inhalation followed by cervical dislocation. A schematic overview of the experimental setup is shown in Figure 7.

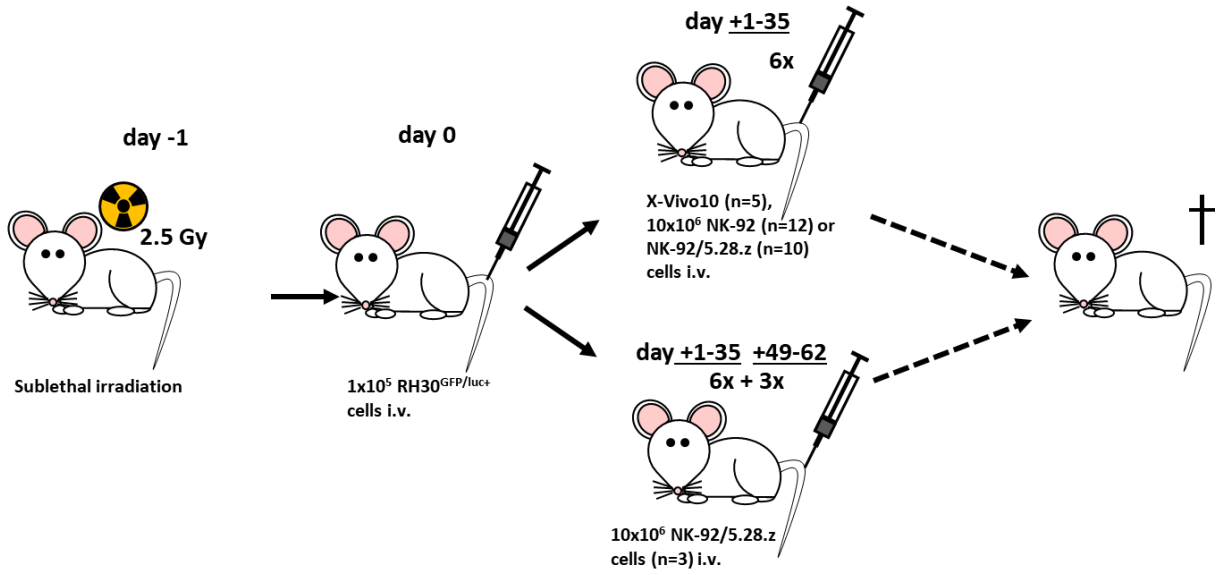

Figure 7: Experimental setup of the xenograft model. Four different treatment groups were used for the evaluation of NK-92/5.28.z cells. In addition to the comparison of NK-92 and untreated mice with one injection course, a fourth group was additionally injected with NK-92/5.28.z in a second course.

2.2.3.4.2 Bioluminescence imaging

Tumor engraftment and growth were monitored via bioluminescence imaging (BLI). Mice were anesthetised with isoflurane and injected with 150 µg *in vivo* grade VivoGlo luciferin resuspended in 100 µl DPBS subcutaneously. After 15 minutes, mice were transferred to the darkroom of an IVIS Lumina II imaging system; exposure times for images ranged between one second and three minutes.

During imaging, mice were kept anesthetised with isoflurane using an anaesthesia mask. After imaging, mice were placed back in their cages and observed until fully awake. Images were analyzed using LivingImage software. The total flux (photon/s) of uniform regions of interest (ROI) was assessed for all mice. Signals of both, the dorsal and ventral images were added to compute the luminoscore for each mouse.

2.2.3.4.3 Analysis of organs

Samples of the peripheral blood (PB), bone marrow (BM), lung, liver, intestine and spleen were assessed for tumor and effector cells. BM was flushed out of femura and tibiae of mice. PB and BM were incubated with red blood cell lysis buffer according to the manufacturer's instructions and washed once with DPBS. Liver, lung and spleen were photographed for macroscopic analysis and spleen size was analyzed using Fiji software [168]. The organs were cut in half and one half was preserved in formaldehyde for subsequent fluorescence microscopy staining. The other half was incubated with Collagenase D solution, filtered through a 70 µm cell strainer, and washed with DPBS. Cell suspensions were analyzed by flow cytometry and quantitative polymerase chain reaction (qPCR).

2.2.3.4.3.1 Flow cytometry

5 µl of cell suspensions from mouse organs were placed in FACS tubes, washed once with DPBS and stained with APC/Cy7-conjugated anti-human CD45 antibody for 20 minutes. After an additional washing step, samples were analyzed using a BD Canto 10c instrument.

2.2.3.4.3.2 Quantitative Polymerase chain reaction (qPCR)

Genomic DNA was extracted from murine organ cell suspensions using the Extractme genomic DNA Kit. By using a real-time quantitative approach specifically amplifying the human albumin gene, the amount of human cells in general was quantified. In a second step, the proportions of NK-92 cells, NK-92/5.28.z cells and/or tumor cells were discriminated using a human-specific STR genotyping approach. The Powerplex 16 STR system was performed according to the manufacturers protocol. The biodistribution and tumor burden was assessed in liver, lung and bone marrow and for effector cell quantification, additionally the spleen as a secondary lymphatic organ was analyzed. Furthermore, NK-92/5.28.z cells were verified by qPCR targeting the CD8 hinge region of the CAR construct. qPCR experiments were performed by Hermann Kreyenberg.

2.2.3.4.3.3 Histology and fluorescence microscopy

Organs were fixed in 4 % buffered formalin immediately after isolation, paraffin-embedded, sliced, and stained with hematoxylin-eosin (HE). Diagnostic immunohistochemistry (IHC) for RMS markers CD56, MyoD1, Desmin and Myogenin was performed by Elise Gradhand. Stained tissue sections were rated by an experienced pathologist (-, negative; +, low grade; ++, intermediate grade; +++, high grade).

Immune cell infiltration in organs and tumors was analyzed by fluorescence immunohistology. These experiments were performed by Sabine Harenkamp. Organ sections were deparaffinized and rehydrated. After antigen retrieval and blocking, primary mouse anti-human CD45 antibody and rabbit anti-GFP antibody were added. Secondary antibodies F(ab`)$_2$ fragment goat-anti-mouse conjugated to Alexa647 and goat-anti-rabbit IgG Alexa488 were used. In addition, nuclei were stained with 4´,6-diamidino-2-phenylindol (DAPI).The exact localisation of immune cells within the tumor tissue with respect to blood vessels was assessed by staining with rat-anti-mouse Meca32 antibody and a secondary anti-rat Alexa546 antibody. The specimens were mounted on and examined using a Keyence BZ-X800 microscope.

2.2.3.5 Combination therapy approaches

Targeting molecules on the tumor cell surface, e.g. PD-L1 inhibition may be used to increase cytotoxic capacity of CAR cell approaches. In addition, cancer cells may be sensitized towards CAR cell-mediated killing by a combinatorial treatment with anticancer therapies.

2.2.3.5.1 PD-1 immune checkpoint blockade

2.2.3.5.1.1 PD-L1 surface expression on aRMS cells

PD-L1 surface expression on RH30, RH41, RMS102, RMS127 and RMS335 was analyzed by flow cytometry. For this purpose, 1x10^5 cells of each cell line were put into two FACS tubes and washed once with DPBS. One tube was stained with anti-PD-L1 antibody conjugated to PE and the other tube was stained with the corresponding isotype. After 20 minutes of incubation, the samples were washed again with DPBS and were subsequently analyzed using a BD Canto 10c instrument.

2.2.3.5.1.2 PD-1 and NK-92/5.28.z combinatorial treatment

NK-92/5.28.z cells were incubated for 30 minutes with 10 µg anti-PD-1 antibody before being assessed against RH30 cells by ERA. NK-92/5.28.z cells without checkpoint inhibition were used as control. Co-culture analyses were performed for a period of three hours.

2.2.3.5.2 Bortezomib

This subproject was mainly carried out by Leonie Hartig as her master thesis project under my supervision. Western blot and qPCR analyses were performed by Nadine Weinelt.

2.2.3.5.2.1 EC_{50} value evaluation

A modified Luc Tox assay was used to determine the EC_{50} values of RH30, RH41 and RMS335 with respect to bortezomib. 5000 target cells were used within dilution series with bortezomib (concentrations ranging from 0 to 1 mM). D-luciferin was added to a final concentration of 0.5 mM per after seven hours and readouts were performed after 7, 24 and 48 hours as described above.

2.2.3.5.2.2 DR4 and DR5 surface expression after bortezomib treatment

Upregulation of DR4 and DR5 on the surface of RH30, RH41 and RMS335 cells upon treatment with bortezomib ranging from 0 to 50nM was expected. The cells were washed with DPBS and were stained with APC-conjugated DR4 antibody or PE-conjugated DR5 antibody. Cells stained with the corresponding isotypes were used as controls. After incubation cells were washed with DPBS and analyzed on a BD Canto 10c instrument.

2.2.3.5.2.3 Caspase activity

Upon bortezomib treatment of RMS cells caspase-3/-7 activity was quantified using CaspaseGlo®3/7 assay system. The assay was performed according to the manufacturer's instructions. RH30, RH41 and RMS335 cells were seeded in 6-well plates and treated with 0.5, 10 or 25 nM bortezomib. Cells treated with 1 µM staurosporine, a non-selective kinase inhibitor inducing apoptosis, were used as positive control. After 24 hours, $1x10^4$ cells were seeded in triplicates in a white 96 well plate and Caspase-Glo® 3/7 reagent was added 1:1. The plate was mixed gently, incubated for one hour and the luminescence signal was measured using a GloMAX Multi+ instrument.

2.2.3.5.2.4 Combination of NK-92/5.28.z and bortezomib

The Luc Tox assay was performed targeting RMS cell lines RH30 and RH41 with 0, 10, 25 or 50nM bortezomib for 24 hours. Patient-derived tumor organoid RMS335 was treated with 0, 5, 10 and 25nM bortezomib. $7.5x10^4$ of bortezomib-pre-treated cells were coincubated with NK-92/5.28.z cells at E:T ratios ranging from 1:1 to 20:1 on white 96-well plates for three hours. Untreated cells were used as controls.

2.2.3.5.2.5 qPCR

qPCR analysis was used to assess NFκB pathway in RH30 and RH41 cells. $5x10^5$ cells were coincubated with untreated cells, cells pre-treated with 10nM bortezomib, and NK-92/5.28.z cells with or without bortezomib pre-treatment of target cells at E-T ratios of 1:1. After 1 hour of coincubation, supernatants were removed and the adherent RMS cells were washed twice with DPBS. DPBS was carefully removed and the plate was immediately frozen at -80°C. RNA from all samples was isolated using the peqGOLD Total RNA isolation kit according to manufacturer's instructions. Cells were lysed with RNA lysis buffer and transferred to peqGOLD RNA Homogenizer columns. After centrifugation at 13,000xg for one minute, 70% ethanol was added to the flow through and the mixture was loaded onto a peqGOLD RNA Mini Column. Centrifugation at 10,000xg for one minute was followed by a washing step with RNA Wash buffer and two washing steps with 80% ethanol. The columns were dried by centrifugation at 12,000xg for two minutes and the RNA was eluted in nuclease-free water by centrifugation. For cDNA synthesis, 0.5 µg of RNA was used in the RevertAid H Minus First Strand Kit according to the manufacturer's instructions. Gene expression levels of p100, p65, JNK and BCL-XL were analyzed by SYBR green-based quantitative real-time PCR using the 7900GR Fast Real-time PCR system. Target gene expression data were normalized to 18S-rRNA and RPII expression, and relative gene expression levels were calculated using the ΔΔCt method.

2.2.3.5.2.6 Western blot analysis

The effect of bortezomib treatment on selected signaling pathways in RMS cells was analyzed by western blot. Briefly, $5x10^5$ RH30 or RH41 cells were seeded in 6-well plates and treated with 0, 5, 10 or 25 nM bortezomib for 24 hours. Cells were then detached with TrypZean, washed in DPBS and seeded in 6-well plates at a density of $5x10^5$ cells per well. Next, NK-92/5.28.z cells were added in a 1:1 ratio to with or without bortezomib pre-treatment of RMS. After 2 hours incubation, RMS cells were washed thoroughly to remove residual NK-92/5.28.z cells. Then RMS cells were detached and washed again with DPBS. Cell pellets were stored at -80°C until used in further experiments. Having obtained

a sufficient samples size, cell pellets were resuspended in 50 µl lysis buffer and incubated for 30 minutes on ice. Cell debris was removed by centrifugation at 18000xg, supernatants were transferred to a new tube. The protein concentration within the samples was quantified by the Pierce™ BCA Protein Assay Kit. Protein concentration was adjusted to 4.16 µg/µl with sodium dodecylsulfate polyacrylamide gel electrophoresis (SDS-PAGE) loading buffer to a total volume of 20 µl. Samples were then boiled at 92°C for 10 minutes. 10 % SDS-PAGE gels were prepared, 12 µl of each sample (= 50 µg proteins) were loaded and 4 µl of PageRuler was used as ladder. After separation with 120 V, the proteins were transferred to a nitrocellulose membrane using a Trans-Blot SD device at 180 mA for 105 minutes. After blocking, the membrane was washed three times with DPBS-T and cut into sections. Sections were incubated with appropriate antibodies for 24 hours at 4°C. After three washing steps with DPBS-T, the secondary antibody conjugated to horseradish peroxidase (HRP) diluted 1:10,000 in blocking buffer was added and incubated for one hour. After three washing steps with DPBS-T, the membranes were wet with chemiluminescent HRP substrate and exposed to an X-ray film. After an incubation time of 5s to 60 minutes, depending on the signal intensity, the film was developed and scanned for analysis.

2.2.3.5.2.7 Bortezomib and TRAIL co-treatment

To determine synergistic or additive effects between bortezomib- and TRAIL-mediated killing, a Luc Tox assay was performed with RH30 and RH41 cells treated with 0, 5, 10, 25 nM bortezomib and 0, 25, 50, 100 or 200 ng/ml purified TRAIL protein for 16 hours. Untreated target cells were used as controls. Data were modelled with by Zero Interaction Potency (ZIP) model [173] to evaluate of synergistic or additive effect.

2.2.4 Non-viral generation of CAR-CIK cells with *Sleeping beauty transposon system*

2.2.4.1 CIK generation

PBMCs of healthy volunteer donors were isolated from buffy coat or peripheral blood. Starting material was diluted with at least twice the volume of DPBS and then carefully layered on top of 15 ml Histopaque-1077 solution in a 50 ml tube. After centrifugation at 800xg for 20 minutes without deceleration, the layer containing the immune cells was transferred to a new tube. Cells were washed twice in 50 ml DPBS. The cells were then resuspended in RPMI++, counted and seeded in a cell culture flask at a density of $3x10^6$ cells per millilitre. For monocyte stimulation, 1000 U/ml INF-γ was added. After 24h, 500 U/ml IL-2 and 100 ng/ µl soluble anti-CD3 (OKT3) were added for stimulation. On day three, cells were counted and adjusted to a density of $1x10^6$ per millilitre in RPMI+ containing 50 ng/ml

IL-15. Every three to four days the cell count was adjusted to a density of $1x10^6$ cells per millilitre and cells were restimulated with RPMI++ containing 50 ng IL-15 per millilitre.

2.2.4.2 Phenotyping

CIK cell subpopulations were characterized by FACS staining on day zero and day 10 of culture. For this, 100 µl of cell were transferred to FACS tubes, cells were washed with DPBS and antibodies were added. For T cell subtypes, antibodies against CD3 (conjugated to PerCP), CD4 (PE-Cy7) and CD8 (APC) were used and for T-NK and NK phenotyping, antibodies against CD3 (PerCP) and CD56 (PE-Cy7) were used. After 20 minutes of incubation at 4°C, cells were washed again and then analyzed using a BD Canto 10c instrument.

2.2.4.3 Nucleofection protocol using MC Venus

As a first step, minicircle (MC) Venus, a minicircle construct encoding eGFP, was used for transfection.. Unless otherwise stated, all experiments were then performed according to the following protocol: CIK nucleofection was performed using P3 Primary Cell 4D-Nucleofector™ X Kit S and 4D-Nucleofector™ X Unit. In general, $2x10^6$ cells were washed with DPBS, resuspended in 20 µl P3 solution (room temperature), MC DNA and SB100x mRNA were added and immediately pulsed in the 4D-Nucleofector™ using the T cell program EO-115. 80 µl of the medium RPMMI++ was added. Strips were incubated at 37°C for 20 minutes to allow for cell recovery. The cells were then transferred to 48-well plates with 400 µl of prewarmed RPMI++ medium, resulting in a final volume of 500 µl per well. After a recovery phase of at least two hours, cytokines were added according to the CIK cell protocol. Non-nucleofected Cells were used as control. Cells were counted every three to four days and diluted to $1x10^6$ cells per millilitre. GFP expression and viability were quantified by flow cytometry. 100 µl cell suspension were transfered to a FACS tube. After washing with DPBS, cells were incubated with 100 µl of Zombie Violet® diluted 1:500 in DPBS for 15 minutes. After an additional washing step, flow cytometry analysis was performed using a BD Canto 10c instrument. On day 10, CIK phenotype was additionally analyzed as described above. Where indicated, cells were used in Luc Tox assays on day 10 of CIK cell culture.

2.2.4.3.1 Proof of principle

First the stable integration of the CAR sequence into the CIK cell genome was assessed. CIK cells were transfected with 4 µg SB100x mRNA and 1 µg MC Venus (4:1 ratio) or with 1 µg MC Venus only on day four of CIK cell culture. GFP expression was quantified on days three, seven, 10 and 15 after nucleofection.

2.2.4.3.2 Timing

For T cells it is known that activated cells are transfected more efficiently than resting cells [174, 175], for CIK cells no optimal time point for transfection has been reported. Therefore, three different time points were investigated: day zero (non-activated cells), day three (activated cells) and day seven (activated cells + IL-15 stimulation). Cells were transfected with 4 µg SB100x mRNA and 1 µg MC Venus.

2.2.4.3.3 Autologous feeder Monocytes

The differentiation of PBMCs into CIK cells depends on signals from activated monocytes. Since monocytes may not survive nucleofection in sufficient numbers, autologous monocytes were isolated prior to nucleofection and added after nucleofection. Nucleofection was performed on day four of CIK culture and SB100x mRNA and MC Venus were added at a 4:1 ratio. For monocyte isolation, the plastic adherence of these cells was used and the adhered cells were scrapped, counted and added to the suspension cells in a 1:10 ratio after nucleofection. GFP expression and viability were analyzed at three, seven and 10 days after nucleofection.

2.2.4.4 Nucleofection protocol using ErbB2-CAR-Minicircle

2.2.4.4.1 Minicircle generation

After the initial steps of CIK nucleofection with MC Venus and SB100x mRNA, the next step was to produce a MC carrying the CAR construct. Due to its smaller size, the MC is less cytotoxic for the immune cells with positive effects seen in terms of cell viability and CAR expression [154]. Since the ITRs are the recognition region for the SB transposase, a plasmid carrying the CAR construct flanked by ITR sequences was manufactured. The 5.28.z sequence was cloned into the pT2 plasmid carrying the ITRs by Malena Bodden. Before the MC was generated by PlasmidFactory, a nucleofection experiment was performed to verify the stable integration of the CAR sequence into the CIK cell genome. CIK cells were nucleofected on day zero using 1 µg pT2-5.28.z plasmid and 4 µg SB100x mRNA. Stable GFP expression was monitored until day 21. The following experiments were performed with manufactured MC ErbB2-CAR.

2.2.4.4.2 GFP expression and CAR expression

A GFP signal peptide was integrated into the MC ErbB2-CAR construct. This can be used to quantify CAR-expression on the cells. Therefore it is of importance that the GFP signal corresponds to the CAR expression. The ErbB2-CAR expression of CAR-CIK cells was determined by flow cytometry. $2x10^6$ cells were washed with DPBS. CIK cells were used as control. To avoid non-specific binding, cells were

incubated with Human TruStain FcX™ (Fc Receptor Blocking Solution) for 20 minutes at 4°C. After washing with DPBS, the cells were incubated with 10 µg of recombinant ErbB2 with human Fc Tag for 20 minutes at 4°C. After two additional washing steps, an APC-conjugated antibody directed against the Fc Tag was added. Cells were washed again and resuspended in 300 µl DPBS for analysis by a BD FACS Canto 10c instrument.

2.2.4.4.3 Time point

An additional series of experiments was performed to determine the optimal time point for nucleofection. Cells were nucleofected with SB100x mRNA and the MC ErbB2-CAR at a 4:1 ratio on day 0, 4 or 7. GFP and therefore CAR expression was analyzed on day 7, 10 and 14.

2.2.4.4.4 Autologous feeder PBMCs

The use of autologous feeder PMBCs to support CAR-CIK cell manufacturing was considered, as previously reported [112]. PBMCs were γ-irradiated with 30 Gy using a ^{137}Cs source. Cells were then washed once in DPBS and added to the nucleofected CIK cells in a 1:10 ratio on day 0. GFP expression was analyzed on day 7, 10 and 14 after nucleofection.

2.2.4.4.5 Medium

The CIK phenotype is characterized by a high percentage of T-NK cells. Therefore, a NK cell culture medium was considered to support cell expansion following nucleofection. Cells were nucleofected with 4 µg SB100x mRNA and 1 µg MC ErbB2-CAR on day 0 and subsequently incubated in RPMI++ or X-Vivo+ medium. Cells were stimulated according to the CIK cell protocol and GFP expression and viability were assessed on days 7, 10 and 14 after nucleofection.

2.2.4.4.6 MC:SB ratio

Next, the ideal amount of DNA that led to high CAR expression and sufficient cell viability was assessed. A ratio of 4:1 was reported to be best for T cell transfection [154]. CIK cells were nucleofected on day 0 with SB100x mRNA and MC ErbB2-CAR at 4:1 or 4:2 ratios and subsequently cultured in X-Vivo 10+ medium. GFP expression and viability were determined on day 7, 10 and 14. In addition, Luc Tox assays were performed on day 10.

2.2.4.5 Viral vs SB100x CAR-CIK cells

As a final step, CAR-CIK cells generated by SBTS were compared to conventionally virally transduced (LV) CAR-CIK cells. For this comparison, CIK cells from the same donors were virally transduced and in parallel modified by SBST. The viral transduction was performed by Laura Moser: CIK cells were seeded in 6-well plates at $3x10^6$ cells/ml on day 0 using RPMI ++ and stimulated as described above. On day two, cell suspension was removed to leave residual $0.5x10^6$ CIK cells per well in 1ml of total volume., 500 µl of ErbB2-CAR lentivirus and 16 µg polybrene was added. After spinfection at 800xg (4/0) for 60 minutes at 32°C, cells were incubated for 24 hours. On day 3 of culture IL-15 (50ng/mL) was added. On day five cells were washed, counted and then cultured according to the CIK manufacturing protocol.

For SBTS-modified CAR-CIK cells, cells were nucleofected with SB100x mRNA and MC ErbB2-CAR at a 4:2 ratio according to the above mentioned protocol and cultured in X-Vivo10+ supplemented with cytokines. Both cultures were phenotypically and functionally characterized on day 10.

2.2.4.5.1 In vitro experiments

2.2.4.5.1.1 Flow cytometry

$1x10^5$ cells were transferred into FACS tubes, washed once with DPBS and stained with panel 1 (CD45-PerCP, CD16-PE, CD56-BV421, TCRα/β-BUV737 and CD3-BUV395) or panel 2 (CD45-PerCP, CD3-BV786, CD45RO-BV711, CD56-BV421,CD62L-BUV737 and CD8-BUV395) for 20 minutes. After an additional washing step, samples were analyzed by a BD Celestar instrument.

2.2.4.5.1.2 Cytotoxicity assays

The cytotoxic capacity of LV or SBTS ErbB2-CAR-CIK cells was evaluated by a 20 h Luc Tox assay against RH30 cells. In addition, CAR-CIK cells were functionally assessed within a 3D spheroid assay. In this assay, 5,000 RH30 mCherry/luc cells were seeded in 96 well U-bottom ultralow attachment plates. Plates were centrifuged at 1000xg for 10 minutes without deceleration. After spheroids were established, 12,500 or 25,000 either LV or SBTS CAR-CIK cells were added. Unmodified CIK cells and untreated spheroids were used as controls. Spheroids with and without CAR-CIK effector cells were monitored for 7 days using an IncuCyte instrument measuring red fluorescence. Spheroid growth was assessed by quantifying red fluorescence using the IncuCyte 2020B software.

2.2.4.5.2 In vivo experiment

LV and SBTS CAR-CIK cells from a single donor were evaluated and compared in a preclinical xenograft model of metastatic RMS.

2.2.4.5.2.1 Treatment

Female NSG mice, 10-12 weeks old were sublethally irradiated with 2.5 Gy (d-1). On the next day (d0) $1x10^5$ RH30 GFP/luc cells were injected. Another 24 hours later (d+1), $2.5x10^6$ wiltype CIK cells (n=6), LV CAR-CIK (n= 10) or SBTS CAR-CIK cells (n=5) were injected. Untreated controls injected with 100 µl DPBS served as control animals (n=7).

Animals were monitored daily for signs of disease and adverse reactions. Mice showing signs of health problems or physical abnormalities were painlessly sacrificed by isoflurane inhalation followed by cervical dislocation.

2.2.4.5.2.2 Analysis of organs

Liver, lung, spleen, BM and PB were analyzed for human immune cell persistence. The organs were incubated in Collagenase D solution for 30 minutes and then filtered through a 70µm strainer. Resulting cell suspension was washed one time with DPBS. BM was flushed out from tibiae and femura and incubated in red blood cell lysis buffer. PB was exposed to red cell lysis buffer for 10 minutes, and BM and PB were washed once with DPBS. Cell suspensions were analyzed by flow cytometry.

5 µl of cell suspensions were added to FACS tubes, washed once with DPBS and stained with antibody directed against human CD45 conjugated to PerCP for 20 minutes. After an additional washing step, the samples were analyzed by a BD Celestar instrument.

2.2.5 Data analysis

All flow cytometry data were acquired using Diva software (Version 8.0.2) and analyzed using FlowJo (Version 10.8.1). Statistical analysis and graphs were performed using GraphPad PRISM (Version 9). Data are given as mean ± standard error of the mean (SEM). Differences between groups were evaluated by two-tailed Student´s t test or one-way ANOVA using the Bonferroni-Dunn (nonparametric) method. Overall survivals are given as median with 95 % confidence interval and differences between the survival of different treatment groups were analyzed by the log-rank (Mantel–Cox) test. Differences with $p < 0.05$ (*), $p < 0.01$ (**), and $p < 0.001$ (***) were considered statistically significant.

3 Results

3.1 RMS cells

3.1.1 ErbB2 surface expression of RMS cells

ErbB2 is a known TAA in various tumors [22]. RMS cell lines do express this CAR-target at low but detectable levels [20, 25]. The patient-derived aRMS tumor organoid cells RMS127 (PAX3-FOXO1 fusion), RMS335 (PAX7-FOXO1 fusion) und RMS102 (PAX3-FOXO1 fusion) had not been previously examined in terms of ErbB2 surface expression. Our results showed, that all tumor organoids express ErbB2 on their surface. Figure 8 shows representative histograms for ErbB2-detection via flow cytometry in RMS127(A), RMS335(B) and RMS102(C) and the median fluorescence intensity (MFI) for each cell line. MFI was 136.7 ± 17.9 (mean ± SEM) for RMS127, 56.5 ± 15.3 for RMS335 and 73.4 ± 12.0 for RMS102. Additionally, the ErbB2 receptor number was quantified for each RMS tumor organoid (292.5 ± 63.1 receptors per cell (RMS127), 87.9 ± 19.8 (RMS335) and227.5 ± 73.3 (RMS102)).

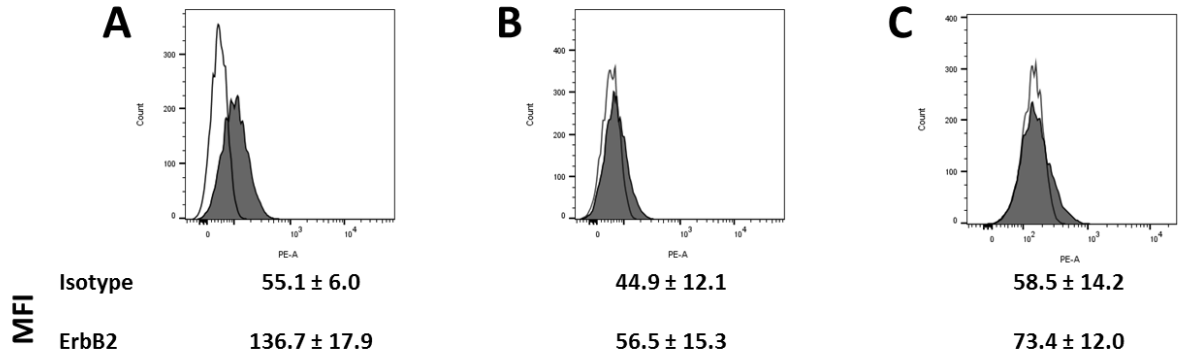

Figure 8: ErbB2 expression of patient-derived RMS organoid cells. RMS127 (A), RMS335 (B) and RMS102 cells (C) were stained with PE-conjugated anti-ErbB2 antibody (filled histograms) or corresponding isotype controls (unfilled histograms). MFIs are given as mean ± SEM and histograms of one representative experiment out of three independent experiments are shown. Adapted from [169].

3.1.2 Lentiviral transduction

For further experiments Luciferase expression was introduced in RMS cells: RH41, RMS335, RMS127 and RMS102 cells were transduced with the GFP/luc construct by lentiviral transduction (plasmid name: pSL2GW). In RMS127 cells, transduction was not possible. Figure 9 shows fluorescence images of RH41 (A), RMS102 (B) and RMS335 (C) cells on day five after transduction. RMS102 cells did not survive long term in culture, probably due to genetic instability. In addition, GFP expression was assessed in RH41 and RMS335 cells by flow cytometry at day 12 after transduction. In more than 96% of cells GFP signals were detectable, not necessitating further sorting approaches before being used in

experiments. The stable GFP expression especially after freezing and rethawing was verified for each cell line.

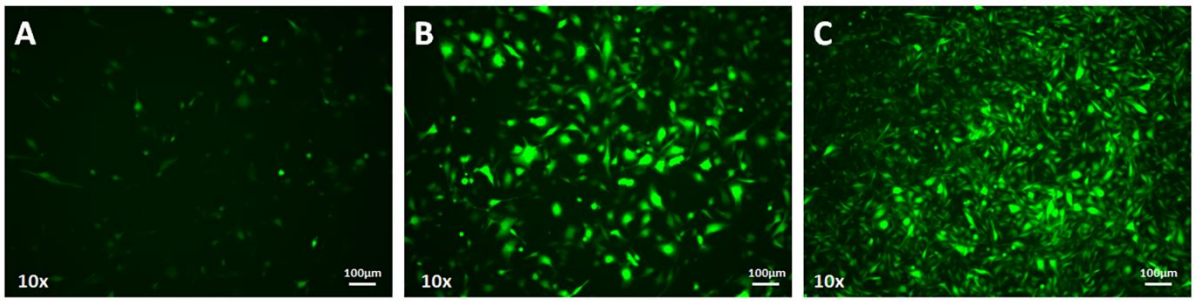

Figure 9: Fluorescence microscopy images of RMS cells five days after transduction. RH41 (A), RMS102 (B) and RMS335 (C) cells were examined for GFP expression using a Keyence BX800 microscope.

3.2 NK-92/5.28.z as innate CAR-cell line for RMS treatment

3.2.1 CAR evaluation & 2D cytotoxicity assays

The monoclonal NK-92/5.28.z cell line derived from the NK-92 cell line is bearing a ErbB2-specific CAR [91, 176]. Since the CAR is stably integrated into the cell genome by lentiviral transduction, almost 100% of the NK-92/5.28.z cells are expected to express the CAR. The filled histogram in Figure 10, representing the NK-92/5.28.z cells, showing ErbB2-specific CAR in 98.4% of these cells. Parental NK-92 cells (unfilled histogram) were used as a controls.

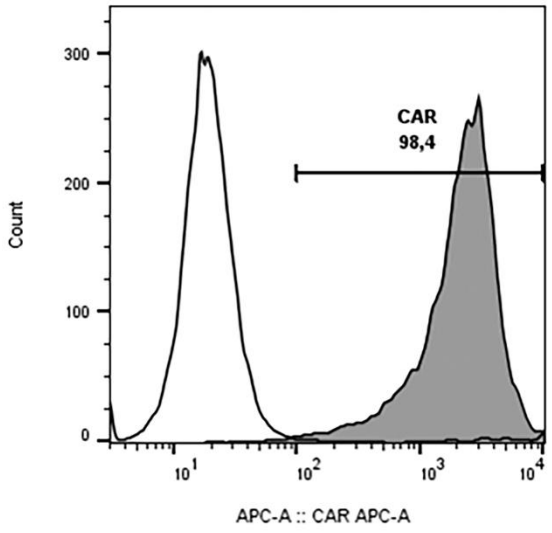

Figure 10: CAR expression of NK-92/5.28.z cells. ErbB2-specific CAR of CAR-NK-92 cells (filled histogram) was stained with an ErbB2-Fc chimera followed by APC-conjugated antibody directed against human Fc of the chimera. Parental NK-92 cells (unfilled histogram) were used as a control. Adopted from [169].

In a proof of concept analysis, NK-92/5.28.z cells demonstrated cytotoxicity against the RMS cell lines RH30 and RH41 in 2D short-term assays [26]. In this work, complementary assays with more complex RMS models including patient-derived tumor organoids were used, to demonstrate cytotoxicity. Cell lysis of RMS127 (A), RMS335 (B) and RMS102 (C) cells after three hours of co-incubation with NK-92/5.28.z cells was assessed by ERA, shown in Figure 11. RMS cells were effectively lysed even at low E:T ratios of 5:1 and 2.5:1. The cytotoxicity of NK-92/5.28.z cells correlated with the ErbB2 surface expression on RMS cells and significantly increased cytotoxicity compared to parental NK-92 cells, indicate CAR-mediated cytotoxicity.

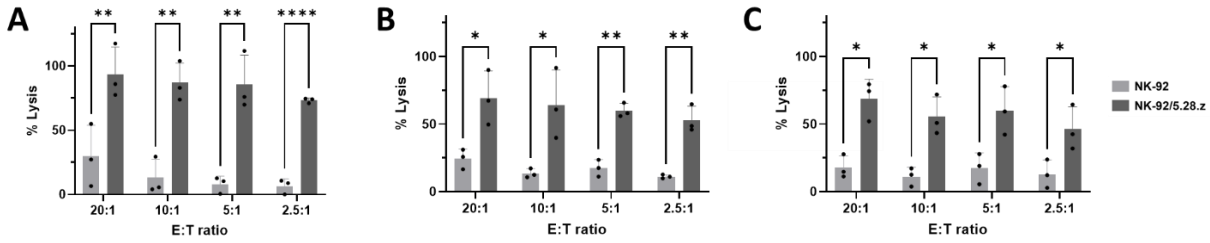

Figure 11: Cytotoxicity of NK-92/5.28.z against primary aRMS cells. NK-92 or NK-92/5.28.z was co-incubated with RMS127 (A), RMS335 (B) or RMS102 (C) cells for three hours and target cell lysis was assessed by europium release assay. Adapted from [169].

3.2.2 Irradiation of NK-92/5.28.z cells

Due to their malignant origin, both the parental NK-92cells and their derivative cells must be γ-irradiated prior to application in patients. NK-92/5.28.z cells were irradiated with 10 Gy according to the FDA standard for adaptively transferred cell products. Non-irradiated control cells proliferated and doubled in number within three days, whereas the number of irradiated cells decreased to half of the original number of cells after three days (Figure 12A), clearly showing that NK-92/5.28.z cells are not able to proliferate after irradiation with 10 Gy. In parallel, the cytotoxicity potential was assessed against RH30$^{GFP/luc}$ cells on day zero, one and two after irradiation (Figure 12B). No significant difference was seen between irradiated and non-irradiated effector cells on days zero and one. But the cytotoxic capacity of NK-92/5.28.z cells significantly decreased two days after irradiation, indicating that NK-92/5.28.z cells retain their intrinsic cytotoxicity for at least 24 hours following irradiation.

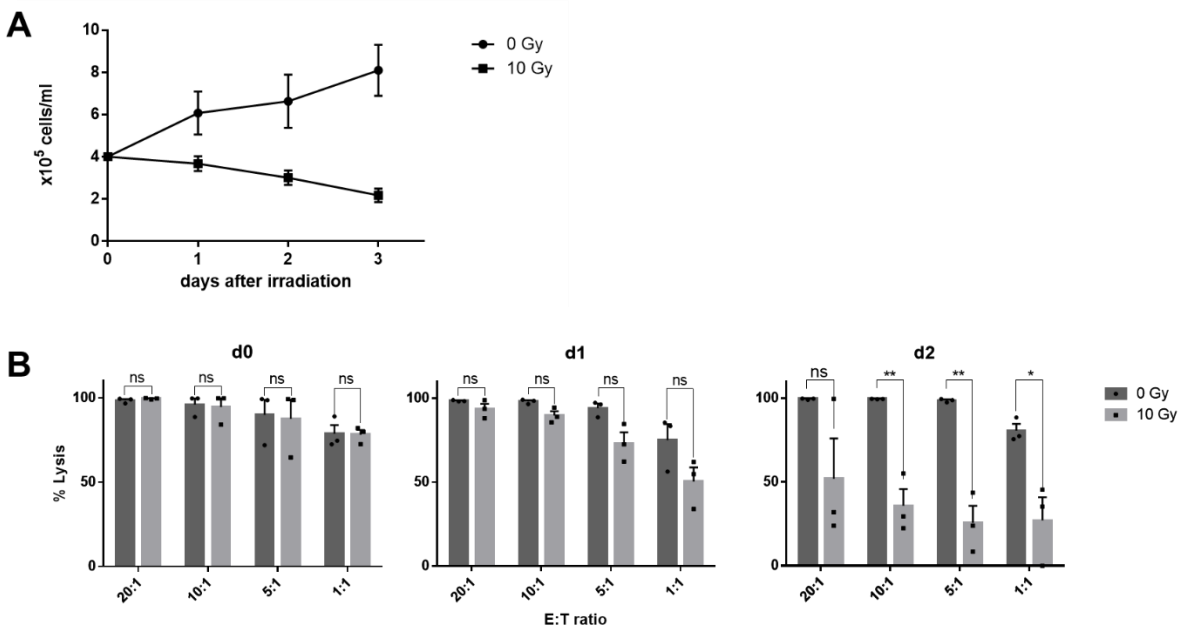

Figure 12: Proliferation and cytotoxicity of irradiated and untreated NK-92/5.28.z cells. (A) NK-92/5.28.z cells were irradiated with 10 Gy and cell numbers were evaluated for three days. (B) The cytotoxic capacity of irradiated NK-92/5.28.z cells against RH30$^{GFP/luc}$ cells was analysed by Luc Tox after 16 hours of co-incubation and compared to untreated NK-92/5.28.z cells. Mean ± SEM of three independent experiments are shown and unpaired Student´s t-test was performed. Adopted form [169].

3.2.3 3D spheroids

Because 2D RMS cell cultures and therefore 2D cytotoxicity assays do not mimic the clinical situation, 3D tumor spheroids were established. In Figure 13A six day co-cultures of green fluorescent tumor spheroids with or without effector cells are shown. NK-92, and even more NK-92/5.28.z cells clustered around tumor spheroids, indicated by non-fluorescent cell clusters. Cytotoxicity was assessed by quantifying the green fluorescent area of tumor spheroids (Figure 13B). Parental NK-92 cells significantly inhibited growth of the spheroids, while NK-92/5.28.z cells significantly reduced tumor size even more compared to untreated controls and NK-92 cell treatment.

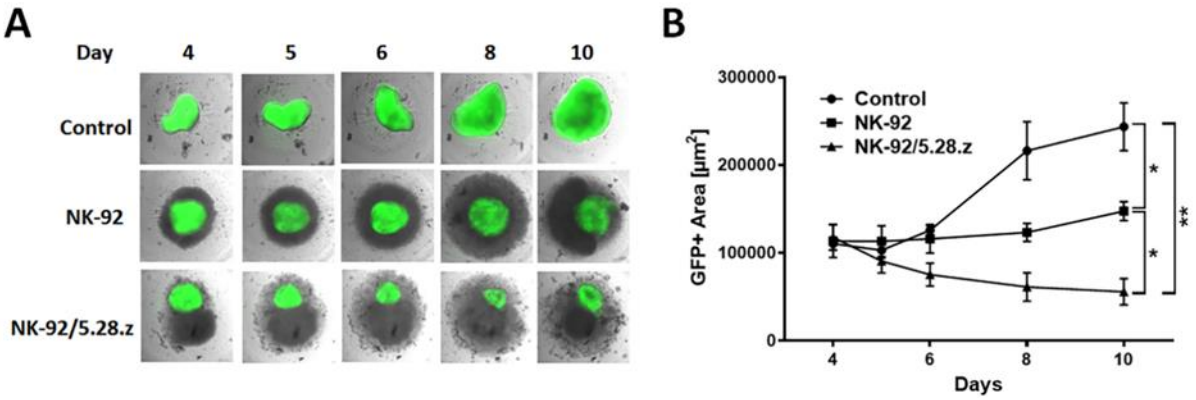

Figure 13: 3D spheroid cytotoxicity assay. (A) RH30$^{GFP/luc}$ spheroids were seeded and NK-92, NK-92/5.28.z cells were added on day 4. Fluorescence and brightfield images of the spheroids and co-cultures were taken until day 10 and a representative experiment is shown. (B) The green fluorescent area and therefore the spheroid size was quantified using Fiji software. Mean ± SEM was calculated from three independent experiments and one-way ANOVA of endpoints was performed. Adopted from [169].

3.2.4 *In vivo* experiment (tumor engraftment and survival)

The ability of NK-92/5.28.z cells to home to, to infiltrate into, and to persist at tumor sites was assessed in a xenograft model of metastatic RMS *in vivo*. Engraftment and growth of tumors were monitored by BLI (Figure 14A). Tumor signals were detectable on day 22 ± 7.5 in the untreated control group, on day 30 ± 5.5 in NK-92 cell and day 30 ± 5.3 in the NK-92/5.28.z cell treatment cohorts. The NK-92/5.28.z cell treated animals also showed a more moderate BLI signal compared to the untreated controls and the NK-92 cell treated animals. Quantification of BLI signals using the luminoscore (Figure 14B) showed a significant inhibition of the tumor growth obtained by NK-92/5.28.z cell therapy compared to parental NK-92 cell treatment and untreated controls. Of note, two out of ten animals within the NK-92/5.28.z treatment group even achieved long-term complete remission. Parental NK-92 cells did not significantly inhibit tumor growth compared to NK-92/5.28.z cell treated and untreated animals.

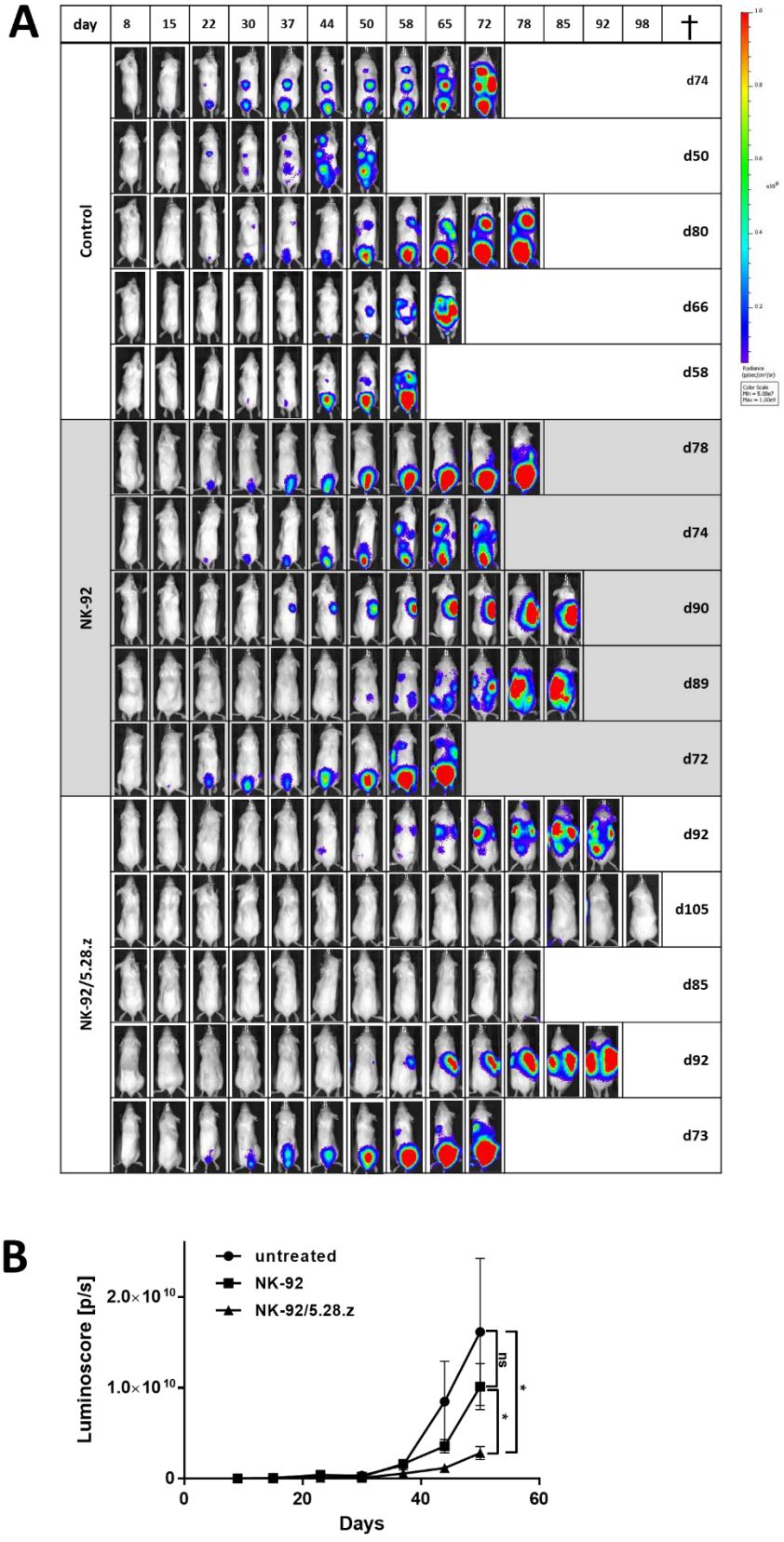

Figure 14: Monitoring of tumor progression by BLI. (A) Bioluminescence images of representative animals of different treatment groups. (B) The total flux of dorsal and ventral BLI images was quantified and was added to the luminoscores. The mean of all animals within a treatment group (untreated n=5, NK-92 n=13, NK-92/5.28.z n=10) was calculated and is shown with SEM. One-way ANOVA was performed. Adapted from [169].

Overall survival of animals is shown in Figure 15. Tumor engraftment became life limiting between days 50 and 80 for controls resulting in a median overall survival of 66.0 ± 13.4 days in this group. Treatment with parental NK-92 cells did not significantly impact survival (median, 72.5 ± 6.1 days). However, NK-92/5.28.z cells significantly prolonged survival resulting in a median overall survival of 81.0 ± 8.8 days compared to the NK-92 treatment group and the untreated controls. Animals without visible signs for tumor engraftment or adverse side effects were sacrificed on day +105.

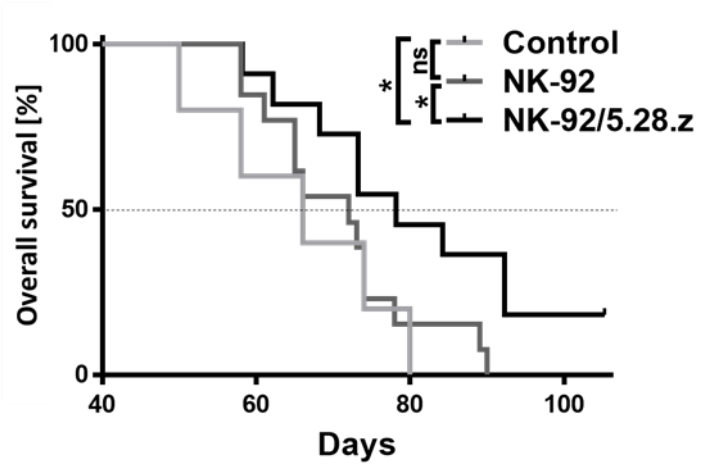

Figure 15: NK-92/5.28.z prolonged the overall survival of the animals. Animals showing visible signs of disease progression, physical abnormalities, or discomfort were sacrificed. Animals without health problems were followed until the end of the experiment on day +105. The overall survival of untreated (n=5), animals treated with NK-92 (n=13) or NK-92/5.28.z (n=10) is shown. Statistical analysis was performed using the log-rank test (Mantel-Cox). Adapted from [169].

3.2.4.1 2nd course NK-92/5.28.z

Three animals out of the NK-92/5.28.z cell treatment group were randomly selected to receive three additional NK-92/5.28.z cell infusions after tumor manifestation. The additional treatment showed an inhibition of tumor growth of established tumors as long as the immunotherapy was applied. But tumors again progressed shortly thereafter (Figure 16A). However, this resulted in a prolonged overall survival with a median of 90.0 ± 0.9 days compared to the untreated controls, and animals treated with only one cycle of NK-92/5.28.z cell therapy (Figure 16B).

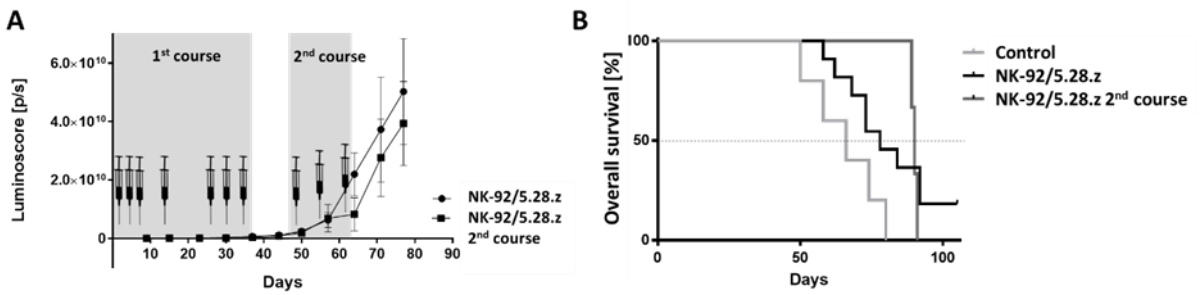

Figure 16: 2nd course of NK-92/5.28.z inhibits tumor progression. Three additional injections of NK-92/5.28.z in NK-92/5.28.z treated mice (2nd course, n = 3) inhibited the tumor growth (A) compared to single course treatment (n=10) and prolonged survival (B) compared to untreated controls (n=5). Luminoscores are shown as mean ± SEM for each treatment group.

3.2.4.2 Irradiated NK-92/5.28.z

Mice treated with irradiated NK-92/5.28.z cells showed a slightly increased tumor growth compared to NK-92/5.28.z cell treated mice without prior irradiation (Figure 17A). Median survival in this cohort was 72.0 ± 19.9 days. In addition, treatment did not lead to a complete remission in any of the treated animals (Figure 17B).

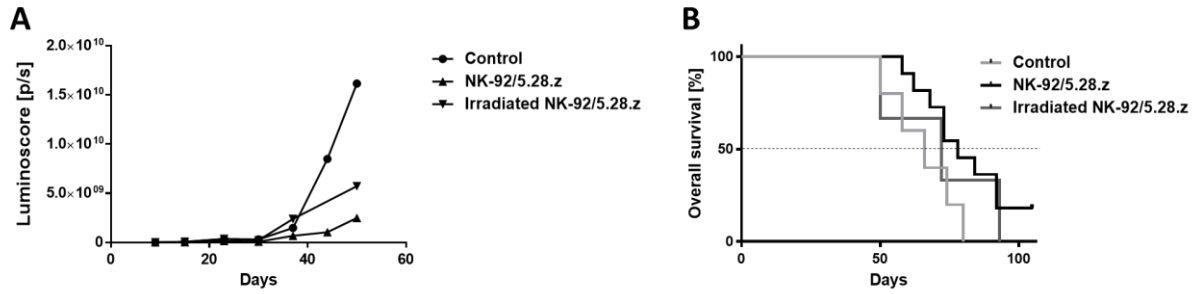

Figure 17: Irradiated NK-92/5.28.z cells inhibit tumor growth and prolong survival. (A) BLI signals showed that irradiated NK-92/5.28.z cells (n=3) inhibited tumor growth compared to untreated control animals (n=5), but not as much sufficient as non-irradiated cells (n=10). (B) Irradiated NK-92/5.28.z cells also prolonged the overall survival of the animals, but also not to the same extent as non-irradiated cells (B).

3.2.4.3 Flow cytometry and qPCR of in vivo samples

At the end of experiments, the organs were analyzed for homing to, infiltration into, and persistence at tumor sites of effector cells. Blood, BM, liver, lung and spleen samples were stained for human CD45 and analyzed by flow cytometry. The representative example shown in Figure 18, demonstrates that positive cells were distinguishable from negative mouse cells. NK-92 and NK-92/5.28z cells were found in all treated animals. As expected, prior irradiation of NK-92/5.28.z cells abrogated persistence of immune cells *in vivo*.

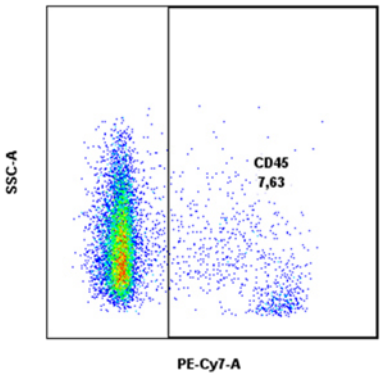

	Blood	BM	Liver	Lung	Spleen
Untreated	0/5	0/5	0/5	0/5	0/5
NK-92	5/12	12/12	11/12	6/12	12/12
NK-92/5.28.z	8/10	7/10	5/10	4/10	8/10
NK-92/5.28.z 2nd course	0/3	2/3	0/3	3/3	2/3
Irradiated NK-92/5.28.z	0/3	0/3	0/3	0/3	0/3

Figure 18: Effector cells were detected in all tissues by flow cytometry. Organs were harvested and single cell suspensions were prepared. Cells were stained for human CD45 and were analysed by flow cytometry. Detected effector cells are summarized up in the table.

Due to the autofluorescence of tissues, tumor cells were not detectable by flow cytometry. Therefore, the tumor cell infiltration was assessed by qPCR. Biodistribution and engraftment of tumor cells is shown in Figure 19A. Highest tumor burdens were found in livers and lowest in BM samples of mice. Tumor burden decreased upon treatment, and was lowest in NK-92/5.28.z cell treated animals. A second course of NK-92/5.28.z cell therapy further decreased tumor load. Irradiation of NK-92/5.28.z cells prior to iv application resulted in a slightly higher tumor burden compared to the iv application of non-irradiated NK-92/5.28.z cells.

Biodistribution and persistence of effector cells was confirmed by qPCR (Figure 19B). Large numbers of effector cells were detected in spleens, a secondary lymphoid organ, but were also detectable in tumor-bearing organs. In addition, qPCR analyses demonstrated presence of CAR cells (Figure 19C). qPCR analysis was performed by Hermann Kreyenberg.

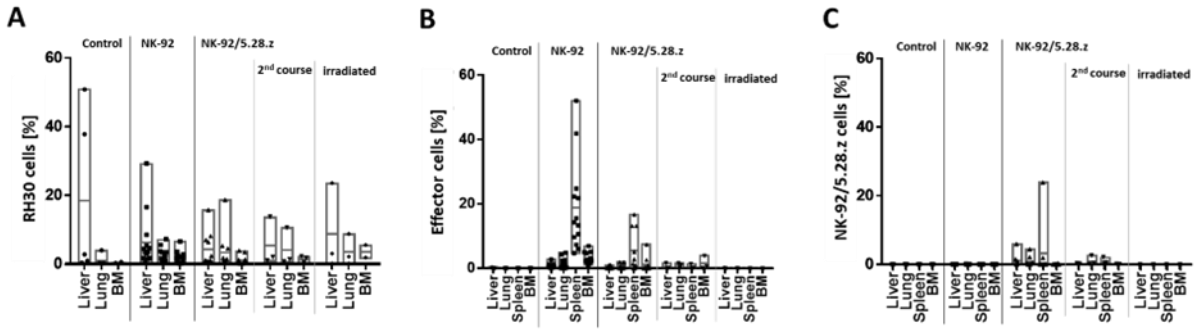

Figure 19: Homing and persistence of tumor and effector cells. (A) Tumor cells were detected by qPCR in tumor-bearing organs (liver, lung, BM). Effector cells (B) and NK-92/5.28.z (C) were quantified in liver, lung, spleen and BM. The results are shown as boxplots for the different treatment groups control (n=5), NK-92 cells (n=13), NK-92/5.28.z (n=10), 2nd course NK-92/5.28.z cells (n=3) and irradiated NK-92/5.28.z cells (n=3).

3.2.4.4 IHC and immunofluorescence microscopy

Tumor tissues were then characterized for integrity and immune cell infiltration using microscopic techniques. IHC staining was used to confirm the RMS phenotype. Staining and rating was performed by Elise Gradhand. As listed inTable *17*, RMS tumors expressed CD56, MyoD, Desmin and Myogenin throughout the entire experiment.

Table 17: RMS markers expressed on xenograft tumors. Tumor bearing mouse organs were isolated and tissues were stained for characteristic RMS tumor markers. Protein expression was graded by an experienced pathologist (-, negative; +, low grade; ++, intermediate grade; +++, high grade).

	CD56	MyoD1	Desmin	Myogenin
Untreated (n=2)	+++ membranous	+++ nuclear	+ cytoplasmic	++ nuclear
NK-92 (n=2)	+++ membranous	+++ nuclear	+ cytoplasmic	++ nuclear
NK-92/5.28.z (n=2)	+++ membranous	+++ nuclear	+ cytoplasmic	++ nuclear

Macroscopically analysis of the spleen sizes revealed significantly enlarged spleens in the immunotherapeutically treated animals due to immune cell infiltration (Figure 20). The spleen size between animals treated with parental NK-92 or NK-92/5.28.z showed no significant difference. Nevertheless, no enlarged spleens were observed in animals treated with irradiated NK-92/5.28.z cells.

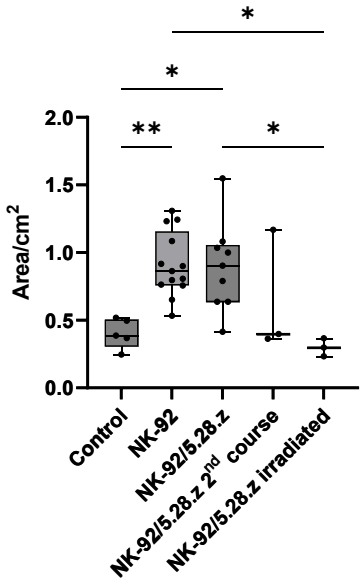

Figure 20: Spleen size of different treatment groups. Macroscopic images of spleens were analyzed with Fiji and spleen size of each animal was assessed. One-way ANOVA was performed. Adapted from [169].

Figure 21 shows whole organs and organ sections. Macroscopically, the livers showed cystic tumor lesions. Immunofluorescence staining showed that NK-92 and NK-92/5.28.z cells were detectable at tumor sites in livers and lungs as well as in spleens. Effector cells were absent in untreated controls and mice treated with irradiated NK-92/5.28.z cells. Immunofluorescence staining and microscopy was performed by Sabine Harenkamp.

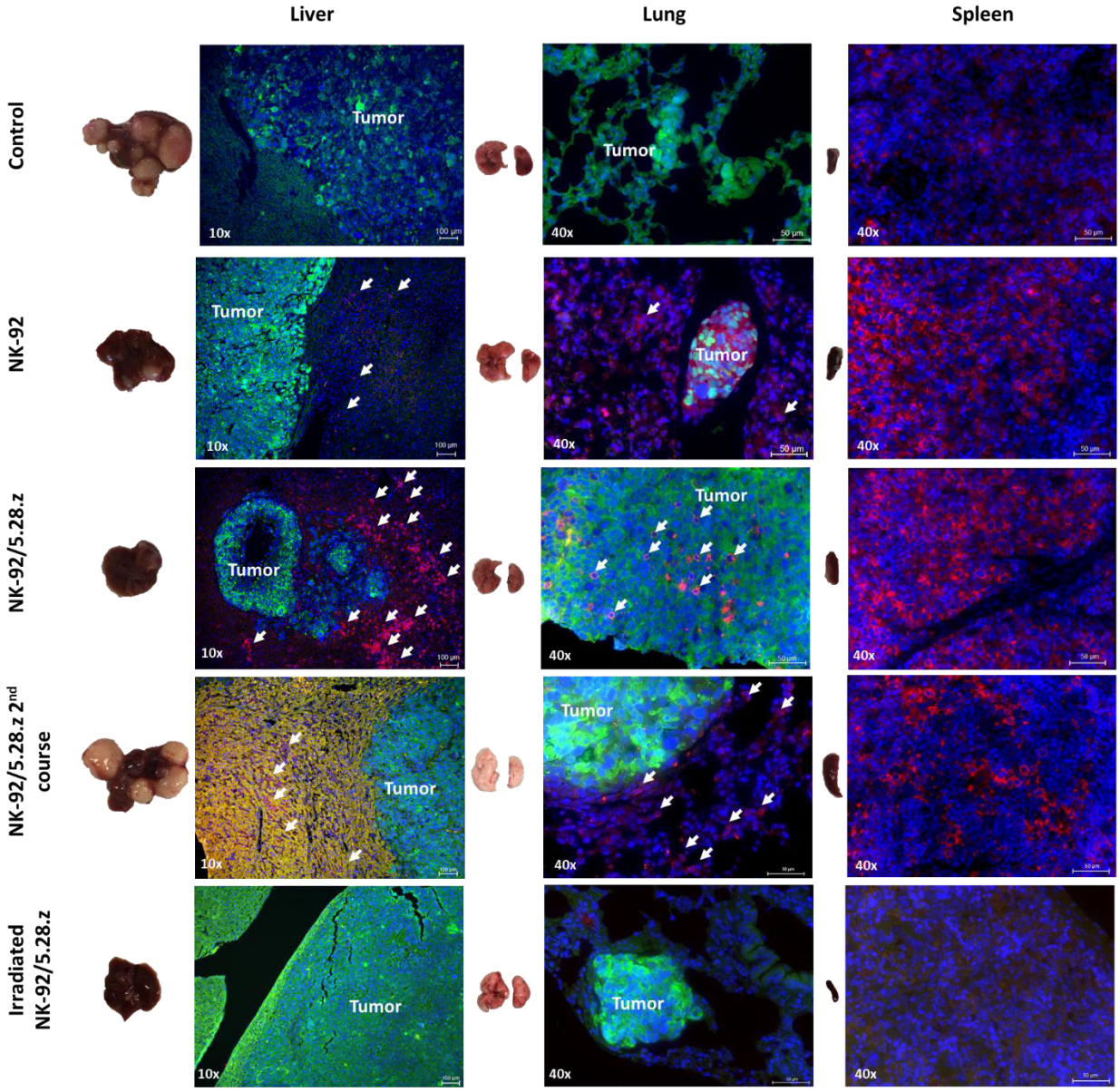

Figure 21: Macroscopic tumor lesions and immunofluorescence staining of metastatic tumors and spleens. Tumor cells (Alexa 488, green) and human immune cells (Alexa 647, red, additionally indicated by arrows in liver and lung) are shown; cell nuclei were stained with DAPI. Exemplary animals with tumor engraftment were selected. NK-92 cells, and to a more pronounced extent NK-92/5.28.z cells, preferentially homed to spleens as well as to metastatic tumor sites in lung and liver, whereas the irradiation of NK-92/5.28.z abrogated the persistence completely. Adapted from [169].

Meca32 staining, a protein expressed by mouse endothelial tissue of blood vessels, allowed for the exact location of the effector cells. NK-92 and NK-92/528.z cells were delivered by the blood circulation to the tumor site and infiltrated the tumor tissues through the blood vessels (Figure 22).

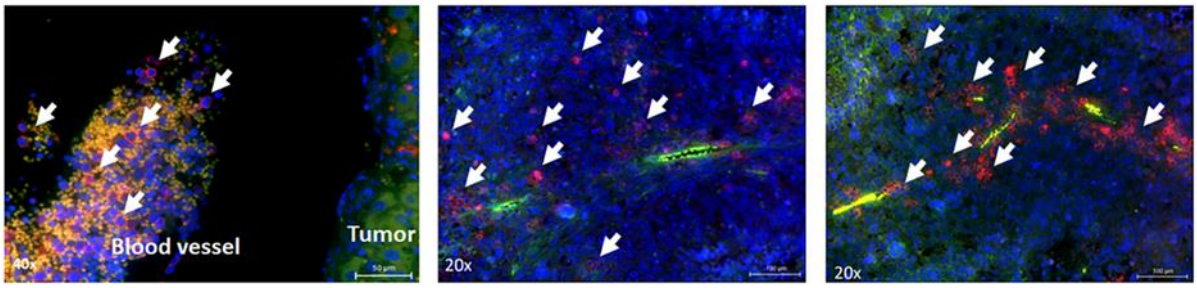

Figure 22: NK-92 and NK-92/5.28.z cells are distributed by blood circulation and infiltrate tumor tissue. Tumor tissue was stained for effector cells against human CD45 (Alexa647, red, indicated by arrows) and blood vessels against Meca32 (green, Alexa488). Additionally, all cell nuclei were stained with DAPI (blue). Adopted form [169].

In conclusion, NK-92/5.28.z cell and to a lesser extent parental NK-92 therapy inhibited tumor growth as long as the therapies were applied, thereby prolonging survival *in vivo*.

3.2.5 Combinational treatment

Combinatorial treatment of NK-92/5.28.z cell with small molecules or immune checkpoint inhibitors may address the limited persistence following irradiation *in vivo*. The successful application of ErbB2-CAR-T cell therapy in combination with PD-1 blockade had been reported as a single case in a child with metastatic RMS [128].

3.2.5.1 PD-1

PD-L1 was expressed on RH30 cells (18.8% ± 3,0%), and on patient-derived RMS organoids RMS335 (3.2% ± 0.9%) and RMS102 (1.6% ± 0.1%) as determined via flow cytometry (Figure 23A). NK-92/5.28.z cells were incubated with PD-1 inhibitors prior to use in a three-hour ERA against RH30 cells. NK-92/5.28.z cells without PD-1 inhibitor treatment were used as controls. Tumor cell lysis of RH30 cells with and without PD-1 blockade is shown in Figure 23B. PD-1 inhibition resulted in a slight but not significant increase of tumor cell lysis.

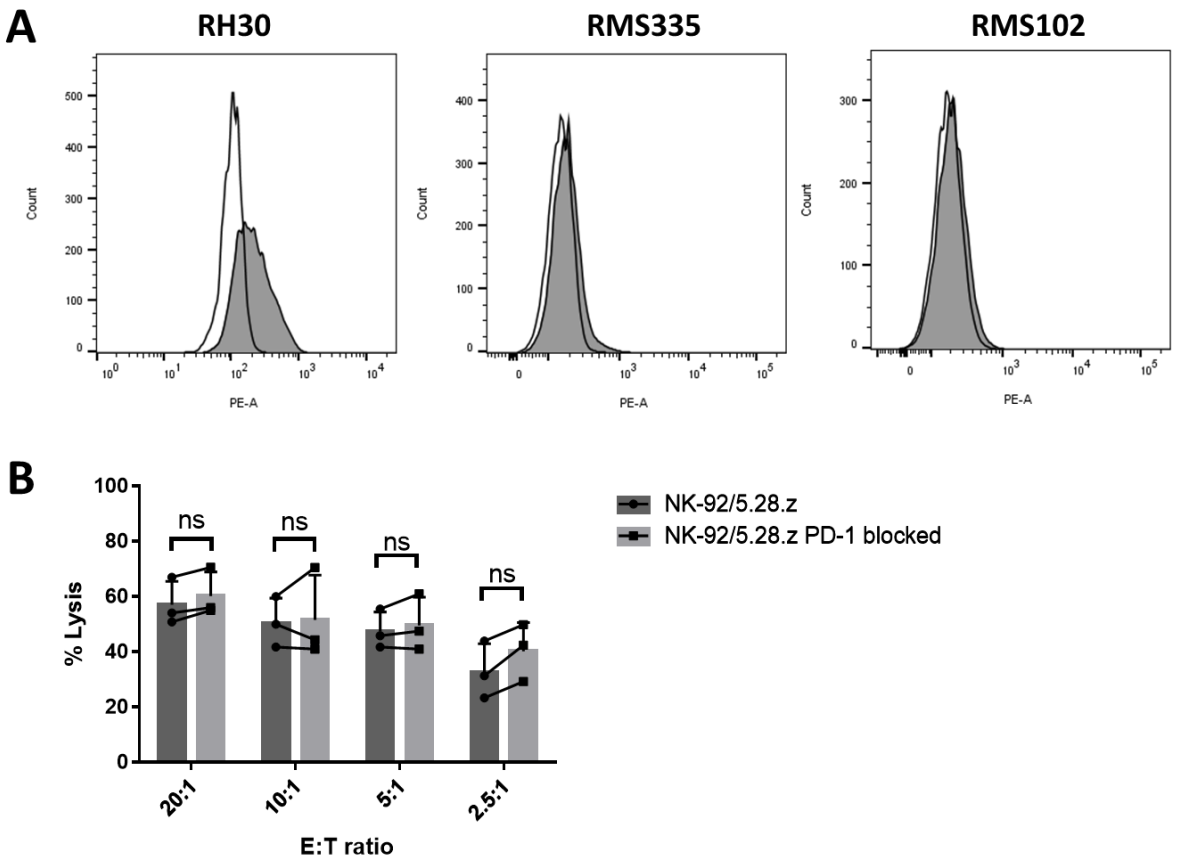

Figure 23: PD-L1 expression on RMS cells and combination therapy with NK-92/5.28.z and PD-1 blockade. (A) RMS cells were stained with PE-conjugated anti-PD-L1 antibody (filled histograms) or corresponding isotype controls (unfilled histograms). RMS cell line RH30 expressed high levels of PD-L1, while PD-L1 was expressed at low levels on the surface of patient-derived RMS organoids RMS102 and RMS335. One of three representative experiments is shown. (B) Blockade of PD-1 on NK-92/5.28.z cells resulted in slightly increased lysis of RH30 cells in a short-term 3 hour ERA cytotoxicity assay. Mean ± SEM of three independent experiments are shown and unpaired Student´s t-test was performed.

However, this model of combinatorial treatment did not assess effects on bystander T cells within the tumor microenvironment and the results can therefore not directly be translated into the patient setting.

3.2.5.2 Bortezomib

Another promising candidate to enhance the cytotoxicity of NK-92/5.28.z could be the proteasome inhibitor bortezomib. This inhibitor is clinically used for the treatment of MM [177] and has been successfully tested in combination with CAR-NK-92 *in vivo* for the treatment of renal carcinoma [146]. The following results were obtained during the supervision of a master thesis, the experiments were mainly performed by Leonie Hartig. qPCR and Western blots were guided by and/or performed by Nadine Weinelt.

3.2.5.2.1 EC_{50} values

Bortezomib treatment induces apoptosis in tumor cells, however its potential has not yet been assessed for the treatment of aRMS tumors in combination with immunotherapy. RH30 cells were incubated with 0 to 1 mM bortezomib for seven (Figure 24A), 24 (Figure 24B) and 48 hours (Figure 24C). A saturation was reached after 48 hours of treatment, resulting in an EC_{50} value of 2.1 nM. 24 hour of bortezomib treatment resulted in sigmoidal saturation curves with calculated EC_{50} values of 29.6nM (RH30, Figure 24B), 23.7 nM (RH41, Figure 24D) and 6.1 nM (RMS335, Figure 24E). The patient-derived RMS organoid RMS335 cell were more sensitive towards bortezomib treatment than the RMS cell lines RH30 and RH41.

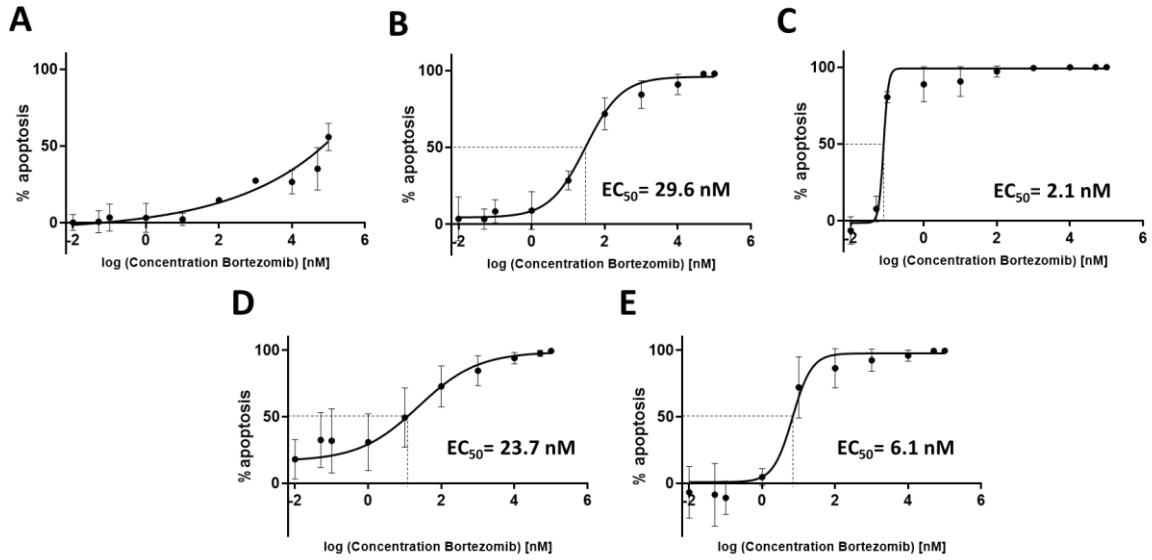

Figure 24: Timing and EC_{50} value determination. RH30 cells were treated with bortezomib for 7 (A), 24 (B) or 48 hours (C). RH41 (D) and RMS335 (E) were incubated with bortezomib concentrations ranging from 0 to 1 mM for 24 hours. Remaining viable cells were quantified by the luciferase activity and EC_{50} values were calculated from the sigmoidal curves of the 24-hour treatment. Means ± SEM of at least three independent experiments are shown.

3.2.5.2.2 Caspase activity

Next, caspase activity, a prerequisite for apoptosis, was evaluated following bortezomib treatment. Western Blot (WB) analysis of RH30 cells (Figure 25A, left) and RH41 cells (Figure 25A, right) revealed caspase-3 cleavage upon 25 nM and 10 nM bortezomib treatment, respectively. In RH41, the cleaved caspase-3 increased in a dose-dependent manner. In addition, caspase-3/-7 activation was confirmed by the Caspase Glo assay (Figure 25B-D). Caspase activation increased with bortezomib treatment in a dose-dependent manner. Differences were significant compared to untreated controls (RH30, Figure 25B and RH41, Figure 25C), but not in RMS335 (Figure 25D). Caspases-3/-7 activation was seen in all cells after incubation with staurosporine (positive control). Thus, bortezomib-induced caspase activation may lead to programmed cell death in RMS cells.

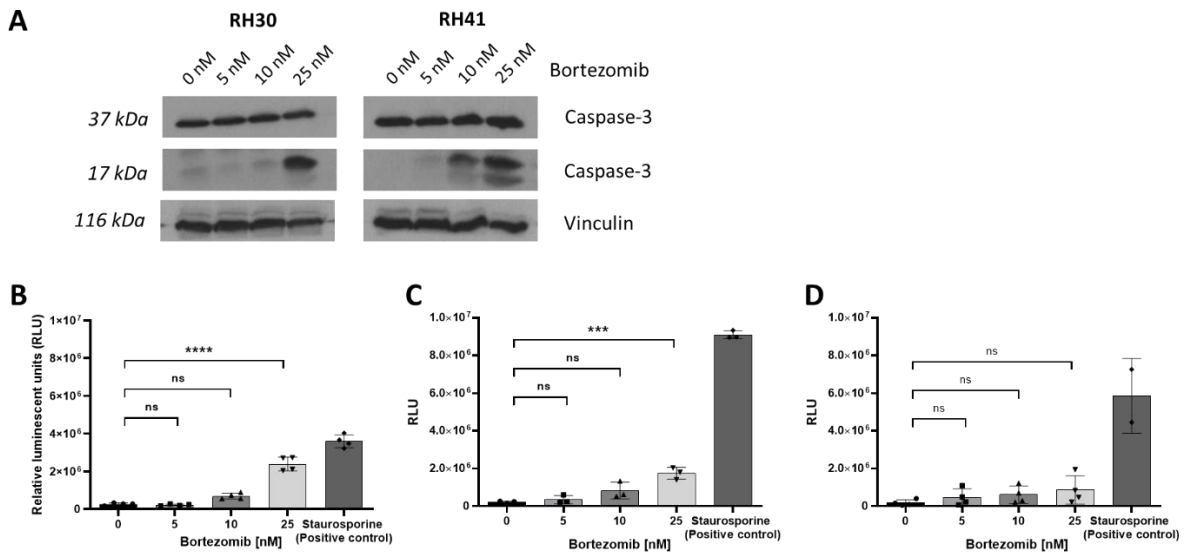

Figure 25: Caspase cleavage and activity. (A) Caspase-3 cleavage in RH30 (left hand side) and RH41 (right hand side) caused by bortezomib was detected by western blot analysis. One representative experiment out of two is shown. (B-C) In addition, caspase glow assay detected an increased caspase activity in RH30 (B) and RH41 (C) after treatment with 25nM bortezomib, but not in RMS335 cells (D). Mean ± SEM of three independent experiments are shown, and one-way ANOVA with Bonferroni correction was used for statistically analysis.

3.2.5.2.3 TRAIL receptors DR4 and DR5

Bortezomib is known to increase the expression of TRAIL receptors DR4 and DR5 on various cancer cells [143, 178]. DR4 and DR5 expression on the surface of aRMS cells RH30, RH41 and RMS335 was analyzed by flow cytometry after 24 hours incubation with 0 to 50 nM bortezomib. DR5 but not DR4 was upregulated on aRMS cells in a dose-dependent manner (Figure 26A). p53 [179, 180], JNK [181] and c-Rel [182, 183] are known to be involved in the upregulation of DR5. These proteins were assessed in RH30 (Figure 26, left) and RH41 (Figure 26B, right) cell lysates after treatment with 0,5,10 and 25 nM bortezomib by WB. c-Rel was not altered, but p53 and JNK phosphorylation and therefore activation was increased upon 10 nM and 25 nM bortezomib treatment, suggesting DR5 upregulation via the JNK pathway. p53 was not detected in RH41 cells, as this cell line harbours a p53 mutation that causes a frame shift resulting in a truncated p53 [184].

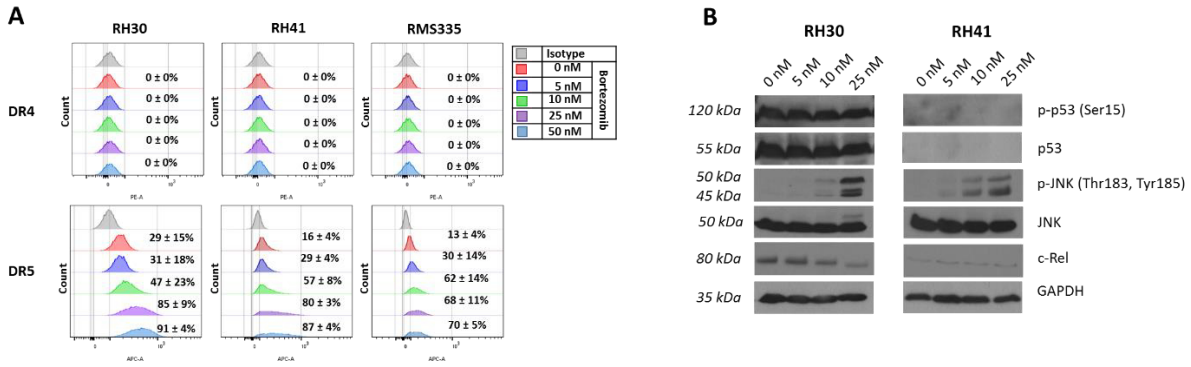

Figure 26: DR4 and DR5 expression after bortezomib treatment and expression of potential mediators. (A) TRAIL receptor DR4 and D5 expression on aRMS cells after bortezomib treatment with concentrations ranging from 0 to 50 nM was assessed by flow cytometry. One representative experiment out of three is shown. (B) Western blot analysis of proteins associated with pathways mediating TRAIL receptor upregulation. One representative experiment out of two is shown.

3.2.5.2.4 TRAIL surface expression of NK-92/5.28.z cells

TRAIL protein is expressed on NK cells and T cells [185], but also on NK-92 cells [90, 186]. TRAIL expression was found on the surface of NK-92/5.28.z cells after coincubation with RH30 cells (Figure 27) by flow cytometry. In addition, TRAIL mRNA was detected by qPCR. Thus, TRAIL is expressed at low but detectable levels on NK-92/5.28.z cells.

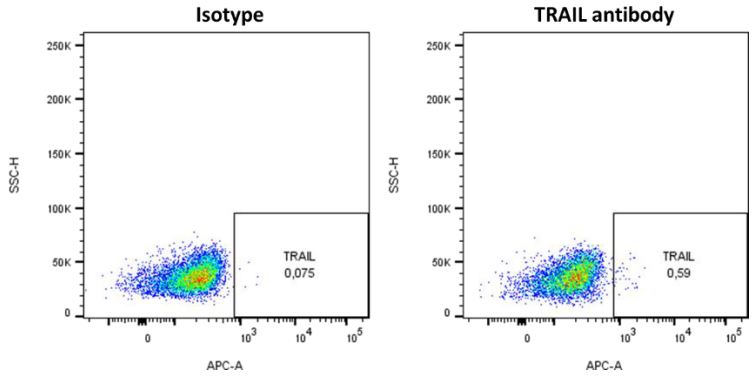

Figure 27: TRAIL surface expression on NK-92/5.28.z cells. NK-92/5.28.z cells were co-incubated with RH30 cells for 1 hour and then stained with APC-conjugated TRAIL antibody (right side) or corresponding isotype (left side). Representative flow cytometry blots out of three independent experiments are shown.

3.2.5.2.5 Tumor cell lysis by combinatorial treatment of bortezomib and NK-92/5.28.z cells

Pre-treatment with bortezomib for 24 hours significantly increased tumor cell lysis in a three-hour Luc Tox assay (Figure 28). RH30 (A) and RH41 (B) cell lines were pre-treated with 0, 10, 25 or 50 nM bortezomib. The more sensitive patient-derived tumor organoid RMS335 (C) was pre-treated with 0, 5, 10 and 25 nM bortezomib. All analyzed tumor targets showed a high susceptibility towards combinatorial treatment with bortezomib and NK-92/5.28.z cells.

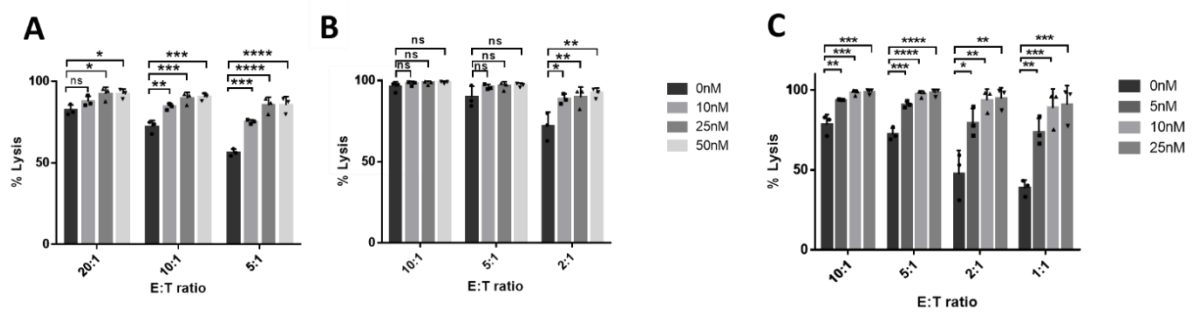

Figure 28: Lysis of aRMS cells by combinatorial treatment. RH30 (A), RH41 (B) and RMS335 cells (C) were pre-treated with indicated concentrations of bortezomib for 24 hours and then co-incubated with NK-92/5.28.z for 3 hours in a Luc Tox assay. Mean ± SEM of at least three independent experiments are shown, and one-way ANOVA with Bonferroni correction was used for statistical analysis.

3.2.5.2.6 qPCR and western blot analysis of selected pathways

NFκB and JNK pathways may be involved in the susceptibility of target cells (RH30, Figure 29A and RH41 Figure 29B) upon bortezomib, NK-92/5.28.z cell, and/or combinatorial treatment [187, 188]. qPCR revealed significantly increased levels of p100 mRNA in RMS cell lines after treatment with NK-92/5.28.z cells. In RH30 cells, JNK mRNA levels significantly decreased after NK-92/5.28.z or combinatorial treatment. At the protein level (Figure 29C), p-p100 and p-JNK, were increased in RH30 cells, but not in RH41 cells upon treatment. However, caspase-3 was cleaved in both cell lines. Thus, indicating towards an inhibition of the non-canonical NFκB pathway, an activation of the JNK pathway and the caspase cascade in RMS tumors upon combinatorial treatment.

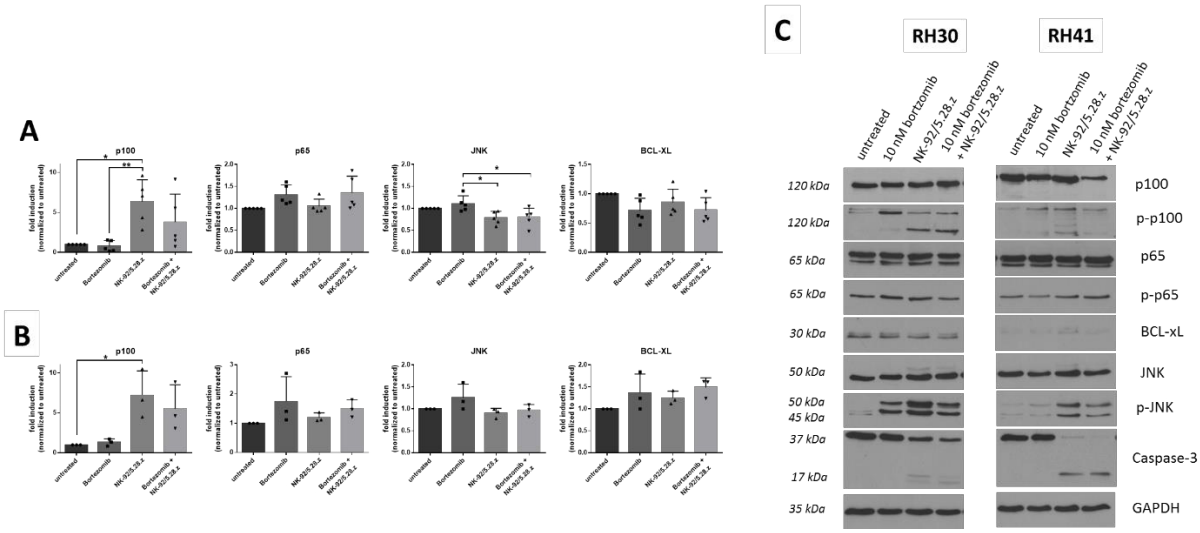

Figure 29: Inhibition of non-canonical NFκB pathway and induction of JNK pathway. qPCR analysis of p100, p65, JNK and Bcl-xL mRNA levels in RH30 (A) and RH41 (B) cells after single agent treatment with bortezomib, or NK-92/5.28.z cells, or combinatorial treatment of both in relation to untreated controls. qPCR analysis in RH41 cells. (C) Western blot analysis of p100, p65, JNK and phosphorylated form of these proteins as well as BCL-XL and caspase 3. GAPDH was used as loading control. Mean ± SEM of at least three independent experiments are shown, and one-way ANOVA with Bonferroni correction was used for statistically analysis.

3.2.5.2.7 Synergistic or additive effect?

Cytotoxicity of NK-92/5.28.z cell is mediated through degranulation of effector molecules and besides the CAR, through a variety of receptor/ligand interactions. To investigate whether the observed effects of DR5 upregulation and TRAIL-mediated apoptosis are synergistic, Luc Tox assays were performed with purified TRAIL protein and bortezomib. The ZIP model was applied for data interpretation (Figure 30). The ZIP reverence confirmed a TRAIL sensitivity in RH30 cells (Figure 30A) and TRAIL resistance in terms of RH41 cells (Figure 30B) and RMS335 cells (Figure 30C). Additionally, combined bortezomib and TRAIL treatment showed synergistic effects in RH30 cells (p = 1.43e-5) and RMS335 cells (p = 4.58e-3), detected by the ZIP synergy score. In RH41 cells (p = 1.9e-1) we observed at least a trend towards synergism. Bioinformatic modelling was performed by Emilia Salzmann-Manrique.

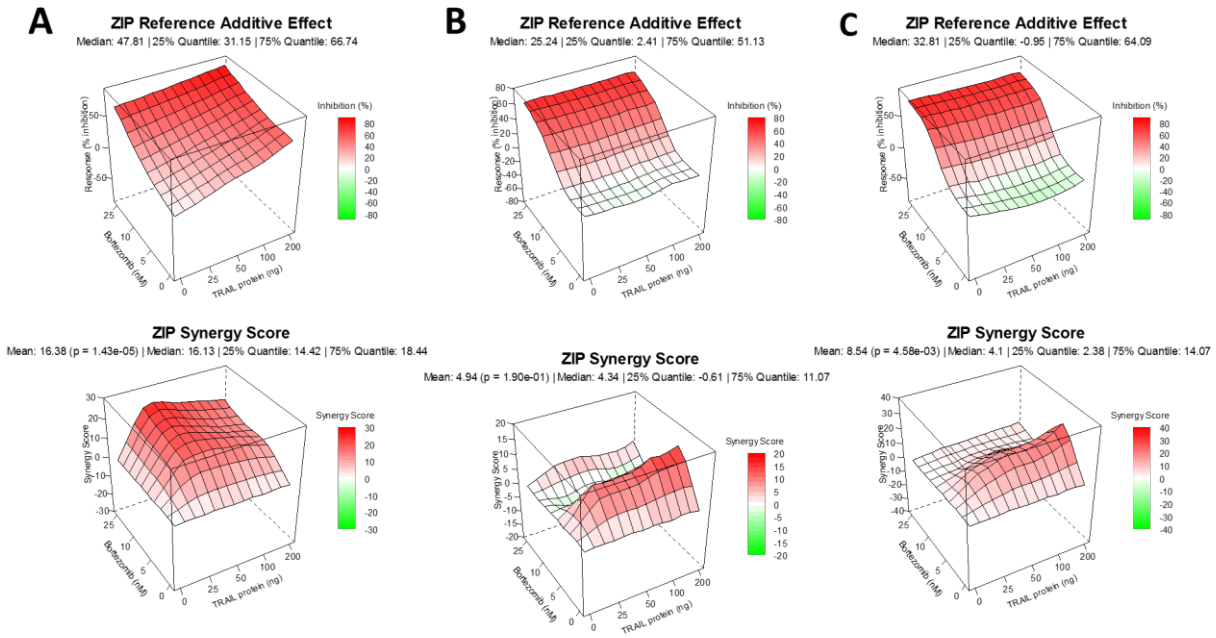

Figure 30: Synergistic or additive effects of bortezomib and TRAIL were analysed using the ZIP model. RH30 (A), RH41 (B) and RMS335 cells (C) were co-incubated with 0, 5, 10 or 50 nM bortezomib and 0, 25, 50, 100 or 200 ng purified TRAIL protein. The ZIP model was applied to the empirical data to identify synergistic effects. At least four independent experiments were used for modeling.

3.2.5.2.8 Sensitivity of NK-92/5.28.z cells to bortezomib

The proteasome inhibitor bortezomib may also affect NK-92/5.28.z cells. After five hours of co-incubation with 5, 10 and 25 nM bortezomib, no cytotoxic effects were observed against NK-92/5.28.z cells (Figure 31). However, after 24 hours of co-incubation up to 80% of the NK-92/5.28.z cells were lysed, indicating an cytotoxic effect through the bortezomib treatment. Therefore, the wash out and timing is crucial when combining bortezomib and NK-92/5.28.z cells for the treatment of metastatic RMS.

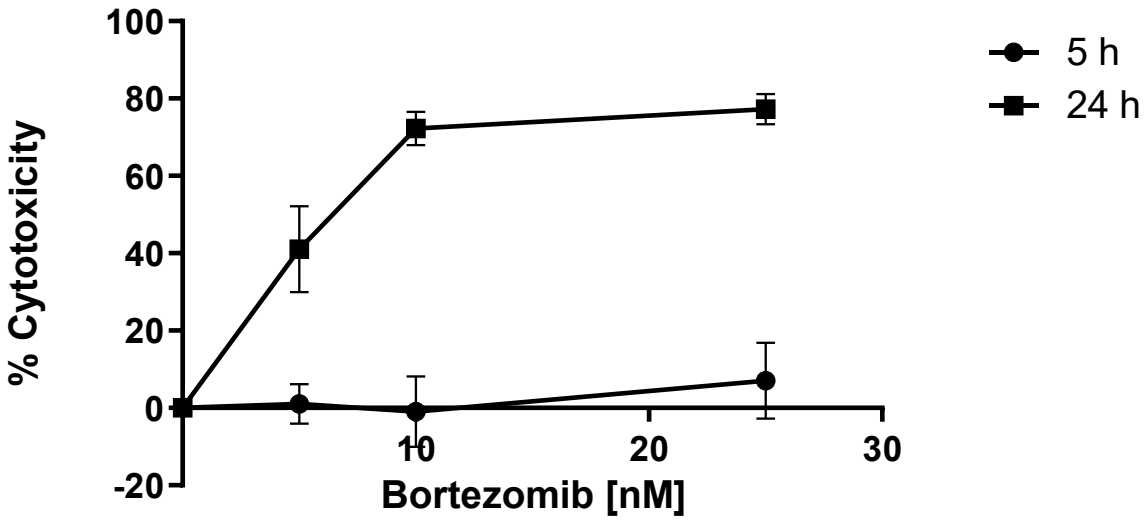

Figure 31: Sensitivity of NK-92/5.28.z cells to bortezomib. NK-92/5.28.z cells were incubated with 0, 5, 10 or 25 nM for 5 or 24 hours and lysed cells were quantified by CytoTox-Glo assay. The Mean ± SEM of four independent experiments is shown.

3.3 Non-viral Sleeping beauty transposon system for engineering of CIK cells

CIK cells lentivirally transduced with a similar ErbB2-specific CAR like that of NK-92/5.28.z cells showed high and specific cytotoxicity against RMS *in vitro* and *in vivo* [115]. Due to regulatory reasons, a non-viral method was considered for manufacturing of CAR-CIK cells. Manufacturing and clinical protocols are available for T cells generated in that manner [189]. Based on the publications of Magnani et al. [112, 113, 190] and experience with T cells [154, 191–193], a protocol for the SBTS-based transfection of CIK cells was established. First experiments were performed with MC Venus, a minicircle plasmid encoding eGFP instead of the CAR construct.

3.3.1 Protocol optimization

3.3.1.1 Proof of principle

CIK cells were nucleofected with SB100x mRNA and MC Venus at a 4:1 ratio or with MC Venus alone. Nucleofection was performed on day four of culture. GFP expression was analysed by flow cytometry on days seven, 10 and 14 (Figure 32). GFP signals decreased over time in cells nucleofected with MC Venus only. Whereas the GFP gene was stably expressed on CIK cells nucleofected with both MC Venus and SB100x mRNA.

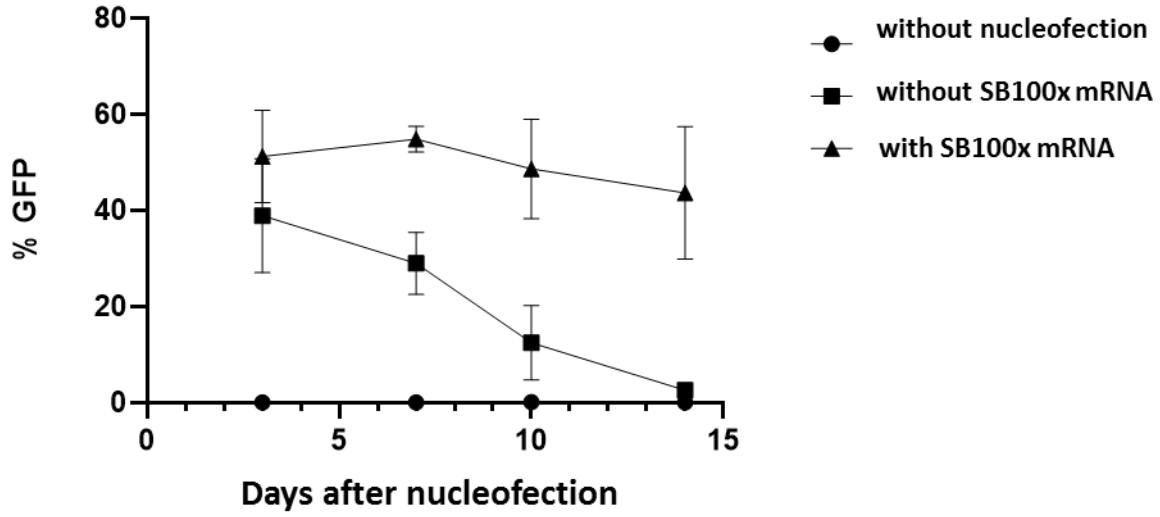

Figure 32: Stable integration of the GFP gene into the CIK cell genome. CIK cells were nucleofected with MC Venus or with MC Venus and SB100x mRNA. The GFP expression in CIK was monitored by flow cytometry until day 14 after nucleofection. Mean ± SEM of three independent experiments are shown.

3.3.1.2 Timing

In T cells a higher gene integration was observed in activated cells [174, 175]. In contrast, nucleofection was reported on day zero of the CIK cell manufacturing protocol [113]. Next, the optimal time point for CIK nucleofection was to be determined. With 45.0 ± 8.3 % GFP+ cells day zero revealed a lower

percentage of GPF expressing cells than days four (67.4 ± 12.3 %) and seven (64.2% ± 17.3 %) (Figure 33A). However, nucleofection on days zero and four resulted in an improved proliferation than seen on day seven (Figure 33B). Therefore, day four, resulting in a high number of GFP+ cells with high proliferative capacities was determined for nucleofection.

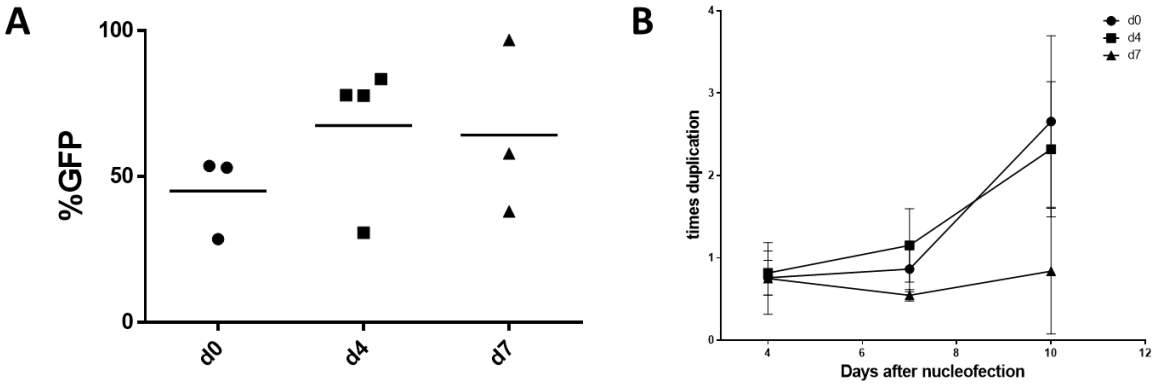

Figure 33: Timing of CIK modification by SBTS. CIK cells were nucleofected on day zero, four or seven of the CIK cell protocol. (A) GFP expression was analysed by flow cytometry on day 7 after nucleofection. (B) Cell number was determined on day four, seven and 10 after nucleofection and multiplication was calculated.

3.3.1.3 Autologous feeder Monocytes

Monocytes are essential for CIK cell manufacturing especially during the first days of *in vitro* culture. Feeder monocytes were added after the nucleofection to support activation and expansion of CIK cells. The percentage of GFP+ cells (Figure 34A) and proliferative capacities (Figure 34B) with and without the addition of autologous feeder cells is shown in Figure 34. Feeder monocytes did not significantly benefit the amount of GFP+ cells and proliferative capacities. Therefore, subsequent experiments were performed without feeder monocytes.

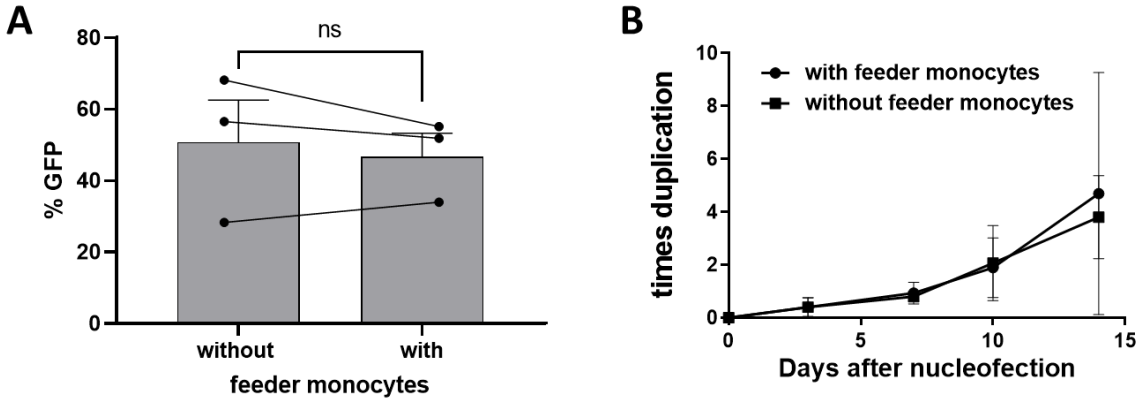

Figure 34: Addition of autologous feeder monocytes does not support CIK cells after nucleofection. After nucleofection, autologous feeder monocytes were added in a 1:10 ratio to support nucleofected CIK cells. (A) The percentage of GFP expressing cells was analysed by flow cytometry on day seven after nucleofection. (B) Proliferation of cultures with or without

feeder monocytes was followed until day 14. Mean ± SEM of three independent experiments are shown and unpaired Student´s t-test was performed.

3.3.1.4 Minicircle generation

Proof of concept experiments showed that integration of the GFP gene into the CIK cell genome by SBTS is possible. For the SBTS gene transfer of the ErbB2-CAR construct, the protocol was adapted. First, the ErbB2-CAR sequence with attached GFP, flanked by ITRs was cloned into a pT2 plasmid. Cloning was performed by Malena Bodden and resulted in the plasmid pT2-5.28.z. Nucleofection with the plasmid showed a stable integration into the cell genome of CIK cells (6.8 % GPF+ cells, Figure 35A). GFP expression was still detected at day 21, suggesting stable integration (Figure 35B). After demonstrating that the pT2-5.28.z plasmid is suitable for SBTS-based engineering of CIK cells, a minicircle (MC ErbB2-CAR) was generated by PlasmidFactory.

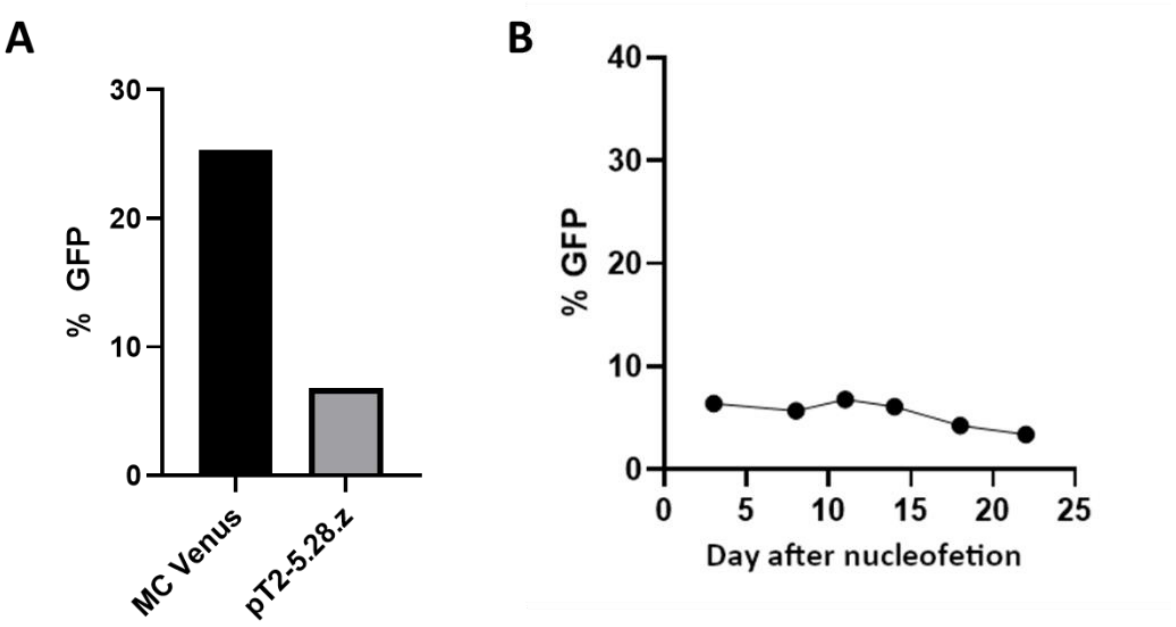

Figure 35: Stable integration of the CAR sequence into the genome of CIK cells. (A) CIK cells were nucleofected with pT2-5.28.z plasmid or MC Venus and mSB100x RNA. GFP+ expression was detected at day 11 after nucleofection. (B) The stable integration of the CAR sequence was analysed by the GFP reporter protein attached to the CAR by an IRES sequence.

3.3.1.5 GFP and CAR expression

As GFP is attached to the CAR sequence via an IRES sequence, the next step was to determine, if the GFP signal could be used for quantification of the CAR. Both, GFP expression and CAR expression are shown in Figure 36 . GFP signals corresponded with CAR expression levels.

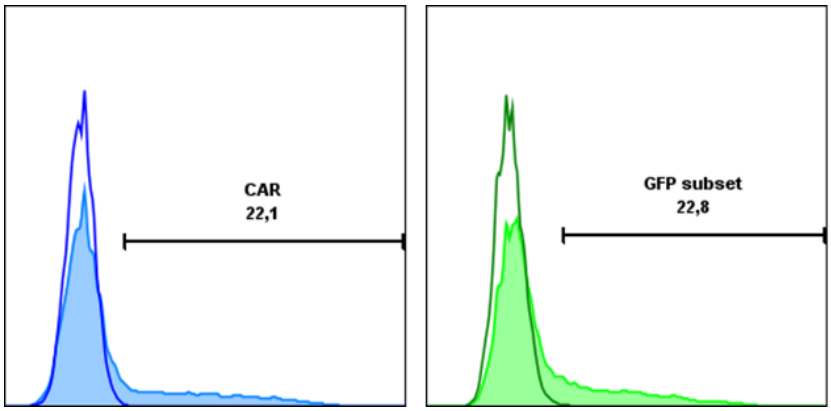

Figure 36: GFP expression is correlates with CAR expression. CAR integration by SBTS was analysed by indirect CAR detection with ErbB2-Fc chimera and secondary antibody staining or by the expression of the GFP attached to the CAR sequence via IRES sequence (filled histograms). Non-transfected CIK cells were used as controls (unfilled histograms). One representative out of three independent experiments is shown.

3.3.1.6 Timing

The optimal time point for nucleofection was determined with the MC ErbB2-CAR. CIK cells were nucleofected on days zero and three or on days zero and seven. The percentage of GFP+ cells and viability were analyzed by flow cytometry (Figure 37). Nucleofection on days zero or three resulted comparable rates in terms of transfection efficiency, viability and expansion (Figure 37). Nucleofection on day seven showed lower percentages of GFP+ cells, lower viability, and lower proliferation of CIK cells (Figure 37B). Therefore, days zero and three were considered suitable for SBTS-based transfection of CIK cells. As nucleofection on day zero allowed for shorter *in vitro* culture periods and higher numbers of ErbB2-CAR-CIK cells on day 10, this time point was chosen for subsequent experiments.

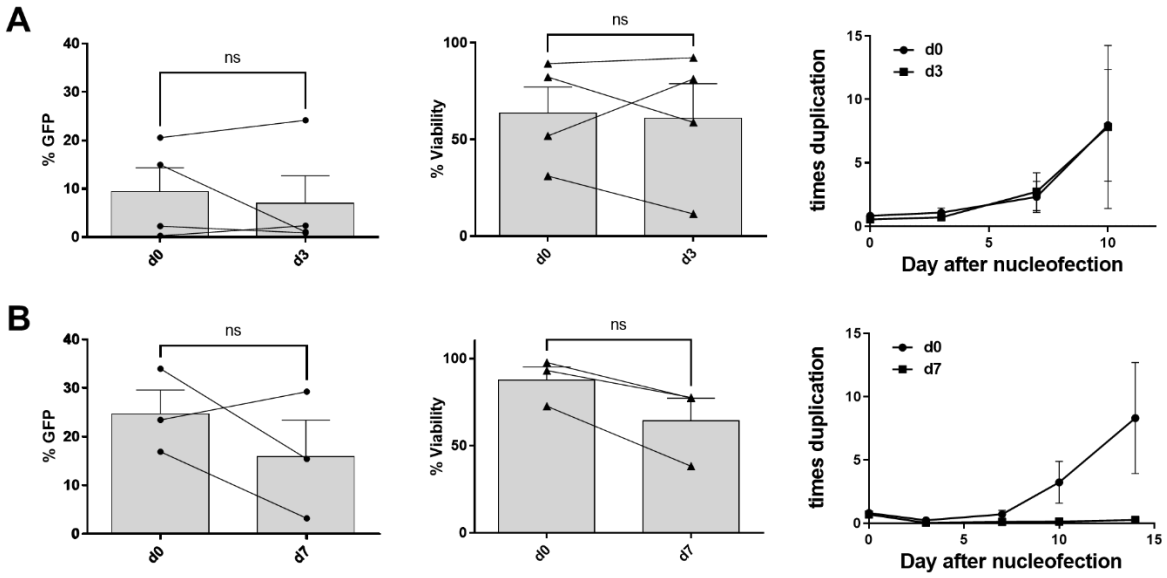

Figure 37: Nucleofection with MC ErbB2-CAR and SB100x mRNA on day 0, 4 or 7. (A) CIK cells from the same donor were nucleofected with SB100x mRNA and MC ErbB2-CAR in a 4:1 ratio on day zero or day three (n =4). The percentage of GFP+ cells and cell viability were analysed on day seven after nucleofection. (B) The experimental setup was performed accordingly

with CIK cells nucleofected on day zero and seven. Mean ± SEM of three independent experiments are shown and unpaired Student´s t-test was performed.

3.3.1.7 Autologous irradiated feeder PBMCs

Magnani et al. [113] used autologous feeder PBMCs to enhance viability and proliferation of SBTS CAR-CIK cells. PBMC feeder cells were irradiated with 30 Gy prior to use, to prevent overgrowth of PBMCs. With this, trends towards higher transfection efficacy and higher viability were observed. But, the addition of feeder PBMCs resulted in lower expansion rates of CIK cells. Therefore, addition of irradiated feeder PBMCs was not considered beneficial in this context.

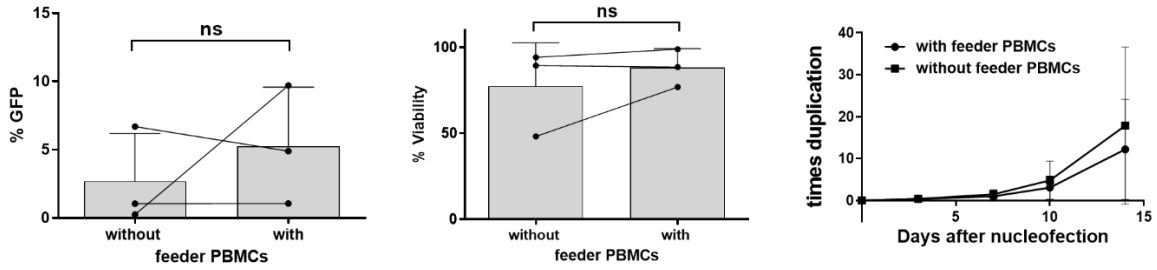

Figure 38: Irradiated autologous PBMCs were added as feeder cells to the CAR-CIK cells. CIK cells were nucleofected with SB100x mRNA and MC ErbB2-CAR on day zero and autologous PBMCs irradiated with 30 Gy were added as feeder cells. Nucleofected CIK cells without feeder cells were used as control. Mean ± SEM of three independent experiments are shown and unpaired Student´s t-test was performed.

3.3.1.8 Medium

The cell culture medium may impact differentiation, activation and expansion of CIK cells. RPMI is used as a standard medium for preclinical research [99]. X-Vivo10 medium supplemented with 5% FFP (X-Vivo+), which is designed to meet *in vitro* needs of NK cells, may also be beneficial for T-NK cells and T cells [108].

CAR-CIK cells from the same donors were cultured in RPMI or X-Vivo+ according to the CIK manufacturing protocol. While GFP expression was not affected by the X-Vivo+ medium, CAR-CIK cells showed significantly increased viability and proliferation rates up to 14 days after nucleofection (Figure 39A). Furthermore, the phenotype of CAR-CIK cells was altered towards a more cytotoxic population. The amount of T-NK, NK, and CD8+ T cells was increased, whereas CD4+ T cell numbers decreased (Figure 39B). Subsequent experiments were performed in the presence of X-Vivo10+ medium.

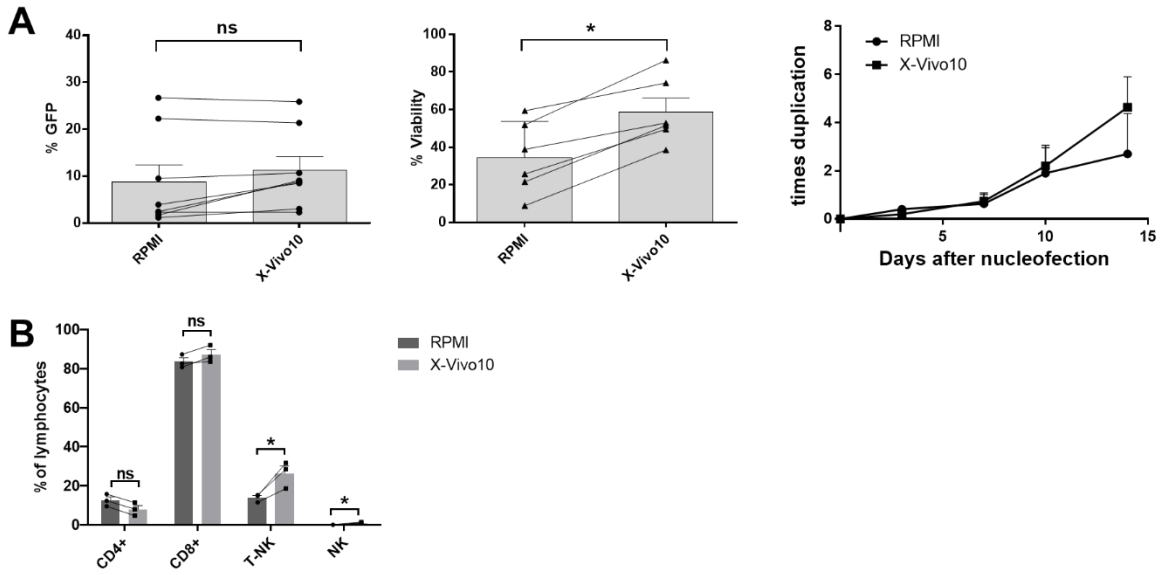

Figure 39: Cultivation of CAR-CIK cells in standard medium RPMI or NK cell medium X-Vivo 10. (A) After nucleofection, CAR-CIK cells were cultured in RPMI or X-Vivo10 supplemented with 5% FFP according to CIK cell protocol. GFP expression and viability were analysed on day 7 after nucleofection and cell proliferation was calculated. (B) The effect of the NK cell medium X-Vivo10 on the different CIK cell types including T cells (CD4 and CD8), T-NK and NK cells were compared to the phenotype in the standard medium RPMI. Mean ± SEM of at least three independent experiments are shown and unpaired Student´s t-test was performed.

3.3.1.9 MC:SB ratio

Beneficial effects of X-Vivo+ on the viability of CAR-CIK cells allowed for the usage of higher amounts of DNA resulting in higher CAR expression rates. 2 µg MC ErbB2-CAR was used at ratios of 4:2 SB100x mRNA to MC ErbB2-CAR. An increased GFP expression, but lower viability rate was observed (Figure 40A). At a ratio of 4:2, GFP-expression and viability were increased (Figure 40B). The usage of higher amounts of DNA achieved comparable total cell numbers at day 10 like seen with at the 4:1 ratio (Figure 40C). Therefore, the use of the 4:2 SB100x mRNA:MC ErbB2-CAR ratio was used in subsequent experiments.

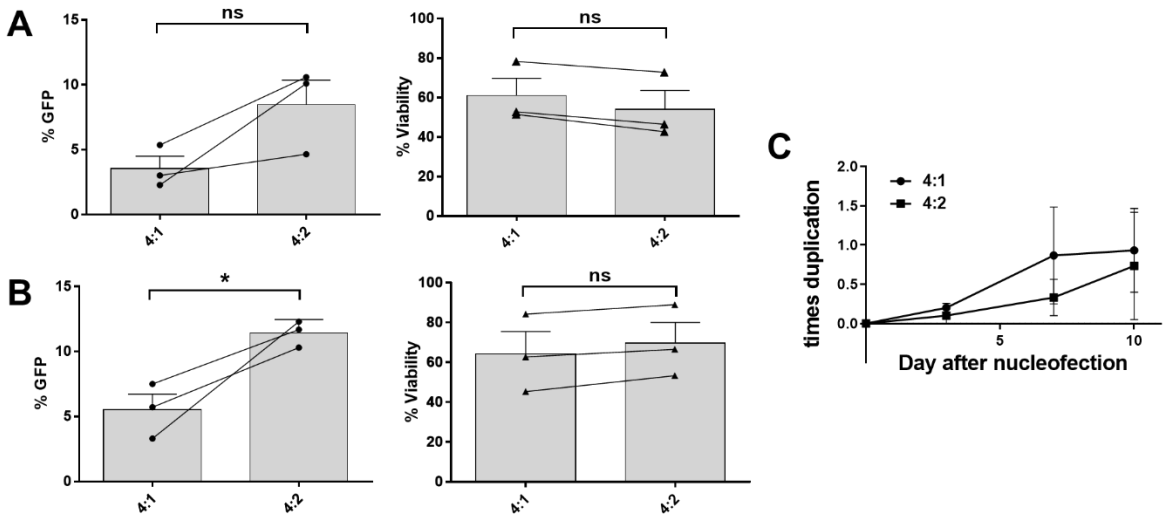

Figure 40: Nucleofection with 4:1 or 4:2 SB100x mRNA:MC ErbB2-CAR ratio. CIK cells were nucleofected with different SB100x mRNA: MC ErbB2-CAR ratios at day 0. GFP expression and viability were analysed at day seven (A) and day 10 (B). Mean ± SEM of three independent experiments are shown and unpaired Student´s t-test was performed.

3.3.2 Functional analyses

For functional analyses CAR-CIK cells were generated according to the conditions shown in Table 18. PBMCs were nucleofected on day zero with SB100x mRNA and MC ErbB2-CAR in a 4:2 ratio. The cells were cultivated in X-Vivo10 supplemented with 5% human FFP without the addition of feeder cells and were stimulated with cytokines according to the CIK cell protocol.

Table 18: Key aspects of the protocol for the non-viral generation of ErbB2-specific CAR-CIK cell via SBTS.

Timing	SB100x : MC ErbB2-CAR ratio	Medium	Feeder cells
Day zero	4:2	X-Vivo10 + 5% FFP(AB)	-

3.3.2.1 Stable CAR expression

The CAR expression of CAR-CIK was repetitive analysed over 28 cells by flow cytometry and showed that the CAR sequence was stably integrated into the CIK cell genome and that the percentage of cells expressing the CAR remained stable or even increases over time (Figure 41). GFP expression was donor-dependent and was not detectable before day seven. CAR-bearing cells (donor 1) increased from day seven to ten and remained stable thereafter. CAR-CIK cells generated from donor 2 increased to over 50% of CAR expressing cells on day 28. CAR expression of CIK cell subpopulations was analyzed on day ten (Figure 41). CAR expression was detectable in T, NK and T-NK CIK cell subpopulations.

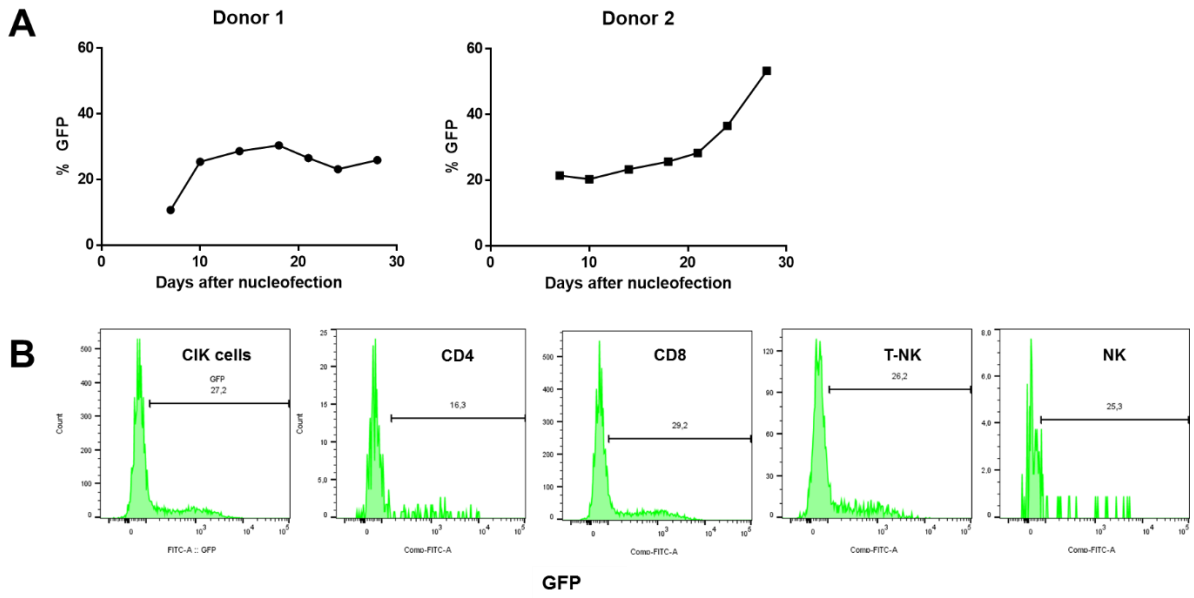

Figure 41: Stability of CAR expression and CAR expression in different CIK cell subtypes. (A) CAR expression was monitored for 28 days after nucleofection for two donors. (B) The CAR expression within the different cell types is shown in a representative example with an overall CAR expression of 27.2% on day 10.

3.3.2.2 Cytotoxicity

Finally, the criterion for the successful generation of SBTS ErbB2-CAR-CIK cells is their cytotoxic capacity against tumor cells. SBTS CAR-CIK cells superiorly lysed the ErbB2-positive aRMS cell line RH30 compared to parental CIK cells derived from the same donor (Figure 42). Therefore, the cytotoxic potential of the SBTS ErbB2-CIK cells was significantly enhanced by the expression of the 5.28.z CAR construct integrated by use of the SBTS. Even with low transfection rates of 7.21%.

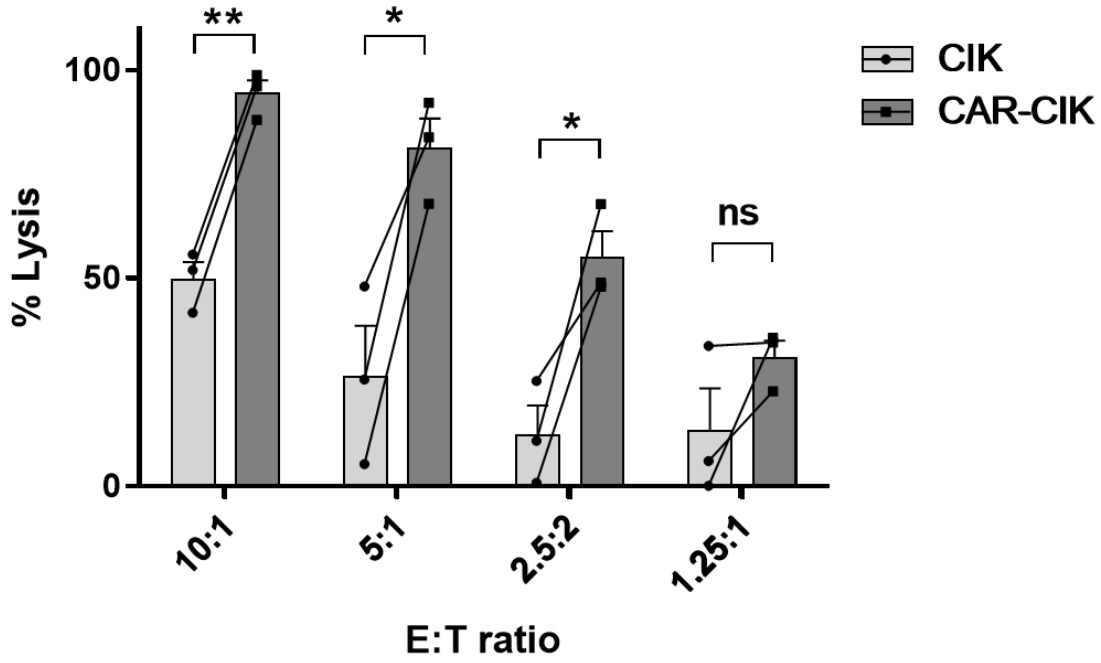

Figure 42: Cytotoxicity of CIK and CAR-CIK cells against the aRMS cell line RH30. The cytolytic capacity of CIK and CAR-CIK cells against RH30 cells was assessed in a 20 hour Luc Tox assay. Mean ± SEM of three independent experiments are shown and unpaired Student´s t-test was performed.

3.3.3 Comparison between lentiviral and SBTS generated CAR-CIK cells

In a final set of experiments, SBTS ErbB2-CAR-CIK cells were compared with LV ErbB2-CAR-CIK cells from the same donor. LV ErbB2-CAR-CIK cells were generated by Laura Moser and functional assessments were performed in close collaboration.

3.3.3.1 Phenotype and CAR expression

The lentiviral transduction resulted in higher CAR expression rates (39.3% ±10.9%) than the SBTS-based transfection (9.7% ± 3.6%). In contrast, SBTS CAR-CIK cells showed higher cell viability (81.2% ± 2.7%) than LV CAR-CIK cells (30.0% ± 6.8%) (Figure 43).

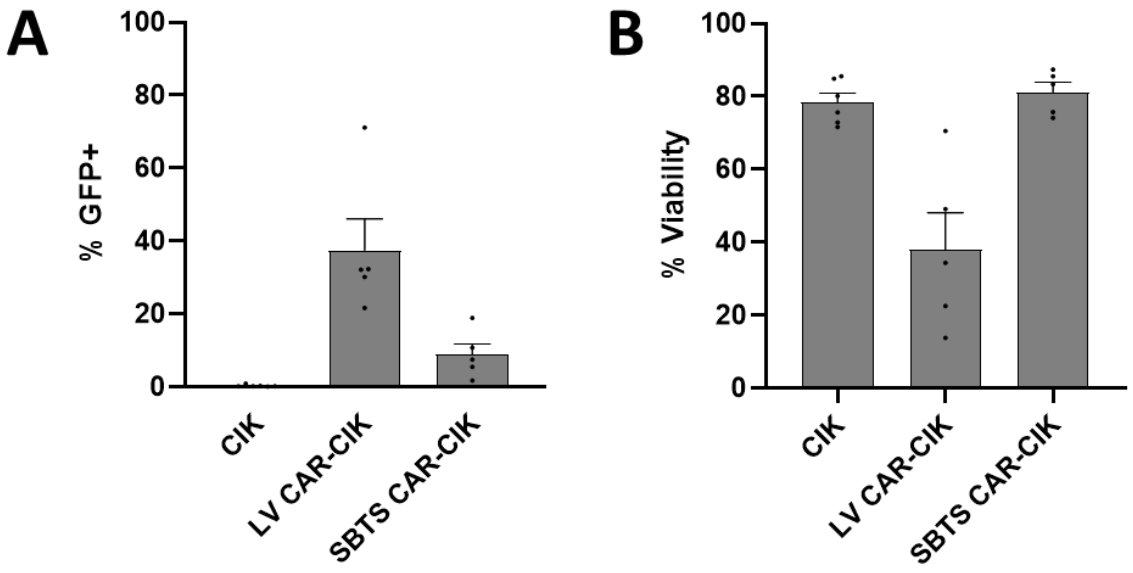

Figure 43: CAR expression and viability of CAR-CIK cells after lentiviral transduction or SBTS modification. (A) The CAR expression of CAR-CIK cells generated by lentiviral transduction or SBTS was analysed by flow cytometry using the GFP reporter protein. (B) In addition, viability was determined by flow cytometry using Zombie Violet dye. Parental CIK cells were used as controls.

The genetic modification was not equally distributed among CIK cell subpopulations (Figure 44A). The percentage of NK cells ranged from 1.2 % ± 0.4 % among parental CIK cells to 2.1 % ± 0.4 % among LV CAR-CIK cells and 0.6 % ± 0.1 % among SBTS CAR-CIK cells. The percentage of T cells was 82.4 % ± 4.5 % (parental CIK cells), 71.7 % ± 4.2 % (LV CAR-CIK cells), and 45.5 % ± 4.2 % (SBTS CAR-CIK cells). The percentage of T-NK cells was 16.1 % ± 4.8 % within parental CIK cells, 24.8 % ± 4.8 % within LV CAR-CIK cells, and 53.6 % ± 4.4 % within SBTS CAR-CIK cells. However, as SBTS CAR-CIK cells, unlike parental CIK cells and LV CAR-CIK cells were cultured in X-Vivo+, the higher proportion of T-NK cells may also be caused by the medium and not exclusively by the genetic modification. T-NK cell populations showed a CD8+ cytotoxic phenotype in SBTS CAR-CIK cells (98.5 % ± 0.3 %), LV CAR-CIK cells (79.9 % ± 4.0 %), and parental CIK cells (76.9 % ± 3.4 %). The same trend was observed for CD8+ T cell subpopulations (SBTS CAR-CIK cells, 88.5 % ± 2.0 %; parental CIK cell, 73.0 % ± 3.6 %; LV CAR-CIK cells, 38.6 % ± 2.2 %) (Figure 44B). In addition, T and T-NK cell subpopulations among SBTS-modified CAR-CIK cells exclusively showed a late effector memory phenotype. Parental and LV CAR-CIK cells were composed of naïve, central and effector memory cells (Figure 44C). Thus, SBTS CAR-CIK cells showed a highly cytotoxic phenotype.

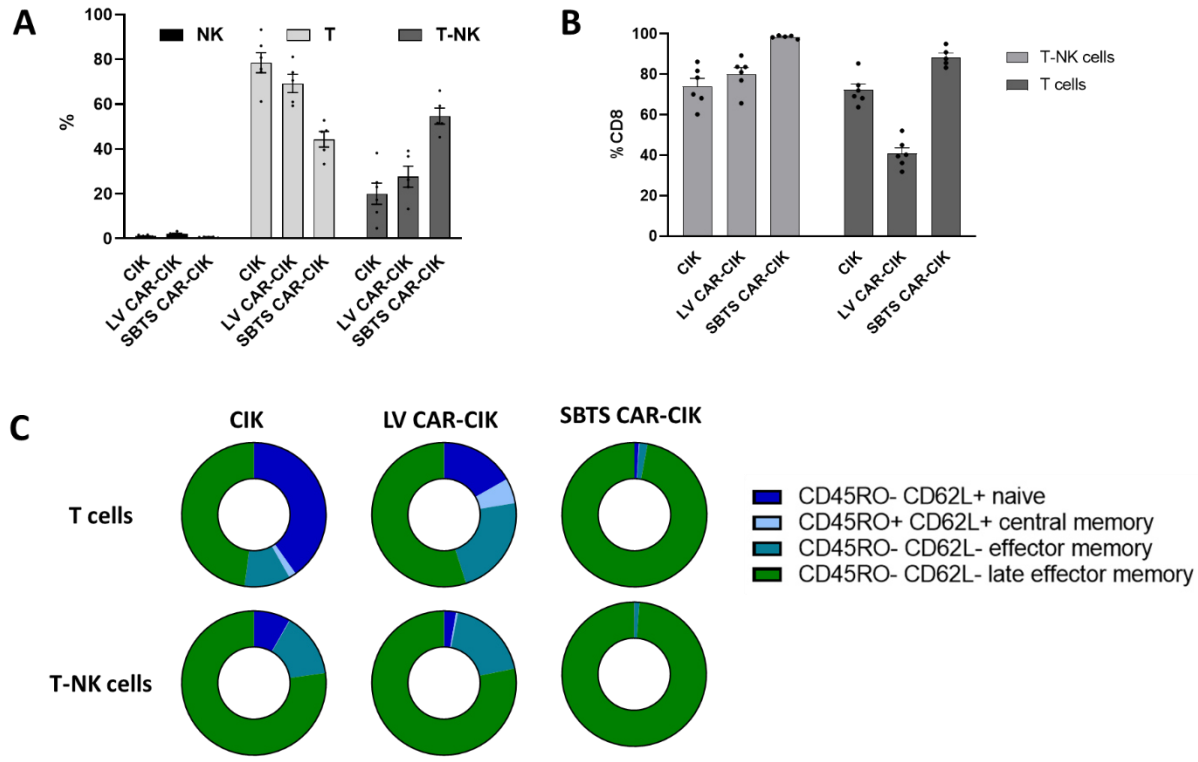

Figure 44: CAR-CIK phenotype. (A) Distribution of CAR-CIK cell subpopulations after lentiviral of SBTS modification. (B) Proportion of CD8+ cells within T-NK and T cells. (C) Memory phenotype within T (upper row) and T-NK (lower row) populations.

3.3.3.2 Cytotoxicity

2D cytotoxicity was assessed in a 20 hour Luc Tox assay against RH30 cells (Figure 45). SBTS CAR-CIK cells were more efficient in killing of RH30 cells than LV CAR-CIK cells, even at low E:T ratios of 2.5:1. Of note, CAR expression ranged from 13.1 % to 25.4 % among SBTS CAR-CIK cells, whereas CAR expression among lentivirally transduced cells was 22.9 % to 69.6 %.

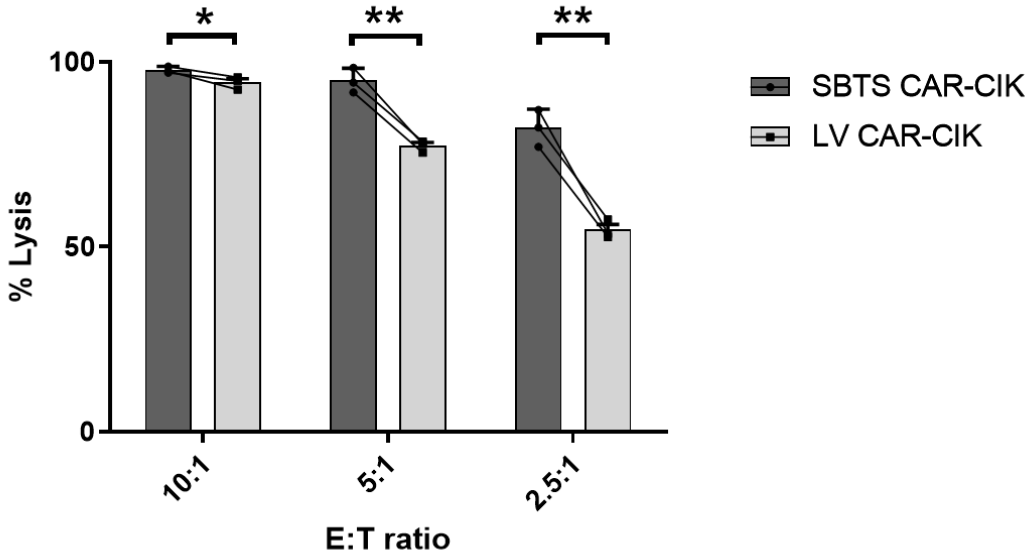

Figure 45: Cytotoxicity of CAR-CIK cells generated by viral transduction or SBTS. CAR-CIK cells from the same donor were virally transduced or were nucleofected with SBTS and cytotoxicity against RH30 was assessed on day 10 of CIK cell culture in a 20 hour Luc Tox assay. Mean ± SEM is shown and unpaired Student´s t-test was performed.

3.3.3.3 Spheroids

In a 3D long-term spheroid assay, SBTS and LV CAR-CIK cells were added to RH30 spheroids, while parental CIK cells and untreated spheroids served as controls (Figure 46). 25,000 parental CIK or SBTS and LV CAR-CIK cells effectively killed tumor spheroids. 12,500 effector cells inhibited tumor growth. The highest cytotoxic effect was observed with LV CAR-CIK cells.

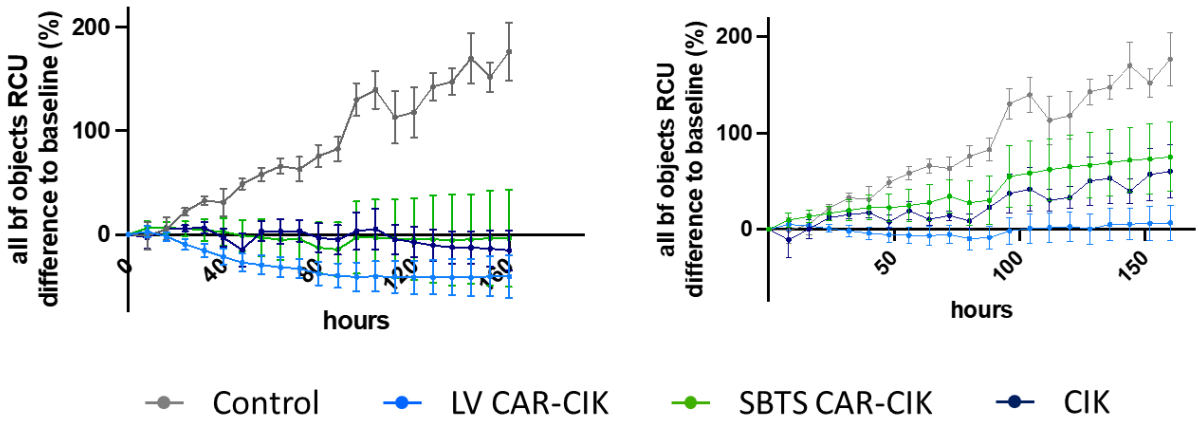

Figure 46: Long-term spheroid assay. RH30 spheroids were co-incubated with 25,000 (left) or 12,500 (right) parental CIK cells (dark blue), lentiviral (light blue) or SBTS modified CAR-CIK cells (green). Untreated spheroids were used as controls (grey). Growth was monitored for 160 hours and spheroid size was quantified by the red fluorescence signal of the RH30 cells.

3.3.3.4 In vivo experiment

LV CAR-CIK cells (96.5 ± 7.2 days) prolonged the survival of mice carrying a RH30 metastatic xenograft. Median survival was not significantly different with SBTS CAR-CIK cell (64 ± 6.4 days), or parental CIK cell treatment (median survival: 60 ± 12.3 days) compared to untreated control animals (63 ± 6.9 days) (Figure 47). Of note, in contrast to parental CIK cells and LV CAR-CIK cells, SBTS CAR-CIK cells were not detectable in murine organs by flow cytometry.

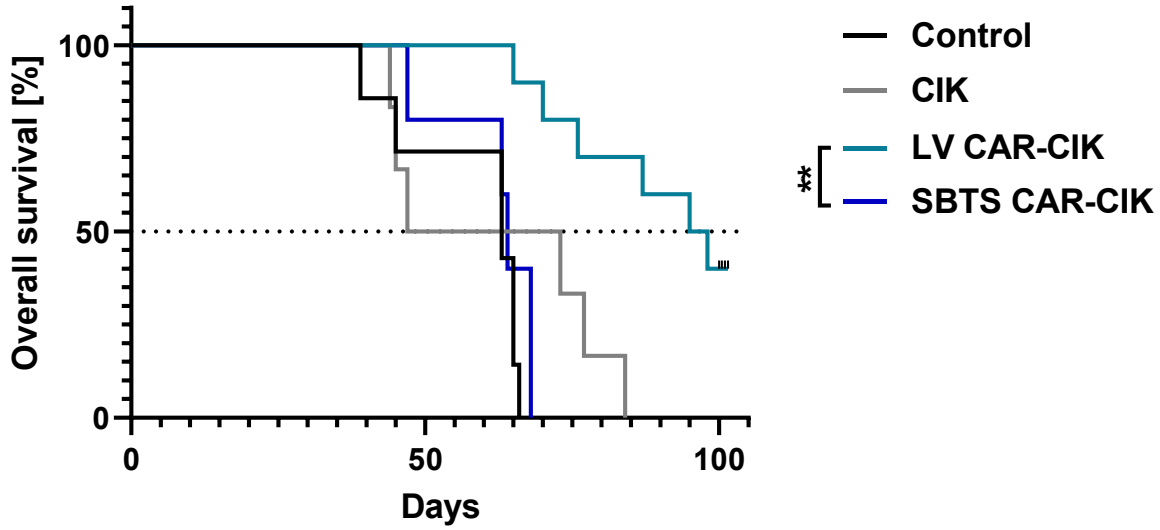

Figure 47: Lentiviral but not SBTS-modified CAR-CIK cells prolonged the overall survival in an aRMS xenograft model. Animals showing visible signs of disease progression, physical abnormalities or discomfort were sacrificed. Animals without health problems were followed until the end of the experiment on day +100. The overall survival of untreated (n=7), animals treated with parental CIK cells (n=6), LV CAR-CIK (n=10) or SBTS CAR-CIK cells (n=5) is shown. Statistical analysis was performed using the log-rank test (Mantel-Cox).

In conclusion, the genetic modification of CIK cells by non-viral SBTS resulted in lower CAR expression levels but higher viability *in vitro*, but not *in vivo*. SBTS ErbB2-CAR-CIK cells showed a more cytotoxic CD8+ late effector memory phenotype with a higher short-term cytotoxicity than LV ErbB2-CAR-CIK cells. But, LV ErbB2-CAR-CIK cells possessed a higher long-term cytotoxicity against 3D aRMS spheroids *in vitro*, and prolong survival of NSG mice carrying a metastatic RMS xenograft.

4 Discussion

4.1 NK-92/5.28.z

Metastatic RMS remains a major unmet medical need in pediatric oncology. For RMS therapy in general significant progress was made in the last 30 years, whereas for metastatic RMS no significant advances have been and durable remissions are not achieved with standard treatments such as radiation, chemotherapy and surgery [11, 194]. The reported complete and durable remission of a child with metastatic RMS after CAR-T cell therapy demonstrated the feasibility of immunotherapy as a safe and effective therapy for RMS [128]. Nevertheless, CAR-T cells occasionally induce severe CRS and/or ICANS and are hampered by limited infiltration and immunosuppressive effects in solid tumors [87, 195]. The intrinsic natural cytotoxicity of NK-92 cells is mainly mediated by signaling though activating NK receptors and is less prone to antigen loss than MHC restricted T cells [196]. Therefore, the use of innate immune cells as carriers for CAR therapy may lead to even more efficient CAR therapies. Previous studies have demonstrated specific recognition and destruction of ErbB2-positive breast carcinoma [55], glioblastoma [176] and also RMS cells [26] by ErbB2-specific CAR-NK cell line NK-92/5.28.z. NK-92/5.28.z demonstrated efficient and specific lysis of aRMS cell lines and patient-derived tumor organoids *in vitro* in 2D short term cytotoxicity assays. In contrast to parental NK-92, which only inhibited RH30 spheroid growth, NK-92/5.28.z cells sufficiently lysed 3D aRMS spheroids, indicating infiltration and long-term cytotoxic potential of the NK-92/5.28.z cells. Therefore, the CAR-NK-92 cell line NK-92/5.28.z is capable of lysing aRMS cells by both CAR mediated and innate immune cell mechanisms, despite the low and heterogenous ErbB2 expression on aRMS tumors. Due to the malignant origin of NK-92 cells, parental cells and derivatives must be irradiated prior to clinical application to prevent uncontrolled outgrowth [91]. While the irradiation with 10 Gy inhibited the proliferation of NK-92/5.28.z cells, the cells remained cytotoxic against aRMS cell line RH30 for at least 24 hours, in agreement with previously reported data [91]. Based on the specific and highly cytotoxic properties of NK-92/5.28.z cells against RMS *in vitro*, it can be assumed that serial injections of the innate CAR-NK cell line NK-92/5.28.z may translate in a safe, effective and affordable therapy for RMS.

Therefore, these cells were evaluated in a preclinical xenograft model for metastatic aRMS. In immunodeficient NSG mice MRD was mimicked by injection of RH30 cells. The developed tumors retained the RMS phenotype and expressed characteristic RMS markers such as MyoD, Desmin and Myogenin. While parental NK-92 cells inhibited tumor growth but did not significantly prolonged survival compared to untreated controls, the serial application of NK-92/5.28.z cells prolonged the overall survival significantly compared to untreated controls and also NK-92-treated animals. The sequential application of NK-92/5.28.z reduced the tumor burden significantly and furthermore inhibited the tumor engraftment completely in two out of ten mice completely. Three additional

injections of NK-92/5.28.z into tumor bearing mice on day 42 again demonstrated inhibition of disease progression as long as the CAR cells were administered, but no durable remission. This response to the second course of NK-92/5.28.z application also indicated that the tumor cells are still accessible for the NK-92/5.28.z and suggesting that no antigen-loss occurred. Notably, both parental and CAR-NK-92 cells infiltrated the tumor tissue as well as the spleen as secondary lymphatic organ after the distribution by the blood stream. The immune effector cells were detected in the organs for up to 56 days after the last application by qPCR and flow cytometry indicating homing, activation and persistence at the tumor sites. Irradiation of NK-92/5.28.z prior to injection prevented the persistence of the CAR-cells, but also resulted in a lower inhibition of tumor growth than that obtained by non-irradiated cells, most likely due to the limited life span and the lack of persistence. Nevertheless, the sequential application of irradiated NK-92/5.28.z cells inhibited the tumor engraftment compared to untreated control animals. Establishing suitable RMS xenograft models and in particular for the evaluation of adoptive immunotherapy, is difficult but can be achieved by using immunodeficient mice. However, in this model lacking almost all immune cells, the priming of autologous immune cells as bystander cells by the NK-92/5.28.z cannot taken into account. This immunomodulatory effect on the hosts immune system has been described by Zhang et al. [92] and is based on a crosstalk between NK-92/5.28.z cells and host dendritic cells, resulting in an immune response and immunological memory, which is particularly important as irradiated NK-92/5.28.z do not persist. Therefore, the attraction and priming of other immune cells is crucial for a durable long-term anti-tumor memory.

However, solid RMS tumors are challenging for NK-92/5.28.z cells due to the low TAA expression and the immunosuppressive TME. Combinational treatment with immune checkpoint blockade or anti-tumor agents/small molecules may lead to improved treatments. PD-1 blocking antibodies are often used in combination with CAR-T cell therapies, resulting in improved efficiency especially in solid tumors [197, 198]. Despite the low expression of PD-1 of NK cells, it has been shown, that the efficiency of NK cells can also be increased by PD-1/PD-L1 blockade [198, 199]. PD-L1 is expressed on 20% of RH30 cells, and it had also been detected on patient-derived tumor organoids and autopsies of RMS tumors [124]. Blocking PD-1 on NK-92/5.28.z resulted in a higher but not significantly increased lysis of RH30 cells *in vitro*. However, *in vivo,* the combination of NK-92/5.28.z and PD-1 antibody may not only support CAR-NK-92 cell cytotoxicity, but also prevent exhaustion of bystander T cells attracted by the NK-92/5.28.z-mediated RMS cell lysis.

The proteasome inhibitor bortezomib was investigated as another agent to enhance the specific lysis of NK-92/5.28.z cells. The efficient combination of CAR-NK-92 cells and bortezomib against renal carcinoma was previously demonstrated in a xenograft model [146]. The aRMS cell lines RH30 and RH41 and the patient-derived tumor organoid cells RMS335 were sensitive to single treatment with

bortezomib at low nanomolar concentrations with EC_{50} values ranging from 6.1 to 29.6 nM. Bortezomib dose-dependent caspase-3 cleavage and caspase-3/-7 activation indicated an caspase-mediated apoptosis. In addition, the expression of the TRAIL receptor DR5, but not DR4 was upregulated by bortezomib in a dose-dependent manner. JNK [181, 200], c-Rel [182, 183, 200]and p53 [179, 180] have been reported as regulators for DR5 expression. Therefore, the aRMS cell lines were examined these proteins by Western blot upon bortezomib treatment. Dose-dependent activation of JNK, a regulator of many cellular processes including apoptosis and proliferation [201, 202], indicated the involvement of this pathway in the DR5 upregulation. Despite the low level of TRAIL expression on NK-92/5.28.z cells, the combinatorial treatment of aRMS cell lines RH30 and RH41 and patient-derived tumor organoid cells RMS335 with bortezomib and NK-92/5.28.5 resulted in significantly higher tumor cell lysis than single agent treatment. Notably, the co-incubation with NK-92/5.28.z cells resulted in an increased level of DR4 mRNA in RH30 and RH41 cells, but was not correlated with an increased surface protein expression. The DR4 mRNA levels were also not affected by bortezomib single treatment. Some aRMS, such as RH41 are known to be resistant to TRAIL mediated apoptosis [130]. Various TRAIL-resistant cancers can be sensitized by bortezomib towards TRAIL-mediated apoptosis [142, 143, 203] and Jane et al. [203] showed that this sensitization is mediated by the inhibition of the canonical NFκB pathway specifically p65. Therefore, the NFκB aan related pathways were analyzed in TRAIL-sensitive RH30 and TRAIL-resistant RH41 cells treated with bortezomib or NK-92/5.28.z single and combinatorial treatment using qPCR and western blot. Interestingly, no inhibition of the canonical NFκB was observed in aRMS cells by bortezomib, but increased p100 mRNA levels were detected by qPCR, but not enhanced p100 protein expression. Hence, increased accumulation of p-p100 protein may be due to inhibited proteasomal degradation, resulting in a blockade of the non-canonical NFκB pathway. Of note, p52, the transcription factor processed from activated p100 is known as driver for tumor progression [204–206]. Additional, single treatment with bortezomib or NK-92/5.28.z and also combinatorial treatment enhanced p-JNK levels, a protein regulating both cell proliferation and cell death [202], suggesting signaling towards cell death in this setting. Last, NK-92/5.28.z and combinatorial treatment resulted in an increased caspase-3 cleavage in aRMS cells. Therefore, the combinatorial treatment with proteasome inhibitor bortezomib and NK-92/5.28.z immunotherapy mediates apoptosis by interacting with various pathways.

Synergistic effects between bortezomib and TRAIL-mediated apoptosis were investigated by further experiments with purified TRAIL protein to exclude non-TRAIL-mediated cytotoxicity of NK-92/5.28.z cells. a synergism between bortezomib treatment and TRAIL-mediated apoptosis was observed in TRAIL-sensitive RH30, but also in TRAIL-resistant RMS335 cells. The TRAIL-resistant aRMS cell line RH41 also responded to combinatorial treatment with bortezomib and TRAIL protein and showed at least a trend towards synergy. Therefore, the cytotoxicity of the clinical usable NK-92/5.28.z against aRMS can

be supported by proteasome inhibitor bortezomib at least *in vitro.* However, NK-92/5.28.z cells are also sensitive to bortezomib treatment after 24 hour co-incubation, but no such effects were observed after 5 hours. Thus, the timing of administration *in vivo* is crucial. The feasibility of combinatorial treatment with bortezomib and CAR-NK-92 cells *in vivo* has already been demonstrated by Zhang et al. [146]. In addition, bortezomib may have a beneficial effect on the bystander T cells recruited by the NK-92/5.28.z cells via dendritic cell priming. Previously, immunomodulatory effects of bortezomib have been described, such as augmenting T cell signaling within the TME [151] and enhancing the effector molecule expression of CD8+ T cells [150].

4.2 Sleeping beauty CIK cells

CIK cells are a heterogenous cell population consisting of T, T-NK and NK cells and therefore combining innate and adaptive immune responses with a high cytotoxic capacity against different cancers [106, 107]. CIK cells generated by an improved protocol including IL-15 stimulation are approved by the National Authority (Paul-Ehrlich-Institute) as ATMP [108]. Merker et al. demonstrated the feasibility of lentiviral transduction with an ErbB2 specific CAR of these cells, resulting in a specific and increased RMS tumor cell lysis *in vitro* [111]. In a metastatic RMS xenograft model these CAR-CIK cells inhibited the tumor engraftment and therefore prolonged the disease free survival significantly [115]. Integrating foreign DNA in a cells genome bears always the risk of insertional mutagenesis and oncogenic transactivation. Thus, the method for genetic modification for adoptive cell therapy must be selected carefully. While genes transferred by viral transduction commonly integrate into active transcription units, SBTS integration is distributed by a close-to-random profile, resulting in a higher genetic safety [162]. Hence, the generation of ErbB2-specific CAR-CIK cells should be transferred to a non-viral modification by SBTS. Previously was shown that higher transfection rates and cell viability are achieved by the use of minicircles instead of plasmids [154] and the hyperactive SB100x [163]. Hence, first proof-of-principle experiments were conducted with SB100x mRNA and MC Venus, a minicircle coding eGFP, and demonstrated the stable integration of the GFP gene in the CIK cells genome, whereas the nucleofection with MC Venus but without SB100x mRNA resulted in a transient expression of GFP, tampering within 18 days. Since nucleofection is a harsh method this process affects the viability and proliferation of the CIK cells. The addition of autologous monocytes as feeder cells and mediators development for CIK cell phenotype [101] neither supported the CIK cell proliferation nor enhanced the transfection efficiency . While reports for gene transfer by SBTS in CIK cells are limited to the experiences of an Italian group [112, 113], for T cells more knowledge is available. Thus, a higher transfection efficiency for activated compared to resting T cells was reported [174, 207], indicating the importance of the appropriate timing for nucleofection. The transfection efficiency and

the proliferation capacity or CIK cells after nucleofection with MC Venus and SB100x mRNA on day zero, four and seven of CIK cell culture was examined. Day four of CIK cell culture was chosen as the transduction for the generation of lentiviral CAR-CIK cells is performed on this time point of CIK culture. While the nucleofection of activated CIK cells on day four and day seven lead to higher transfection efficiency compared to resting CIK cells on day zero, the cells nucleofected on day seven were hampered in their proliferation. Therefore, nucleofection of CIK cells on day four of CIK protocol result in high transfection efficiency combined with high proliferative capacity for MC Venus, confirming the better modifiability of activated lymphocytes. Therefore, SBTS is feasible for the gene transfer from MC Venus in the CIK cell genome.

Next, the 5.28.z CAR was cloned in a pT2 plasmid to provide the ITR sequences required for the gene transfer by SBTS. The functionality of the pT2-5.28.z plasmid was examined in a preliminary experiment, resulting in a low but stable transfection efficiency. Since the plasmid was proven functional, it was used for the MC ErbB2-CAR generation by PlasmidFactory. Of note, the GFP protein attached to the CAR sequence equals the CAR expression and therefore can be used for transfection efficiency analysis. For the MC ErbB2-CAR also the best time point for transfection was determined. As experiments with MC Venus had shown a higher transfection of anti-CD3/CD28 activated lymphocytes, day three instead of day four was chosen to further benefit from the early activation in line with the transfection on the day after activation in T cell SBTS protocols [154]. Beside a low transfection efficiency and viability, transfection on day seven hampers the proliferation severely compared to transfection on day zero. Nevertheless, transfection on day zero and day three resulted in similar efficiency, viability and proliferative capacity. Since CIK cells do not proliferate in the first three days of culture, nucleofection on day three has no benefit regarding the initial cell number, whereas transfection on day zero results in higher cell numbers on day 10, the harvest day of CIK products due to a longer recovery time, thus in subsequent experiments cells were nucleofected on day zero. Magnani et al. [113] also use CIK cells/ PBMCs on day zero of CIK cell culture to generate CAR-CIK cells by SBTS, and additionally add irradiated, autologous PBMCs as feeder cells. Thus, the addition of autologous PBMCs irradiated with 30 Gy were to CIK cells directly after nucleofection on day zero was assessed. However, neither an increased transfection efficiency nor an increased viability or higher proliferation was observed for ErbB2-CAR-CIK cells. As the addition of feeder cells had no beneficial effect on the, in a next step the culture medium as another substantial factor for the welfare of cell growth influencing the nucleofection efficiency of lymphocytes [207] was focused. X-Vivo 10 medium, a medium originally designed for the needs of NK cells, was compared with standard medium RPMI. While the transfection rate was not affected, cells cultured in X-Vivo 10 medium showed significantly increased viability resulting in a higher proliferation. In addition, the NK cell medium significantly encouraged the development of T-NK cells, the characteristic CD3+/CD56+ double-positive population

in CIK cells , and supported the survival of NK cells. The higher viability favoured by X-Vivo 10 medium permitted the usage of a higher DNA amount. Thus, instead of a 4:1 SB100x mRNA:MC ErbB2-CAR ratio, a 4:2 ratio was used resulting in a significant higher amount of GFP expressing cells on day 10, while the viability and also the proliferation was not negatively affected. Summarised, $2x10^6$ PBMCs are nucleofected on day zero of CIK culture with T cell pulse EO-115 and are cultivated without feeder cells in X-Vivo10 medium supplemented with human fresh-frozen plasma according to the CIK cell protocol. Of note, the nucleofection of CIK cells with T cell pulse EO-115 lead to a CAR expression in all cell subtypes including NK cells in distinct amounts and also a stable, permanent CAR expression for at least 28 days. The SBTS generated CAR-CIK cells exhibited a clearly enhanced cytotoxicity against aRMS cell line RH30 in a 20 hour short-term assay.

After protocol establishment CAR-CIK cells generated by SBTS or lentiviral transduction were compared. Lentiviral transduced cells were modified with an higher efficiency than SBTS CAR-CIK cells, but were less viable. On day 10 of CIK culture, in lentiviral CAR-CIK cells T cells were more predominant than T-NK cells, while in SBTS CAR-CIK cells the reversed proportion was observed. NK cells were accounting for only a low number of cells within both cultures. Of note, lentiviral CAR-CIK cells were cultured in RPMI medium, whereas SBTS CAR-CIK cells were cultured in X-Vivo10 medium adapted to the needs of NK and T-NK cells, which may lead to the different subtype proportions. Nearly 100% of the T-NK cells in SBTS CAR-CIK cells were CD8+ cells, while this subpopulation accounted for only 80% of viral CAR-CIK cells. Also for T cells more than 90% of SBTS CAR-CIK cells were CD8+, while less than 50% of the viral CAR-CIK cells were CD8+. In SBTS CAR-CIK cells over 95% of both T-NK and T cells were CD45RO-/CD62L- late effector memory cells, while in viral CAR-CIK cells only 80% of T-NK and 50% of T cells were late effector memory cells and higher percentage of naïve, central memory and effector memory cells were still present. The SBTS CAR-CIK phenotype indicated a highly cytotoxic cell population, which indeed led to a significant higher lysis of RH30 cells compared to viral CAR-CIK cells in short-term *in vitro* assays. However, in long-term 3D spheroid assays the viral CAR-CIK cells lysed the RMS cells more efficient than SBTS CAR-CIK cells, mainly supported by long term effects of CD4+ memory cells. This was also observed in a RH30 xenograft model, where viral CAR-CIK cells persisted and prolonged the survival of animals, whereas SBTS CAR-CIK cells did not provide a life prolonging effect compared to untreated controls. Of note, SBTS CAR-CIK cells did not persisted in the organs of the animals, whereas viral CAR-CIK cells were detected at the end of experiment. Thus, the highly cytotoxic CD8+ dominated SBTS CAR-CIK cells exhibit a sufficient tumor cell lysis in short-term *in vitro* assays, but is not able to inhibit the tumor engraftment and persist *in vivo* due to lacking cell memory provided by CD4+ cells. This cytotoxic phenotype is favoured by the X-Vivo10 medium, therefore the protocol could be adapted using another medium supporting the viability but not affecting the

phenotype. However, the CAR expression, viability and proliferative capacity of CAR-CIK cells of both viral transduction and SBTS is highly donor dependent.

5 Conclusion & Outlook

In this work different ErbB2-specific CAR-cell therapies for the treatment of metastatic RMS were evaluated in preclinical *in vitro* and *in vivo* models. The already therapeutically used, off-the-shelf product NK-92/5.28.z showed excellent CAR-specific cytotoxicity against RMS cell lines and patient-derived tumor organoids in 2D and 3D assays *in vitro*. In addition, the proliferative capacity of NK-92/5.28.z was abolished by irradiation, whereas the cytotoxic potential was retained for at least 24 hours. In a xenograft model carrying a RH30 minimal residual disease NK-92/5.28.z inhibited tumor growth compared to parental NK-92 and untreated controls and therefore prolonged survival of these animals. Despite complete remission in two out of thirteen animals, NK-92/5.28.z treatment inhibited tumor growth as long as it was administered, but tumor growth progressed as shortly after last NK-92/5.28.z cell injection. *In vitro* assessment showed significantly enhanced RMS tumor cell lysis for the combinatorial therapy using NK-92/5.28.z and proteasome inhibitor bortezomib, but further evaluation *in vivo* of this approach is required. In addition, the combination of NK-92/5.28.z cells with PD-1 immune checkpoint blockade might be suitable for RMS treatment, regarding the bystander cells recruited by the NK-92/5.28.z mediated tumor cell lysis. But an immunocompetent RMS xenograft model must be developed to explore this approach *in vivo*.

Additionally a protocol for the generation of non-viral *Sleeping beauty transposon* modified CAR-CIK cells was established. The SBTS CAR-CIKs showed a lower CAR-expression rate than lentiviral transduced CAR-CIK cells, but a higher viability and also short-term cytotoxicity. But in long-term *in vitro* assays as well as in an *in vivo* evaluation the SBTS clearly were inferior to the lentiviral transduced CAR-CIK cells, most likely due to the more cytotoxic and therefore more prone to exhaustion phenotype of the SBTS modified CAR-CIK cells. This phenotype is probably caused by the use of X-Vivo10 medium in the SBTS CAR-CIK protocol. Thus, additional protocol optimization using another medium supporting cell survival, but not effecting the phenotype might be considered to ensure that the low *in vivo* cytotoxicity compared to virally transduced CAR-CIKs is not caused by the non-viral modification method. Additionally, the same number of CAR-CIK cells instead of total cells must be used for *in vivo* application to abolish effects caused by varying CAR proportions, which may result in different persistence characteristics *in vivo*. Despite the protocol for non-viral CAR-CIK cell, also the CAR construct itself can be adapted to achieve higher transfection rates and maybe also longer *in vivo* persistence. Beside a different promotor, the deletion of the GFP signaling protein might result in a

better transfection efficiency and an 4-1BB costimulatory domain instead of the CD28 domain might enhance the *in vivo* persistence.

This work underlines the hard-to-treat characteristic of metastatic RMS. Since ErbB2-specicifc NK-92/5.28.z cells at least prolonged the survival of RMS xenografts the combination with other immunotherapy supporting anti-cancer therapies or immune checkpoint inhibitors might be an expedient strategy for the treatment of these tumors. Also lentiviral CAR-CIK cells were able to prolong the survival of mice in a xenograft model and inhibit the tumor engraftment in some mice completely and a further adaption of the protocol for the generation of non-viral SBTS CAR-CIK cells might translate this approach into clinics.

6 References

1 Yiallouros M, Kube S. Weichteilsarkome und seltene Weichteiltumoren (Kurzinformation). Berlin: Pediatric Oncology and Hematology Publications 2010.

2 Shern JF, Yohe ME, Khan J. Pediatric Rhabdomyosarcoma. *Crit Rev Oncog* 2015;20(3-4):227–43.

3 Dasgupta R, Fuchs J, Rodeberg D. Rhabdomyosarcoma. *Seminars in Pediatric Surgery* 2016;25(5):276–83. https://www.sciencedirect.com/science/article/pii/S105585861630049X.

4 Dziuba I, Kurzawa P, Dopierała M, et al. Rhabdomyosarcoma in children - current pathologic and molecular classification. *Pol J Pathol* 2018;69(1):20–32.

5 Barr FG, Smith LM, Lynch JC, et al. Examination of gene fusion status in archival samples of alveolar rhabdomyosarcoma entered on the Intergroup Rhabdomyosarcoma Study-III trial: a report from the Children's Oncology Group. *J Mol Diagn* 2006;8(2):202–08.

6 Barr FG, Galili N, Holick J, et al. Rearrangement of the PAX3 paired box gene in the paediatric solid tumour alveolar rhabdomyosarcoma. *Nat Genet* 1993;3(2):113–17.

7 Davis RJ, D'Cruz CM, Lovell MA, et al. Fusion of PAX7 to FKHR by the variant t(1;13)(p36;q14) translocation in alveolar rhabdomyosarcoma. *Cancer Res* 1994;54(11):2869–72.

8 Regina C, Hamed E, Andrieux G, et al. Negative correlation of single-cell PAX3:FOXO1 expression with tumorigenicity in rhabdomyosarcoma. *Life Sci Alliance* 2021;4(9). doi:10.26508/lsa.202001002 [published Online First: 29 June 2021].

9 Linardic CM. PAX3-FOXO1 fusion gene in rhabdomyosarcoma. *Cancer Lett* 2008;270(1):10–18.

10 Williamson D, Missiaglia E, Reyniès A de, et al. Fusion gene-negative alveolar rhabdomyosarcoma is clinically and molecularly indistinguishable from embryonal rhabdomyosarcoma. *J Clin Oncol* 2010;28(13):2151–58. doi:10.1200/JCO.2009.26.3814 [published Online First: 29 March 2010].

11 Oberlin O, Rey A, Lyden E, et al. Prognostic factors in metastatic rhabdomyosarcomas: results of a pooled analysis from United States and European cooperative groups. *J Clin Oncol* 2008;26(14):2384–89.

12 Schoot RA, Chisholm JC, Casanova M, et al. Metastatic Rhabdomyosarcoma: Results of the European Paediatric Soft Tissue Sarcoma Study Group MTS 2008 Study and Pooled Analysis With the Concurrent BERNIE Study. *J Clin Oncol* 2022;40(32):3730–40. doi:10.1200/JCO.21.02981 [published Online First: 16 June 2022].

13 Defachelles A-S, Bogart E, Casanova M, et al. Randomized Phase II Trial of Vincristine-Irinotecan With or Without Temozolomide, in Children and Adults With Relapsed or Refractory Rhabdomyosarcoma: A European Paediatric Soft Tissue Sarcoma Study Group and Innovative Therapies for Children With Cancer Trial. *J Clin Oncol* 2021;39(27):2979–90. doi:10.1200/JCO.21.00124 [published Online First: 3 August 2021].

14 Ruhen O, Lak NSM, Stutterheim J, et al. Molecular Characterization of Circulating Tumor DNA in Pediatric Rhabdomyosarcoma: A Feasibility Study. *JCO Precis Oncol* 2022;6:e2100534.

15 Chen C, Dorado Garcia H, Scheer M, et al. Current and Future Treatment Strategies for Rhabdomyosarcoma. *Front Oncol* 2019;9:1458. doi:10.3389/fonc.2019.01458 [published Online First: 20 December 2019].

16 van Erp AEM, Versleijen-Jonkers YMH, van der Graaf WTA, et al. Targeted Therapy-based Combination Treatment in Rhabdomyosarcoma. *Mol Cancer Ther* 2018;17(7):1365–80.

17 Yohe ME, Heske CM, Stewart E, et al. Insights into pediatric rhabdomyosarcoma research: Challenges and goals. *Pediatr Blood Cancer* 2019;66(10):e27869. doi:10.1002/pbc.27869 [published Online First: 21 June 2019].

18 Gutierrez C, Schiff R. HER2: biology, detection, and clinical implications. *Arch Pathol Lab Med* 2011;135(1):55–62.

19 Iqbal N, Iqbal N. Human Epidermal Growth Factor Receptor 2 (HER2) in Cancers: Overexpression and Therapeutic Implications. *Mol Biol Int* 2014;2014:852748. doi:10.1155/2014/852748 [published Online First: 7 September 2014].

20 Ricci C, Landuzzi L, Rossi I, et al. Expression of HER/erbB family of receptor tyrosine kinases and induction of differentiation by glial growth factor 2 in human rhabdomyosarcoma cells. *Int J Cancer* 2000;87(1):29–36.

21 Yu D, Hung MC. Overexpression of ErbB2 in cancer and ErbB2-targeting strategies. *Oncogene* 2000;19(53):6115–21.

22 Oh D-Y, Bang Y-J. HER2-targeted therapies - a role beyond breast cancer. *Nature reviews. Clinical oncology* 2020;17(1):33–48. doi:10.1038/s41571-019-0268-3 [published Online First: 23 September 2019].

23 Baselga J, Swain SM. CLEOPATRA: A Phase III Evaluation of Pertuzumab and Trastuzumab for HER2-Positive Metastatic Breast Cancer. *Clinical Breast Cancer* 2010;10(6):489–91. https://www.sciencedirect.com/science/article/pii/S1526820911701999.

24 Emens LA, Davidson NE. Trastuzumab in breast cancer. *Oncology (Williston Park)* 2004;18(9):1117-28; discussion 1131-2, 1137-8.

25 Varlet P, Bouffet E, Casanova M, et al. Comprehensive analysis of the ErbB receptor family in pediatric nervous system tumors and rhabdomyosarcoma. *Pediatr Blood Cancer* 2022;69(1):e29316.

26 Gossel LDH, Heim C, Pfeffermann L-M, et al. Retargeting of NK-92 Cells against High-Risk Rhabdomyosarcomas by Means of an ERBB2 (HER2/Neu)-Specific Chimeric Antigen Receptor. *Cancers (Basel)* 2021;13(6). doi:10.3390/cancers13061443 [published Online First: 22 March 2021].

27 Ahmed N, Brawley VS, Hegde M, et al. Human Epidermal Growth Factor Receptor 2 (HER2) -Specific Chimeric Antigen Receptor-Modified T Cells for the Immunotherapy of HER2-Positive Sarcoma. *J Clin Oncol* 2015;33(15):1688–96. doi:10.1200/JCO.2014.58.0225 [published Online First: 23 March 2015].

28 Couzin-Frankel J. Breakthrough of the year 2013. Cancer immunotherapy. *Science* 2013;342(6165):1432–33.

29 McNutt M. Cancer immunotherapy. *Science* 2013;342(6165):1417.

30 McCarthy EF. The toxins of William B. Coley and the treatment of bone and soft-tissue sarcomas. *Iowa Orthop J* 2006;26:154–58.

31 Gross G, Waks T, Eshhar Z. Expression of immunoglobulin-T-cell receptor chimeric molecules as functional receptors with antibody-type specificity. *Proc Natl Acad Sci U S A* 1989;86(24):10024–28.

32 Cameron F, Whiteside G, Perry C. Ipilimumab: first global approval. *Drugs* 2011;71(8):1093–104.

33 Poole RM. Pembrolizumab: first global approval. *Drugs* 2014;74(16):1973–81.

34 Raedler LA. Opdivo (Nivolumab): Second PD-1 Inhibitor Receives FDA Approval for Unresectable or Metastatic Melanoma. *Am Health Drug Benefits* 2015;8(Spec Feature):180–83.

35 Tisagenlecleucel (Kymriah) for ALL. *Med Lett Drugs Ther* 2017;59(1532):177–78.

36 Sengsayadeth S, Savani BN, Oluwole O, et al. Overview of approved CAR-T therapies, ongoing clinical trials, and its impact on clinical practice. *eJHaem* 2022;3(S1):6–10.

37 Schwerdtfeger M, Benmebarek M-R, Endres S, et al. Chimeric Antigen Receptor-Modified T Cells and T Cell-Engaging Bispecific Antibodies: Different Tools for the Same Job. *Curr Hematol Malig Rep* 2021;16(2):218–33. doi:10.1007/s11899-021-00628-2 [published Online First: 30 April 2021].

38 Mazinani M, Rahbarizadeh F. CAR-T cell potency: from structural elements to vector backbone components. *Biomark Res* 2022;10(1):70. doi:10.1186/s40364-022-00417-w [published Online First: 19 September 2022].

39 Weinkove R, George P, Dasyam N, et al. Selecting costimulatory domains for chimeric antigen receptors: functional and clinical considerations. *Clin Transl Immunology* 2019;8(5):e1049.

40 Elahi R, Khosh E, Tahmasebi S, et al. Immune Cell Hacking: Challenges and Clinical Approaches to Create Smarter Generations of Chimeric Antigen Receptor T Cells. *Front Immunol* 2018;9:1717.

41 Sheykhhasan M, Manoochehri H, Dama P. Use of CAR T-cell for acute lymphoblastic leukemia (ALL) treatment: a review study. *Cancer Gene Ther* 2022;29(8-9):1080–96. doi:10.1038/s41417-021-00418-1 [published Online First: 5 January 2022].

42 Biermann M, Reya T. Hematopoietic Stem Cells and Regeneration. *Cold Spring Harb Perspect Biol* 2022;14(8). doi:10.1101/cshperspect.a040774 [published Online First: 1 August 2022].

43 Martinez M, Moon EK. CAR T Cells for Solid Tumors: New Strategies for Finding, Infiltrating, and Surviving in the Tumor Microenvironment. *Front. Immunol.* 2019;10:128. doi:10.3389/fimmu.2019.00128 [published Online First: 5 February 2019].

44 Smith AJ, Oertle J, Warren D, et al. Chimeric antigen receptor (CAR) T cell therapy for malignant cancers: Summary and perspective. *Journal of Cellular Immunotherapy* 2016;2(2):59–68. https://www.sciencedirect.com/science/article/pii/S2352177516300127.

45 Chmielewski M, Abken H. TRUCKS, the fourth-generation CAR T cells: Current developments and clinical translation. *Adv Cell Gene Ther* 2020;3(3):e84. https://onlinelibrary.wiley.com/doi/full/10.1002/acg2.84.

46 Petty AJ, Heyman B, Yang Y. Chimeric Antigen Receptor Cell Therapy: Overcoming Obstacles to Battle Cancer. *Cancers (Basel)* 2020;12(4). doi:10.3390/cancers12040842 [published Online First: 31 March 2020].

47 Tomasik J, Jasiński M, Basak GW. Next generations of CAR-T cells - new therapeutic opportunities in hematology? *Front. Immunol.* 2022;13:1034707. doi:10.3389/fimmu.2022.1034707 [published Online First: 28 October 2022].

48 Tokarew N, Ogonek J, Endres S, et al. Teaching an old dog new tricks: next-generation CAR T cells. *British Journal of Cancer* 2019;120(1):26–37.

49 Sun S, Hao H, Yang G, et al. Immunotherapy with CAR-Modified T Cells: Toxicities and Overcoming Strategies. *J Immunol Res* 2018;2018:2386187. doi:10.1155/2018/2386187 [published Online First: 17 April 2018].

50 Guedan S, Calderon H, Posey AD, et al. Engineering and Design of Chimeric Antigen Receptors. *Mol Ther Methods Clin Dev* 2019;12:145–56. doi:10.1016/j.omtm.2018.12.009 [published Online First: 31 December 2018].

51 Moghanloo E, Mollanoori H, Talebi M, et al. Remote controlling of CAR-T cells and toxicity management: Molecular switches and next generation CARs. *Transl Oncol* 2021;14(6):101070. doi:10.1016/j.tranon.2021.101070 [published Online First: 28 March 2021].

52 Majzner RG, Mackall CL. Tumor Antigen Escape from CAR T-cell Therapy. *Cancer Discov* 2018;8(10):1219–26. doi:10.1158/2159-8290.CD-18-0442 [published Online First: 22 August 2018].

53 Harwerth IM, Wels W, Marte BM, et al. Monoclonal antibodies against the extracellular domain of the erbB-2 receptor function as partial ligand agonists. *J Biol Chem* 1992;267(21):15160–67.

54 Wels W, HARWERTH I, HYNES N, et al. Diminution of antibodies directed against tumor cell surface epitopes: A single chain Fv fusion molecule specifically recognizes the extracellular domain of the c-erbB-2 receptor. *The Journal of Steroid Biochemistry and Molecular Biology* 1992;43(1-3):1–7.

55 Schönfeld K, Sahm C, Zhang C, et al. Selective inhibition of tumor growth by clonal NK cells expressing an ErbB2/HER2-specific chimeric antigen receptor. *Mol Ther* 2015;23(2):330–38. doi:10.1038/mt.2014.219 [published Online First: 6 November 2014].

56 Wendel P, Reindl LM, Bexte T, et al. Arming Immune Cells for Battle: A Brief Journey through the Advancements of T and NK Cell Immunotherapy. *Cancers (Basel)* 2021;13(6). doi:10.3390/cancers13061481 [published Online First: 23 March 2021].

57 Vivier E, Tomasello E, Baratin M, et al. Functions of natural killer cells. *Nature Immunology* 2008;9(5):503–10.

58 Su S, Lei A, Wang X, et al. Induced CAR-Macrophages as a Novel Therapeutic Cell Type for Cancer Immune Cell Therapies. *Cells* 2022;11(10). doi:10.3390/cells11101652 [published Online First: 16 May 2022].

59 Kumar BV, Connors TJ, Farber DL. Human T Cell Development, Localization, and Function throughout Life. *Immunity* 2018;48(2):202–13.

60 Xiong Y, Bosselut R. CD4-CD8 differentiation in the thymus: connecting circuits and building memories. *Curr Opin Immunol* 2012;24(2):139–45. doi:10.1016/j.coi.2012.02.002 [published Online First: 2 March 2012].

61 Mohanty R, Chowdhury CR, Arega S, et al. CAR T cell therapy: A new era for cancer treatment (Review). *Oncol Rep* 2019;42(6):2183–95. doi:10.3892/or.2019.7335 [published Online First: 24 September 2019].

62 Waldman AD, Fritz JM, Lenardo MJ. A guide to cancer immunotherapy: from T cell basic science to clinical practice. *Nat Rev Immunol* 2020;20(11):651–68. doi:10.1038/s41577-020-0306-5 [published Online First: 20 May 2020].

63 Allen ES, Stroncek DF, Ren J, et al. Autologous lymphapheresis for the production of chimeric antigen receptor T cells. *Transfusion* 2017;57(5):1133–41.

64 Noaks E, Peticone C, Kotsopoulou E, et al. Enriching leukapheresis improves T cell activation and transduction efficiency during CAR T processing. *Mol Ther Methods Clin Dev* 2021;20:675–87.

65 Wang X, Rivière I. Clinical manufacturing of CAR T cells: foundation of a promising therapy. *Mol Ther Oncolytics* 2016;3:16015. doi:10.1038/mto.2016.15 [published Online First: 15 June 2016].

66 Sanber K, Savani B, Jain T. Graft-versus-host disease risk after chimeric antigen receptor T-cell therapy: the diametric opposition of T cells. *Br J Haematol* 2021;195(5):660–68. doi:10.1111/bjh.17544 [published Online First: 25 May 2021].

67 Turtle CJ, Hanafi L-A, Berger C, et al. CD19 CAR-T cells of defined CD4+:CD8+ composition in adult B cell ALL patients. *J Clin Invest* 2016;126(6):2123–38. doi:10.1172/JCI85309 [published Online First: 25 April 2016].

68 Shah NN, Highfill SL, Shalabi H, et al. CD4/CD8 T-Cell Selection Affects Chimeric Antigen Receptor (CAR) T-Cell Potency and Toxicity: Updated Results From a Phase I Anti-CD22 CAR T-Cell Trial. *J Clin Oncol* 2020;38(17):1938–50. doi:10.1200/JCO.19.03279 [published Online First: 14 April 2020].

69 Sommermeyer D, Hudecek M, Kosasih PL, et al. Chimeric antigen receptor-modified T cells derived from defined CD8+ and CD4+ subsets confer superior antitumor reactivity in vivo. *Leukemia* 2016;30(2):492–500. doi:10.1038/leu.2015.247 [published Online First: 15 September 2015].

70 Melenhorst JJ, Chen GM, Wang M, et al. Decade-long leukaemia remissions with persistence of CD4+ CAR T cells. *Nature* 2022;602(7897):503–09. doi:10.1038/s41586-021-04390-6 [published Online First: 2 February 2022].

71 Flemming A. Cytotoxic CD4+ CAR T cells implicated in long-term leukaemia remission. *Nat Rev Immunol* 2022;22(3):146.

72 Bove C, Arcangeli S, Falcone L, et al. CD4 CAR-T cells targeting CD19 play a key role in exacerbating cytokine release syndrome, while maintaining long-term responses. *J Immunother Cancer* 2023;11(1).

73 Sheth VS, Gauthier J. Taming the beast: CRS and ICANS after CAR T-cell therapy for ALL. *Bone Marrow Transplant* 2021;56(3):552–66. doi:10.1038/s41409-020-01134-4 [published Online First: 24 November 2020].

74 Shimabukuro-Vornhagen A, Gödel P, Subklewe M, et al. Cytokine release syndrome. *J Immunother Cancer* 2018;6(1):56. doi:10.1186/s40425-018-0343-9 [published Online First: 15 June 2018].

75 Liu D, Zhao J, Song Y. Engineering switchable and programmable universal CARs for CAR T therapy. *Journal of Hematology & Oncology* 2019;12(1):69.

76 Langers I, Renoux VM, Thiry M, et al. Natural killer cells: role in local tumor growth and metastasis. *Biologics* 2012;6:73–82. doi:10.2147/BTT.S23976 [published Online First: 5 April 2012].

77 Abel AM, Yang C, Thakar MS, et al. Natural Killer Cells: Development, Maturation, and Clinical Utilization. *Front. Immunol.* 2018;9:1869. doi:10.3389/fimmu.2018.01869 [published Online First: 13 August 2018].

78 Chu J, Gao F, Yan M, et al. Natural killer cells: a promising immunotherapy for cancer. *J Transl Med* 2022;20(1):240. doi:10.1186/s12967-022-03437-0 [published Online First: 23 May 2022].

79 Prager I, Watzl C. Mechanisms of natural killer cell-mediated cellular cytotoxicity. *J Leukoc Biol* 2019;105(6):1319–29. doi:10.1002/JLB.MR0718-269R [published Online First: 20 May 2019].

80 Pan K, Farrukh H, Chittepu VCSR, et al. CAR race to cancer immunotherapy: from CAR T, CAR NK to CAR macrophage therapy. *J Exp Clin Cancer Res* 2022;41(1):119. doi:10.1186/s13046-022-02327-z [published Online First: 31 March 2022].

81 Phan M-TT, Lee S-H, Kim S-K, et al. Expansion of NK Cells Using Genetically Engineered K562 Feeder Cells. *Methods Mol Biol* 2016;1441:167–74.

82 Oberschmidt O, Morgan M, Huppert V, et al. Development of Automated Separation, Expansion, and Quality Control Protocols for Clinical-Scale Manufacturing of Primary Human NK Cells and Alpharetroviral Chimeric Antigen Receptor Engineering. *Hum Gene Ther Methods* 2019;30(3):102–20. doi:10.1089/hgtb.2019.039 [published Online First: 16 May 2019].

83 Allan DS, Chakraborty M, Waller GC, et al. Systematic improvements in lentiviral transduction of primary human natural killer cells undergoing ex vivo expansion. *Mol Ther Methods Clin Dev* 2021;20:559–71. https://www.sciencedirect.com/science/article/pii/S2329050121000085.

84 Robbins GM, Wang M, Pomeroy EJ, et al. Nonviral genome engineering of natural killer cells. *Stem Cell Res Ther* 2021;12(1):350. doi:10.1186/s13287-021-02406-6 [published Online First: 16 June 2021].

85 Zhang Y, Wallace DL, Lara CM de, et al. In vivo kinetics of human natural killer cells: the effects of ageing and acute and chronic viral infection. *Immunology* 2007;121(2):258–65. doi:10.1111/j.1365-2567.2007.02573.x [published Online First: 7 March 2007].

86 Jiang T, Zhou C, Ren S. Role of IL-2 in cancer immunotherapy. *Oncoimmunology* 2016;5(6):e1163462. doi:10.1080/2162402X.2016.1163462 [published Online First: 25 April 2016].

87 Marofi F, Rahman HS, Thangavelu L, et al. Renaissance of armored immune effector cells, CAR-NK cells, brings the higher hope for successful cancer therapy. *Stem Cell Res Ther* 2021;12(1):200.

88 Schwartz RN, Stover L, Dutcher JP. Managing toxicities of high-dose interleukin-2. *Oncology (Williston Park)* 2002;16(11 Suppl 13):11–20.

89 Gong JH, Maki G, Klingemann HG. Characterization of a human cell line (NK-92) with phenotypical and functional characteristics of activated natural killer cells. *Leukemia* 1994;8(4):652–58.

90 Maki G, Klingemann HG, Martinson JA, et al. Factors regulating the cytotoxic activity of the human natural killer cell line, NK-92. *Journal of hematotherapy & stem cell research* 2001;10(3):369–83. https://pubmed.ncbi.nlm.nih.gov/11454312/.

91 Nowakowska P, Romanski A, Miller N, et al. Clinical grade manufacturing of genetically modified, CAR-expressing NK-92 cells for the treatment of ErbB2-positive malignancies. *Cancer Immunol Immunother* 2018;67(1):25–38. doi:10.1007/s00262-017-2055-2 [published Online First: 6 September 2017].

92 Zhang C, Oberoi P, Oelsner S, et al. Chimeric Antigen Receptor-Engineered NK-92 Cells: An Off-the-Shelf Cellular Therapeutic for Targeted Elimination of Cancer Cells and Induction of Protective Antitumor Immunity. *Front. Immunol.* 2017;8:533. doi:10.3389/fimmu.2017.00533 [published Online First: 18 May 2017].

93 Burger MC, Zhang C, Harter PN, et al. CAR-Engineered NK Cells for the Treatment of Glioblastoma: Turning Innate Effectors Into Precision Tools for Cancer Immunotherapy. *Front. Immunol.* 2019;10:2683. doi:10.3389/fimmu.2019.02683 [published Online First: 14 November 2019].

94 Lee SC, Srivastava RM, López-Albaitero A, et al. Natural killer (NK): dendritic cell (DC) cross talk induced by therapeutic monoclonal antibody triggers tumor antigen-specific T cell immunity. *Immunol Res* 2011;50(2-3):248–54.

95 Peterson EE, Barry KC. The Natural Killer-Dendritic Cell Immune Axis in Anti-Cancer Immunity and Immunotherapy. *Front. Immunol.* 2020;11:621254. doi:10.3389/fimmu.2020.621254 [published Online First: 3 February 2021].

96 Cappuzzello E, Sommaggio R, Zanovello P, et al. Cytokines for the induction of antitumor effectors: The paradigm of Cytokine-Induced Killer (CIK) cells. *Cytokine Growth Factor Rev* 2017;36:99–105. doi:10.1016/j.cytogfr.2017.06.003 [published Online First: 3 June 2017].

97 Mulé JJ, Shu S, Rosenberg SA. The anti-tumor efficacy of lymphokine-activated killer cells and recombinant interleukin 2 in vivo. *J Immunol* 1985;135(1):646–52.

98 Rayner AA, Grimm EA, Lotze MT, et al. Lymphokine-activated killer (LAK) cells. Analysis of factors relevant to the immunotherapy of human cancer. *Cancer* 1985;55(6):1327–33.

99 Rettinger E, Kuçi S, Naumann I, et al. The cytotoxic potential of interleukin-15-stimulated cytokine-induced killer cells against leukemia cells. *Cytotherapy* 2012;14(1):91–103. doi:10.3109/14653249.2011.613931 [published Online First: 6 October 2011].

100 Iudicone P, Fioravanti D, Cicchetti E, et al. Interleukin-15 enhances cytokine induced killer (CIK) cytotoxic potential against epithelial cancer cell lines via an innate pathway. *Hum Immunol* 2016;77(12):1239–47.

101 Lopez RD, Waller EK, Lu PH, et al. CD58/LFA-3 and IL-12 provided by activated monocytes are critical in the in vitro expansion of CD56+ T cells. *Cancer Immunol Immunother* 2001;49(12):629–40.

102 Liu Y, Li J, Zhao L, et al. Effects of interleukin-2 concentration and administration method on proliferation and function of cytokine-induced killer cells. *Transl Cancer Res* 2021;10(9):3930–38.

103 Kriegsmann K, Kriegsmann M, Bergwelt-Baildon M von, et al. NKT cells - New players in CAR cell immunotherapy? *Eur J Haematol* 2018;101(6):750–57. doi:10.1111/ejh.13170 [published Online First: 9 October 2018].

104 Meng M, Li L, Li R, et al. A dynamic transcriptomic atlas of cytokine-induced killer cells. *J Biol Chem* 2018;293(51):19600–12. doi:10.1074/jbc.RA118.003280 [published Online First: 17 October 2018].

105 Waldowska M, Bojarska-Junak A, Roliński J. A brief review of clinical trials involving manipulation of invariant NKT cells as a promising approach in future cancer therapies. *Cent Eur J Immunol* 2017;42(2):181–95.

106 Zhang Y, Schmidt-Wolf IGH. Ten-year update of the international registry on cytokine-induced killer cells in cancer immunotherapy. *J Cell Physiol* 2020;235(12):9291–303. doi:10.1002/jcp.29827 [published Online First: 2 June 2020].

107 Meng Y, Yu Z, Wu Y, et al. Cell-based immunotherapy with cytokine-induced killer (CIK) cells: From preparation and testing to clinical application. *Hum Vaccin Immunother* 2017;13(6):1–9. doi:10.1080/21645515.2017.1285987 [published Online First: 22 February 2017].

108 Bremm M, Pfeffermann L-M, Cappel C, et al. Improving Clinical Manufacturing of IL-15 Activated Cytokine-Induced Killer (CIK) Cells. *Front. Immunol.* 2019;10:1218. doi:10.3389/fimmu.2019.01218 [published Online First: 31 May 2019].

109 Kornacker M, Verneris, Kornacker B, et al. The apoptotic and proliferative fate of cytokine-induced killer cells after redirection to tumor cells with bispecific Ab. *Cytotherapy* 2006;8(1):13–23.

110 Oelsner S, Wagner J, Friede ME, et al. Chimeric antigen receptor-engineered cytokine-induced killer cells overcome treatment resistance of pre-B-cell acute lymphoblastic leukemia and enhance survival. *Int J Cancer* 2016;139(8):1799–809. doi:10.1002/ijc.30217 [published Online First: 11 June 2016].

111 Merker M, Pfirrmann V, Oelsner S, et al. Generation and characterization of ErbB2-CAR-engineered cytokine-induced killer cells for the treatment of high-risk soft tissue sarcoma in children. *Oncotarget* 2017;8(39):66137–53. doi:10.18632/oncotarget.19821 [published Online First: 2 August 2017].

112 Magnani CF, Turazzi N, Benedicenti F, et al. Immunotherapy of acute leukemia by chimeric antigen receptor-modified lymphocytes using an improved Sleeping Beauty transposon platform. *Oncotarget* 2016;7(32):51581–97.

113 Magnani CF, Mezzanotte C, Cappuzzello C, et al. Preclinical Efficacy and Safety of CD19CAR Cytokine-Induced Killer Cells Transfected with Sleeping Beauty Transposon for the Treatment of Acute Lymphoblastic Leukemia. *Hum Gene Ther* 2018;29(5):602–13. doi:10.1089/hum.2017.207 [published Online First: 16 April 2018].

114 Kuçi S, Rettinger E, Voss B, et al. Efficient lysis of rhabdomyosarcoma cells by cytokine-induced killer cells: implications for adoptive immunotherapy after allogeneic stem cell transplantation.

Haematologica 2010;95(9):1579–86. doi:10.3324/haematol.2009.019885 [published Online First: 7 April 2010].

115 Merker M, Wagner J, Kreyenberg H, et al. ERBB2-CAR-Engineered Cytokine-Induced Killer Cells Exhibit Both CAR-Mediated and Innate Immunity Against High-Risk Rhabdomyosarcoma. *Front. Immunol.* 2020;11:581468. doi:10.3389/fimmu.2020.581468 [published Online First: 19 October 2020].

116 Linn Y-C, Niam M, Chu S, et al. The anti-tumour activity of allogeneic cytokine-induced killer cells in patients who relapse after allogeneic transplant for haematological malignancies. *Bone Marrow Transplant* 2012;47(7):957–66. doi:10.1038/bmt.2011.202 [published Online First: 10 October 2011].

117 Qin Y, Xu G. Enhancing CAR T-cell therapies against solid tumors: Mechanisms and reversion of resistance. *Front. Immunol.* 2022;13:1053120. doi:10.3389/fimmu.2022.1053120 [published Online First: 8 December 2022].

118 Giraldo NA, Sanchez-Salas R, Peske JD, et al. The clinical role of the TME in solid cancer. *British Journal of Cancer* 2019;120(1):45–53. doi:10.1038/s41416-018-0327-z [published Online First: 9 November 2018].

119 D'Agostino S, Tombolan L, Saggioro M, et al. Rhabdomyosarcoma Cells Produce Their Own Extracellular Matrix With Minimal Involvement of Cancer-Associated Fibroblasts: A Preliminary Study. *Front Oncol* 2020;10:600980. doi:10.3389/fonc.2020.600980 [published Online First: 29 January 2021].

120 Lian X, Bond JS, Bharathy N, et al. Defining the Extracellular Matrix of Rhabdomyosarcoma. *Front Oncol* 2021;11:601957.

121 Kather JN, Hörner C, Weis C-A, et al. CD163+ immune cell infiltrates and presence of CD54+ microvessels are prognostic markers for patients with embryonal rhabdomyosarcoma. *Sci Rep* 2019;9(1):9211. doi:10.1038/s41598-019-45551-y [published Online First: 25 June 2019].

122 DeMartino J, Meister MT, Visser L, et al. Single-cell transcriptomics reveals immune suppression and cell states predictive of patient outcomes in rhabdomyosarcoma 2022.

123 Marin-Acevedo JA, Kimbrough EO, Lou Y. Next generation of immune checkpoint inhibitors and beyond. *Journal of Hematology & Oncology* 2021;14(1):45. doi:10.1186/s13045-021-01056-8 [published Online First: 19 March 2021].

124 Bertolini G, Bergamaschi L, Ferrari A, et al. PD-L1 assessment in pediatric rhabdomyosarcoma: a pilot study. *BMC Cancer* 2018;18(1):652. doi:10.1186/s12885-018-4554-8 [published Online First: 13 June 2018].

125 D'Angelo SP, Mahoney MR, van Tine BA, et al. Nivolumab with or without ipilimumab treatment for metastatic sarcoma (Alliance A091401): two open-label, non-comparative, randomised,

phase 2 trials. *Lancet Oncol* 2018;19(3):416–26. doi:10.1016/S1470-2045(18)30006-8 [published Online First: 19 January 2018].

126 Grosser R, Cherkassky L, Chintala N, et al. Combination Immunotherapy with CAR T Cells and Checkpoint Blockade for the Treatment of Solid Tumors. *Cancer Cell* 2019;36(5):471–82.

127 Qin S, Xu L, Yi M, et al. Novel immune checkpoint targets: moving beyond PD-1 and CTLA-4. *Mol Cancer* 2019;18(1):155. doi:10.1186/s12943-019-1091-2 [published Online First: 6 November 2019].

128 Hegde M, Joseph SK, Pashankar F, et al. Tumor response and endogenous immune reactivity after administration of HER2 CAR T cells in a child with metastatic rhabdomyosarcoma. *Nat Commun* 2020;11(1):3549. doi:10.1038/s41467-020-17175-8 [published Online First: 15 July 2020].

129 Beldi-Ferchiou A, Caillat-Zucman S. Control of NK Cell Activation by Immune Checkpoint Molecules. *Int J Mol Sci* 2017;18(10). doi:10.3390/ijms18102129 [published Online First: 12 October 2017].

130 Petak I, Douglas L, Tillman DM, et al. Pediatric rhabdomyosarcoma cell lines are resistant to Fas-induced apoptosis and highly sensitive to TRAIL-induced apoptosis. *Clin Cancer Res* 2000;6(10):4119–27.

131 Montinaro A, Walczak H. Harnessing TRAIL-induced cell death for cancer therapy: a long walk with thrilling discoveries. *Cell Death Differ* 2023;30(2):237–49. doi:10.1038/s41418-022-01059-z [published Online First: 4 October 2022].

132 Takeda K, Smyth MJ, Cretney E, et al. Critical role for tumor necrosis factor-related apoptosis-inducing ligand in immune surveillance against tumor development. *J Exp Med* 2002;195(2):161–69.

133 ADAMS J. Proteasome inhibition in cancer: Development of PS-341. *Semin Oncol* 2001;28(6):613–19.

134 Teicher BA, Ara G, Herbst R, et al. The proteasome inhibitor PS-341 in cancer therapy. *Clin Cancer Res* 1999;5(9):2638–45.

135 Zhang L, Fang B. Mechanisms of resistance to TRAIL-induced apoptosis in cancer. *Cancer Gene Ther* 2005;12(3):228–37.

136 Wilt LHAM de, Kroon J, Jansen G, et al. Bortezomib and TRAIL: a perfect match for apoptotic elimination of tumour cells? *Crit Rev Oncol Hematol* 2013;85(3):363–72. doi:10.1016/j.critrevonc.2012.08.001 [published Online First: 1 September 2012].

137 Srivastava RK. TRAIL/Apo-2L: mechanisms and clinical applications in cancer. *Neoplasia* 2001;3(6):535–46.

138 Boccadoro M, Morgan G, Cavenagh J. Preclinical evaluation of the proteasome inhibitor bortezomib in cancer therapy. *Cancer Cell Int* 2005;5(1):18. doi:10.1186/1475-2867-5-18 [published Online First: 1 June 2005].

139 Milano A, Iaffaioli RV, Caponigro F. The proteasome: a worthwhile target for the treatment of solid tumours? *Eur J Cancer* 2007;43(7):1125–33. doi:10.1016/j.ejca.2007.01.038 [published Online First: 26 March 2007].

140 Fulda S. Novel insights into the synergistic interaction of Bortezomib and TRAIL: tBid provides the link. *Oncotarget* 2011;2(5):418–21.

141 Rapino F, Abhari BA, Jung M, et al. NIK is required for NF-κB-mediated induction of BAG3 upon inhibition of constitutive protein degradation pathways. *Cell Death Dis* 2015;6(3):e1692. doi:10.1038/cddis.2014.584 [published Online First: 12 March 2015].

142 Koschny R, Holland H, Sykora J, et al. Bortezomib sensitizes primary human esthesioneuroblastoma cells to TRAIL-induced apoptosis. *J Neurooncol* 2010;97(2):171–85. doi:10.1007/s11060-009-0010-6 [published Online First: 20 September 2009].

143 Ames E, Hallett WHD, Murphy WJ. Sensitization of human breast cancer cells to natural killer cell-mediated cytotoxicity by proteasome inhibition. *Clin Exp Immunol* 2009;155(3):504–13.

144 Gras Navarro A, Espedal H, Joseph JV, et al. Pretreatment of Glioblastoma with Bortezomib Potentiates Natural Killer Cell Cytotoxicity through TRAIL/DR5 Mediated Apoptosis and Prolongs Animal Survival. *Cancers (Basel)* 2019;11(7). doi:10.3390/cancers11070996 [published Online First: 17 July 2019].

145 Koschny R, Ganten TM, Sykora J, et al. TRAIL/bortezomib cotreatment is potentially hepatotoxic but induces cancer-specific apoptosis within a therapeutic window. *Hepatology* 2007;45(3):649–58.

146 Zhang Q, Xu J, Ding J, et al. Bortezomib improves adoptive carbonic anhydrase IX-specific chimeric antigen receptor-modified NK92 cell therapy in mouse models of human renal cell carcinoma. *Oncol Rep* 2018;40(6):3714–24. doi:10.3892/or.2018.6731 [published Online First: 24 September 2018].

147 Carlsten M, Namazi A, Reger R, et al. Bortezomib sensitizes multiple myeloma to NK cells via ER-stress-induced suppression of HLA-E and upregulation of DR5. *Oncoimmunology* 2019;8(2):e1534664. doi:10.1080/2162402X.2018.1534664 [published Online First: 2 November 2018].

148 Shi J, Tricot GJ, Garg TK, et al. Bortezomib down-regulates the cell-surface expression of HLA class I and enhances natural killer cell-mediated lysis of myeloma. *Blood* 2008;111(3):1309–17. doi:10.1182/blood-2007-03-078535 [published Online First: 18 October 2007].

149 Maki RG, Kraft AS, Scheu K, et al. A multicenter Phase II study of bortezomib in recurrent or metastatic sarcomas. *Cancer* 2005;103(7):1431–38.

150 Thounaojam MC, Dudimah DF, Pellom ST, et al. Bortezomib enhances expression of effector molecules in anti-tumor CD8+ T lymphocytes by promoting Notch-nuclear factor-κB crosstalk. *Oncotarget* 2015;6(32):32439–55.

151 Pellom ST, Dudimah DF, Thounaojam MC, et al. Bortezomib augments lymphocyte stimulatory cytokine signaling in the tumor microenvironment to sustain CD8+T cell antitumor function. *Oncotarget* 2017;8(5):8604–21.

152 Moretti A, Ponzo M, Nicolette CA, et al. The Past, Present, and Future of Non-Viral CAR T Cells. *Front. Immunol.* 2022;13:867013. doi:10.3389/fimmu.2022.867013 [published Online First: 9 June 2022].

153 Brenner MK. Will T-cell therapy for cancer ever be a standard of care? *Cancer Gene Ther* 2012;19(12):818–21. doi:10.1038/cgt.2012.74 [published Online First: 12 October 2012].

154 Monjezi R, Miskey C, Gogishvili T, et al. Enhanced CAR T-cell engineering using non-viral Sleeping Beauty transposition from minicircle vectors. *Leukemia* 2017;31(1):186–94. doi:10.1038/leu.2016.180 [published Online First: 24 June 2016].

155 Wagner DL, Koehl U, Chmielewski M, et al. Review: Sustainable Clinical Development of CAR-T Cells - Switching From Viral Transduction Towards CRISPR-Cas Gene Editing. *Front. Immunol.* 2022;13:865424. doi:10.3389/fimmu.2022.865424 [published Online First: 17 June 2022].

156 Morita D, Nishio N, Saito S, et al. Enhanced Expression of Anti-CD19 Chimeric Antigen Receptor in piggyBac Transposon-Engineered T Cells. *Mol Ther Methods Clin Dev* 2018;8:131–40. doi:10.1016/j.omtm.2017.12.003 [published Online First: 22 December 2017].

157 Irving M, Lanitis E, Migliorini D, et al. Choosing the Right Tool for Genetic Engineering: Clinical Lessons from Chimeric Antigen Receptor-T Cells. *Hum Gene Ther* 2021;32(19-20):1044–58.

158 Narayanavari SA, Izsvák Z. Sleeping Beauty transposon vectors for therapeutic applications: advances and challenges. *Cell Gene Therapy Insights* 2017;3(2):131–58.

159 Ochmann MT, Ivics Z. Jumping Ahead with Sleeping Beauty: Mechanistic Insights into Cut-and-Paste Transposition. *Viruses* 2021;13(1).

160 Ivics Z, Hackett PB, Plasterk RH, et al. Molecular reconstruction of Sleeping Beauty, a Tc1-like transposon from fish, and its transposition in human cells. *Cell* 1997;91(4):501–10.

161 Mátés L, Chuah MKL, Belay E, et al. Molecular evolution of a novel hyperactive Sleeping Beauty transposase enables robust stable gene transfer in vertebrates. *Nat Genet* 2009;41(6):753–61. doi:10.1038/ng.343 [published Online First: 3 May 2009].

162 Narayanavari SA, Chilkunda SS, Ivics Z, et al. Sleeping Beauty transposition: from biology to applications. *Crit Rev Biochem Mol Biol* 2017;52(1):18–44. doi:10.1080/10409238.2016.1237935 [published Online First: 4 October 2016].

163 Jin Z, Maiti S, Huls H, et al. The hyperactive Sleeping Beauty transposase SB100X improves the genetic modification of T cells to express a chimeric antigen receptor. *Gene Ther* 2011;18(9):849–56.

164 Chicaybam L, Abdo L, Carneiro M, et al. CAR T Cells Generated Using Sleeping Beauty Transposon Vectors and Expanded with an EBV-Transformed Lymphoblastoid Cell Line Display Antitumor Activity In Vitro and In Vivo. *Hum Gene Ther* 2019;30(4):511–22.

165 Magnani CF, Tettamanti S, Alberti G, et al. Transposon-Based CAR T Cells in Acute Leukemias: Where are We Going? *Cells* 2020;9(6). doi:10.3390/cells9061337 [published Online First: 27 May 2020].

166 Magnani CF, Gaipa G, Lussana F, et al. Sleeping Beauty-engineered CAR T cells achieve antileukemic activity without severe toxicities. *J Clin Invest* 2020;130(11):6021–33.

167 Miskey C, Amberger M, Reiser M, et al. Genomic Analyses of SLAMF7 CAR-T Cells Manufactured by Sleeping Beauty Transposon Gene Transfer for Immunotherapy of Multiple Myeloma 2019.

168 Schindelin J, Arganda-Carreras I, Frise E, et al. Fiji: an open-source platform for biological-image analysis. *Nat Methods* 2012;9(7):676–82.

169 Heim C, Moser L, Kreyenberg H, et al. ErbB2 (HER2)-CAR-NK-92 cells for enhanced immunotherapy of metastatic fusion-driven alveolar rhabdomyosarcoma. *Front. Immunol.* 2023;14:1228894.

170 Hinson ARP, Jones R, Crose LES, et al. Human rhabdomyosarcoma cell lines for rhabdomyosarcoma research: utility and pitfalls. *Front Oncol* 2013;3:183. doi:10.3389/fonc.2013.00183 [published Online First: 17 July 2013].

171 Meister MT, Groot Koerkamp, Marian J. A., Souza T de, et al. Mesenchymal tumor organoid models recapitulate rhabdomyosarcoma subtypes. *EMBO Mol Med* 2022;14(10):e16001. doi:10.15252/emmm.202216001 [published Online First: 2 August 2022].

172 Wakuri S, Yamakage K, Kazuki Y, et al. Correlation between luminescence intensity and cytotoxicity in cell-based cytotoxicity assay using luciferase. *Anal Biochem* 2017;522:18–29. doi:10.1016/j.ab.2017.01.015 [published Online First: 20 January 2017].

173 Yadav B, Wennerberg K, Aittokallio T, et al. Searching for Drug Synergy in Complex Dose-Response Landscapes Using an Interaction Potency Model. *Comput Struct Biotechnol J* 2015;13:504–13. doi:10.1016/j.csbj.2015.09.001 [published Online First: 25 September 2015].

174 Aksoy P, Aksoy BA, Czech E, et al. Viable and efficient electroporation-based genetic manipulation of unstimulated human T cells 2018.

175 Chicaybam L, Sodre AL, Curzio BA, et al. An efficient low cost method for gene transfer to T lymphocytes. *PLoS One* 2013;8(3):e60298. doi:10.1371/journal.pone.0060298 [published Online First: 26 March 2013].

176 Zhang C, Burger MC, Jennewein L, et al. ErbB2/HER2-Specific NK Cells for Targeted Therapy of Glioblastoma. *JNCI: Journal of the National Cancer Institute* 2016;108(5):987.

177 Field-Smith A, Morgan GJ, Davies FE. Bortezomib (Velcadetrade mark) in the Treatment of Multiple Myeloma. *Ther Clin Risk Manag* 2006;2(3):271–79.

178 Hellwig CT, Delgado ME, Skoko J, et al. Proteasome inhibition triggers the formation of TRAIL receptor 2 platforms for caspase-8 activation that accumulate in the cytosol. *Cell Death Differ* 2022;29(1):147–55. doi:10.1038/s41418-021-00843-7 [published Online First: 5 August 2021].

179 Willms A, Schittek H, Rahn S, et al. Impact of p53 status on TRAIL-mediated apoptotic and non-apoptotic signaling in cancer cells. *PLoS One* 2019;14(4):e0214847. doi:10.1371/journal.pone.0214847 [published Online First: 4 April 2019].

180 Wu GS, Burns TF, McDonald ER3, et al. Induction of the TRAIL receptor KILLER/DR5 in p53-dependent apoptosis but not growth arrest. *Oncogene* 1999;18(47):6411–18.

181 Fu L, Lin Y-D, Elrod HA, et al. c-Jun NH2-terminal kinase-dependent upregulation of DR5 mediates cooperative induction of apoptosis by perifosine and TRAIL. *Mol Cancer* 2010;9:315. doi:10.1186/1476-4598-9-315 [published Online First: 20 December 2010].

182 Chen X, Kandasamy K, Srivastava RK. Differential Roles of RelA (p65) and c-Rel Subunits of Nuclear Factor κB in Tumor Necrosis Factor-related Apoptosis-inducing Ligand Signaling1. *Cancer Res* 2003;63(5):1059–66.

183 Ravi R, Bedi GC, Engstrom LW, et al. Regulation of death receptor expression and TRAIL/Apo2L-induced apoptosis by NF-kappaB. *Nat Cell Biol* 2001;3(4):409–16.

184 Taylor AC, Shu L, Danks MK, et al. p53 mutation and MDM2 amplification frequency in pediatric rhabdomyosarcoma tumors and cell lines. *Med. Pediatr. Oncol.* 2000;35(2):96–103.

185 Sag D, Ayyildiz ZO, Gunalp S, et al. The Role of TRAIL/DRs in the Modulation of Immune Cells and Responses. *Cancers (Basel)* 2019;11(10). doi:10.3390/cancers11101469 [published Online First: 30 September 2019].

186 Klingemann H. The NK-92 cell line-30 years later: its impact on natural killer cell research and treatment of cancer. *Cytotherapy* 2023. doi:10.1016/j.jcyt.2022.12.003 [published Online First: 5 January 2023].

187 Hideshima T, Ikeda H, Chauhan D, et al. Bortezomib induces canonical nuclear factor-kappaB activation in multiple myeloma cells. *Blood* 2009;114(5):1046–52. doi:10.1182/blood-2009-01-199604 [published Online First: 12 May 2009].

188 Kubiczkova L, Pour L, Sedlarikova L, et al. Proteasome inhibitors - molecular basis and current perspectives in multiple myeloma. *J Cell Mol Med* 2014;18(6):947–61. doi:10.1111/jcmm.12279 [published Online First: 8 April 2014].

189 Prommersberger S, Reiser M, Beckmann J, et al. CARAMBA: a first-in-human clinical trial with SLAMF7 CAR-T cells prepared by virus-free Sleeping Beauty gene transfer to treat multiple myeloma. *Gene Ther* 2021;28(9):560–71. doi:10.1038/s41434-021-00254-w [published Online First: 13 April 2021].

190 Rotiroti MC, Buracchi C, Arcangeli S, et al. Targeting CD33 in Chemoresistant AML Patient-Derived Xenografts by CAR-CIK Cells Modified with an Improved SB Transposon System. *Mol Ther* 2020;28(9):1974–86. doi:10.1016/j.ymthe.2020.05.021 [published Online First: 30 May 2020].

191 Hudecek M, Ivics Z. Non-viral therapeutic cell engineering with the Sleeping Beauty transposon system. *Curr Opin Genet Dev* 2018;52:100–08. doi:10.1016/j.gde.2018.06.003 [published Online First: 12 October 2018].

192 Prommersberger S, Monjezi R, Botezatu L, et al. Generation of CAR-T Cells with Sleeping Beauty Transposon Gene Transfer. *Methods Mol Biol* 2022;2521:41–66.

193 Prommersberger S, Monjezi R, Shankar R, et al. Minicircles for CAR T Cell Production by Sleeping Beauty Transposition: A Technological Overview. *Methods Mol Biol* 2022;2521:25–39.

194 Ferrari A, Gasparini P, Casanova M. A home run for rhabdomyosarcoma after 30 years: What now? *Tumori* 2020;106(1):5–11. doi:10.1177/0300891619888021 [published Online First: 8 November 2019].

195 Sterner RC, Sterner RM. CAR-T cell therapy: current limitations and potential strategies. *Blood Cancer J* 2021;11(4):69. doi:10.1038/s41408-021-00459-7 [published Online First: 6 April 2021].

196 Liu S, Galat V, Galat Y, et al. NK cell-based cancer immunotherapy: from basic biology to clinical development. *Journal of Hematology & Oncology* 2021;14(1):7. doi:10.1186/s13045-020-01014-w [published Online First: 6 January 2021].

197 McGowan E, Lin Q, Ma G, et al. PD-1 disrupted CAR-T cells in the treatment of solid tumors: Promises and challenges. *Biomed Pharmacother* 2020;121:109625. doi:10.1016/j.biopha.2019.109625 [published Online First: 13 November 2019].

198 Oyer JL, Gitto SB, Altomare DA, et al. PD-L1 blockade enhances anti-tumor efficacy of NK cells. *Oncoimmunology* 2018;7(11):e1509819. doi:10.1080/2162402X.2018.1509819 [published Online First: 27 August 2018].

199 Hsu J, Hodgins JJ, Marathe M, et al. Contribution of NK cells to immunotherapy mediated by PD-1/PD-L1 blockade. *J Clin Invest* 2018;128(10):4654–68.

200 Higuchi H, Grambihler A, Canbay A, et al. Bile acids up-regulate death receptor 5/TRAIL-receptor 2 expression via a c-Jun N-terminal kinase-dependent pathway involving Sp1. *J Biol Chem* 2004;279(1):51–60. doi:10.1074/jbc.M309476200 [published Online First: 14 October 2003].

201 Nishina H, Wada T, Katada T. Physiological roles of SAPK/JNK signaling pathway. *J Biochem* 2004;136(2):123–26.

202 Tournier C. The 2 Faces of JNK Signaling in Cancer. *Genes Cancer* 2013;4(9-10):397–400.

203 Jane EP, Premkumar DR, Pollack IF. Bortezomib sensitizes malignant human glioma cells to TRAIL, mediated by inhibition of the NF-{kappa}B signaling pathway. *Mol Cancer Ther* 2011;10(1):198–208.

204 Wright KD, Miller BS, El-Meanawy S, et al. The p52 isoform of SHC1 is a key driver of breast cancer initiation. *Breast Cancer Res* 2019;21(1):74. doi:10.1186/s13058-019-1155-7 [published Online First: 15 June 2019].

205 Hufnagel DH, Wilson AJ, Saxon J, et al. Expression of p52, a non-canonical NF-kappaB transcription factor, is associated with poor ovarian cancer prognosis. *Biomark Res* 2020;8:45. doi:10.1186/s40364-020-00227-y [published Online First: 15 September 2020].

206 Saxon JA, Yu H, Polosukhin VV, et al. p52 expression enhances lung cancer progression. *Sci Rep* 2018;8(1):6078. doi:10.1038/s41598-018-24488-8 [published Online First: 17 April 2018].

207 Zhang Z, Qiu S, Zhang X, et al. Optimized DNA electroporation for primary human T cell engineering. *BMC Biotechnol* 2018;18(1):4. doi:10.1186/s12896-018-0419-0 [published Online First: 30 January 2018].

7 List of Abbrevations

Abbreviation	Definition
ADCC	Antibody dependent cell-mediated cytotoxicity
APC	Allophycocyanin
aRMS	Alveolar rhabdomyosarcoma
BATDA	Bis(acetomethyl)2,2´:6´,2´´-terpyridine-6,6´´-dicarboxylate
BCA	Bicinchoninic acid
BLI	Bioluminescence imaging
BM	Bone marrow
BME	Basement membrane extract
CAR	Chimeric antigen receptor
CD	Cluster of differentiation
CIK cells	Cytokine induced killer cells
CRS	Cytokine release syndrome
CTLA-4	Cytotoxic T-lymphocyte-associated protein 4
Cy7	Cyanine7
DAPI	4´,6-Diamidino-2-phenylindol
DC	Dendritic cells
DcR	Decoy receptor
ddH_2O	Demineralized water
DMEM	Dulbecco´s modified eagle medium
DMEM/F12	Dulbecco´s modified eagle medium/Nutrient mixture F-12
DMSO	Dimethylsulfoxid
DPBS	Dulbecco´s phosphor buffered saline
DR4	Death receptor 4, also known as TRAIL receptor 1
DR5	Death receptor 4, also known as TRAIL receptor 2
DTT	Dithiothreitol
eRMS	Embryonal rhabdomyosarcoma
FACS	Flourescence activated cell sorting
FasL	Fas Ligand
FCS	Fetal Calf Serum
FFP	Fresh frozen (human) plasma (blood type AB)
FLuc	Firefly luciferase from *Photinus pyralis*

GFP	Green fluoreszent protein
GvHD	Graft versus host disease
hEGF	Human epidermal growth factor
HEPES	N-(2-Hydroxyethyl)piperazin-N´-(2-ethansulfonacid)
hFGF	Human fibroblast growth factor
hIGF	Human insulin-like growth factor
HLA	Human leucocyte antigene
HRP	Horseradish peroxidase
ICANS	Immune effector cell-associated neurotoxicity syndrome
IL	Interleukin
INF	Interferon
IRES	Internal ribosomal entry site
ITR	Inverted terminal repeats
JNK	C-Jun N-terminal kinases
MC	Minicircle
MFI	Median fluorescent intensity
MHC	Major histocompatibility complex
MM	Multiple Myeloma
MRD	Minimal residual disease
NP-40	Nonyl phenoxypolyethoxylethanol
NSG mouse	NOD/Scid/IL2Rγ$^{-/-}$ mouse
PB	Peripheral blood
PBMCs	Peripheral blood mononuclear cells
PD-1	Programmed cell death protein 1
PD-L1	Programmed cell death ligand 1
PE	Phycoerythrin
PEI	Polyethylenimine
PerCP	Peridinin chlorophyll
PIC	Protease inhibitor cocktail
PMSF	Phenylmethylsulfonyl fluoride
qPCR	Quantitative polymerase chain reaction
r/r	Refractory and/or relapsed
RIPA buffer	Radioimmunoprecipitation assay buffer
RMS	Rhabdomyosarcoma

RNA	Ribonucleic acid
ROI	Region of interest
RPMI	Roswell Park Memorial Institute medium
SB	*Sleeping beauty* transposase
SB100x	Hyperactive *Sleeping beauty* transposase
SBTS	*Sleeping beauty* transposon system
scFv	Single chain variable fragment
SD	Standard deviation
SDS	Sodium dodecylsulfate
SDS-PAGE	sodium dodecylsulfate polyacrylamide gel electrophoresis
SEM	Standard error mean
STR	Short tandem repeats
TAA	Tumor associated antigen
TE	Transposable element
TEMED	Tetramethylethylenediamine
TME	Tumor microenvironemt
TNFα	Tumor necrosis factor α
TRAIL	Tumor necrosis factor related apoptosis inducing ligand
TRUCKs	T cells redirected for antigen-unrestricted cytokine-initiated killing
WPRE	Woodchuck Hepatitis virus posttranscriptional regulatory element
ZIP model	Zero Interaction Potency model (Drug synergism model)

8 List of Figures

9 List of Tables

10 Declaration

Except when stated otherwise by reference or acknowledgment, the work presented was generated by myself under the supervision of my advisors during my doctoral studies. All contributions from colleagues are explicitly referenced in the thesis. The material listed below was obtained in the context of collaborative research:

Figure 19: Hermann Kreyenberg, Goethe University Frankfurt, Department of Pediatrics, Division for Stem Cell Transplantation, Immunology and Intensive Care Medicine (his/her contribution: qPCR performance; my own contribution: DNA preparation, data evaluation and presentation)

Figure 21 and 22: Halvard Bönig/ Sabine Harenkamp, Department of Cellular Therapeutics/Cell Processing, Institute for Transfusion Medicine and Immunotherapy, Goethe University, Frankfurt (sample preparation, immunofluorescence microscopy; providing the samples, data presentation)

Figure 25, 26, 29: Nadine Weinelt, Institute for Experimental Cancer Research in Pediatrics (supervision or performance of western blots, performance of qPCR; experiment design, sample preparation, data analysis and presentation)

Figure 24-26, 28, 31: Leonie Hartig, Goethe University Frankfurt, Department of Pediatrics, Division for Stem Cell Transplantation, Immunology and Intensive Care Medicine (experiment performance, data analysis; supervision, experiment design, data analysis)

Figure 43-47: Laura Moser, Goethe University Frankfurt, Department of Pediatrics, Division for Stem Cell Transplantation, Immunology and Intensive Care Medicine (generation of viral CAR-CIK cells, performance of *in vitro* and *in vivo* experiment, experiment design; generation of SBTS-CAR-CIK cells, *in vitro* experiment performance, support in *in vivo* experiment, experiment design, data presentation)

Figure 30: Emilia Salzmann-Manrique, Goethe University Frankfurt, Department of Pediatrics, Division for Stem Cell Transplantation, Immunology and Intensive Care Medicine (bioinformatic analysis and modelling; preparation of raw data)

Table 18: Luise Gradhand, Dr. Senckenberg Institute of Pathology, University Hospital Frankfurt (staining and rating of the slices; providing of the samples and data presentation)

Whenever a figure, table or text is identical to a previous publication, it is stated explicitly in the thesis that copyright permission and/or co-author agreement has been obtained.

The following parts of this thesis have been previously published:

- Figures 8, 10-15, 20-22
- Table 16

11 Appendix

Plasmid maps

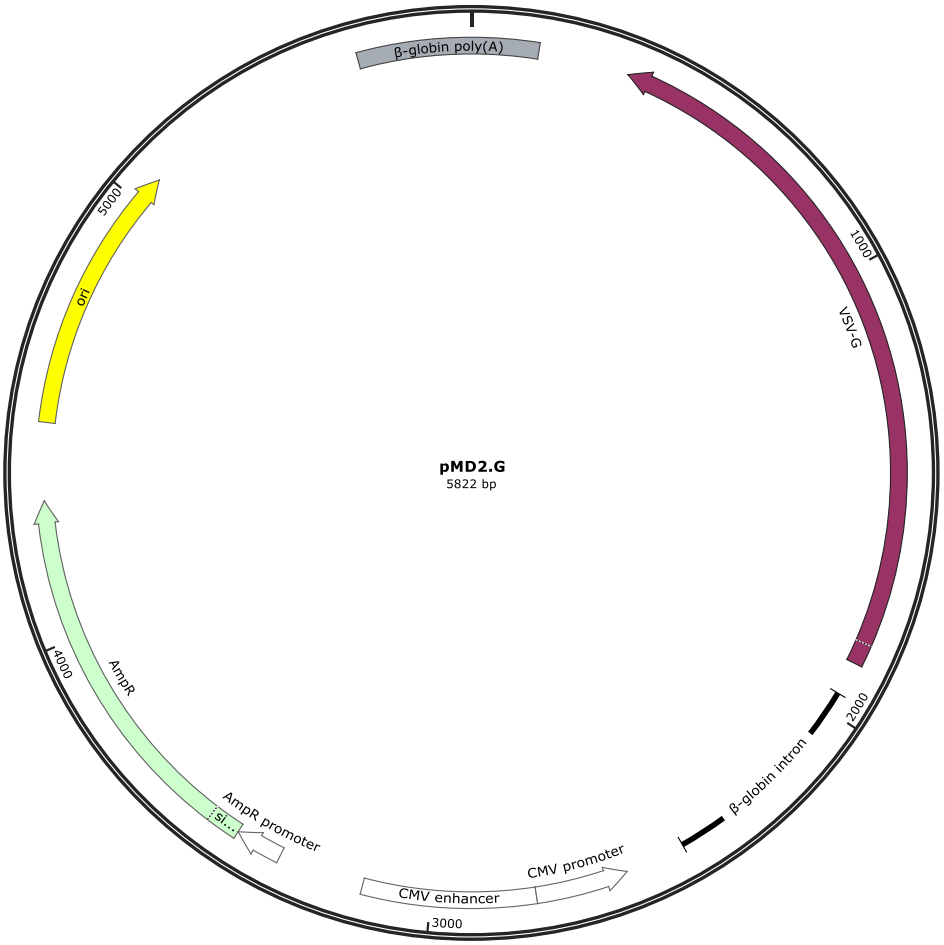

Supplementary figure 1: VSV-G Plasmid. *Packaging plasmid for lentiviral transduction.*

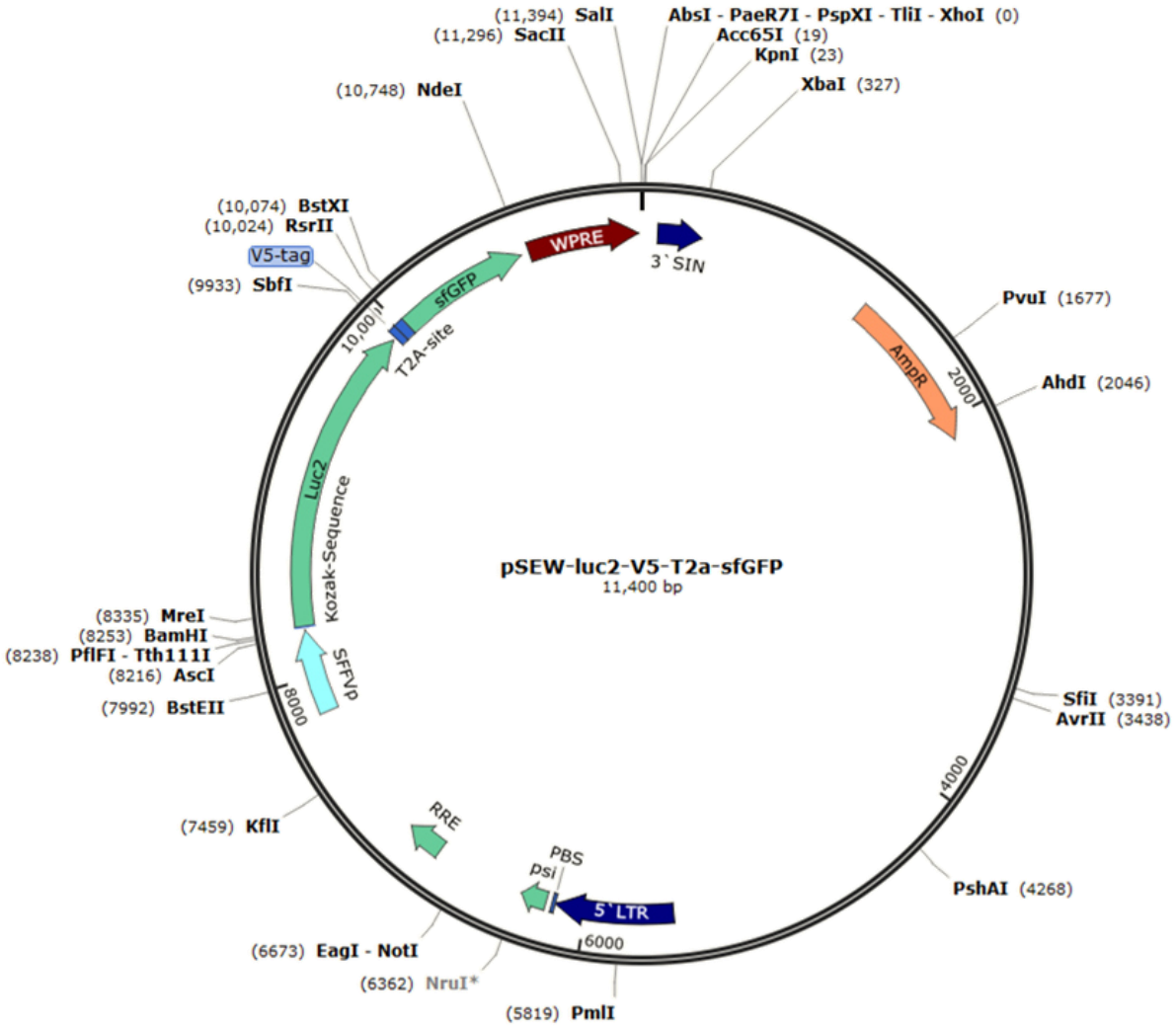

Supplementary figure 2: pSL2GW. *GFP luc gene for lentiviral transfer.*

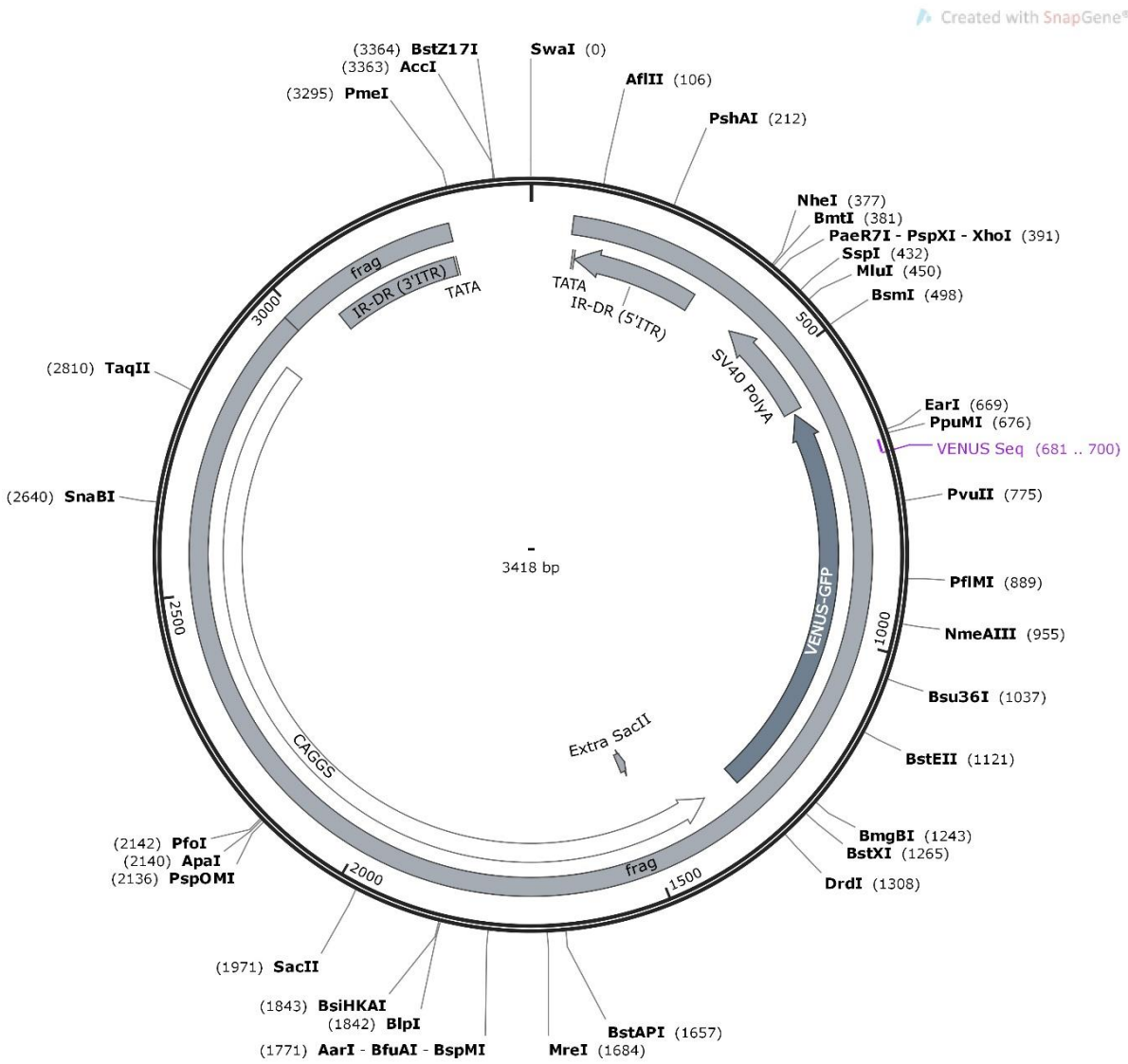

Supplementary figure 3: MC Venus. *Minicircle habouring eGFP flanked by ITR sequences for the transfer by SBTS.*

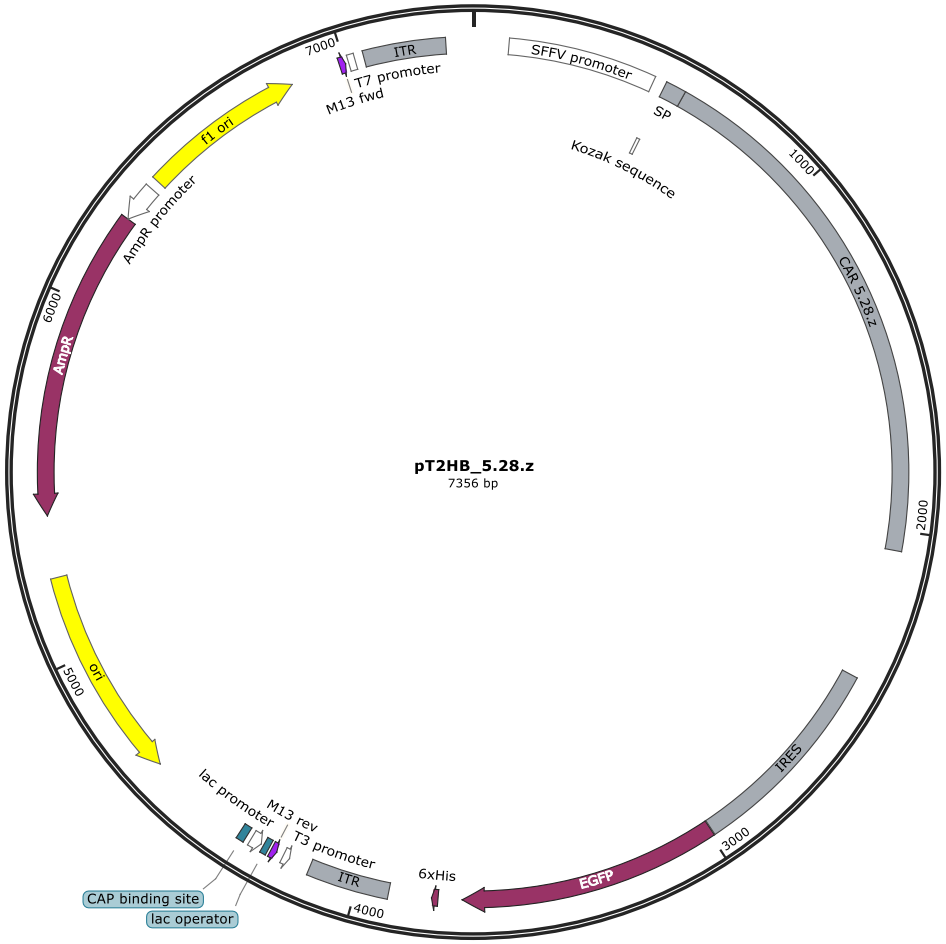

Supplementary figure 4: pT2-5.28.z. *Plasmid encoding the ErbB2-specific 5.28.z CAR with eGFP separated by an IRES sequence flanked by ITR sequences for SBTS transfer. This plasmid was used as starting material for the minicircle generation.*

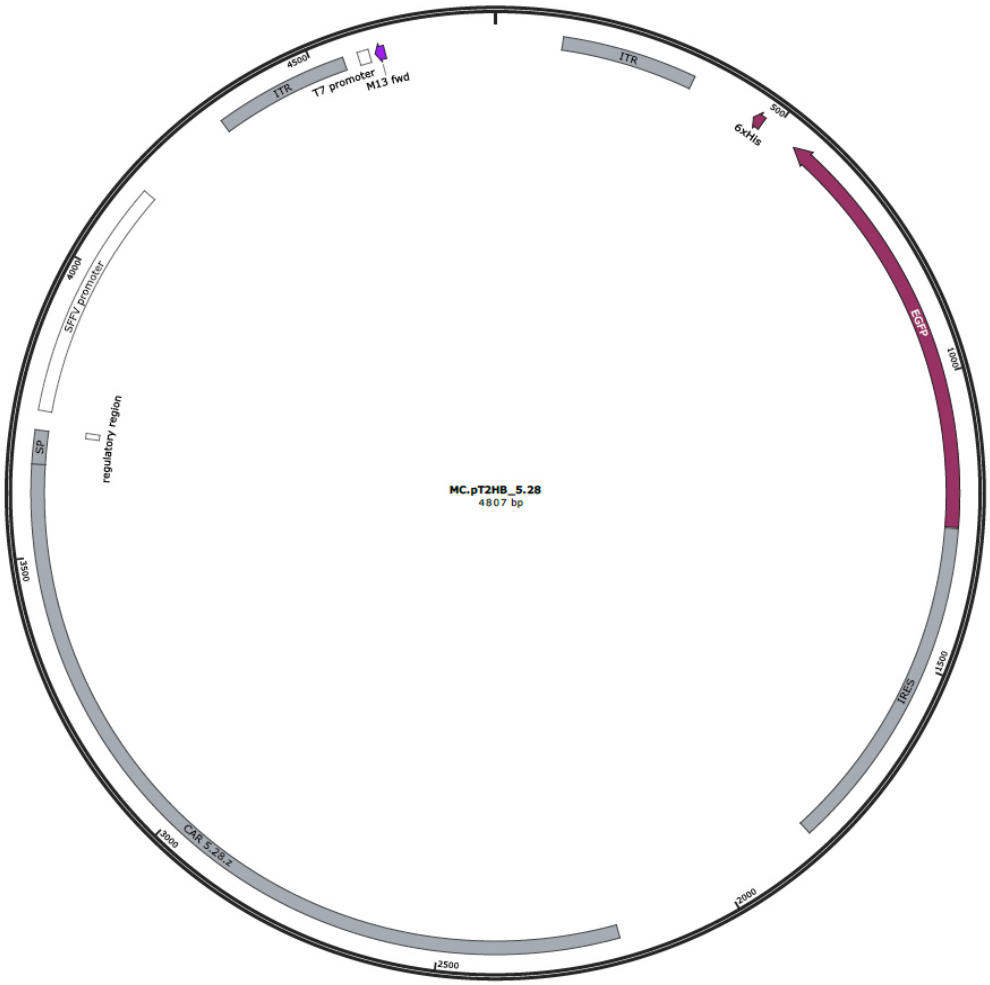

Supplementary figure 5: MC ErbB2-CAR. *Minicircle encoding the ErbB2-specific 5.28.z CAR with eGFP separated by an IRES sequence for SBTS transfer.*

List of Publications

Heim C, Moser LM, Kreyenberg H, Bönig H, Tonn T, Wels WS, Gradhand E, Ullrich E, Meister MT, Koerkamp MG, Holstege FC, Drost J, Klusmann J-H, Bader P, Merker M, Rettinger E. ErbB2 (Her2)-CAR-NK-92 cells for enhanced immunotherapy of metastatic fusion-driven alveolar rhabdomyosarcoma. Front Immunol. 2023 Aug 18;14:1228894. doi: 10.3389/fimmu.2023.1228894.

Gossel LDH, **Heim C**, Pfeffermann L-M, Moser LM, Bönig HB, Klingebiel TE, Bader P, Wels WS, Merker M, Rettinger E. Retargeting of NK-92 Cells against High-Risk Rhabdomyosarcomas by Means of an ERBB2 (HER2/neu)-Specific Chimeric Antigen Receptor. Cancers (Basel). 2021 Mar 22;13(6):1443. doi: 10.3390/cancers13061443.

Merker M, Wagner J, Kreyenberg H, **Heim C**, Moser LM, Wels WS, Bonig H, Ivics Z, Ullrich E, Klingebiel T, Bader P, Rettinger E. ERBB2-CAR-Engineered Cytokine-Induced Killer Cells Exhibit Both CAR-Mediated and Innate Immunity Against High-Risk Rhabdomyosarcoma. Front Immunol. 2020 Oct 19;11:581468. doi: 10.3389/fimmu.2020.581468.

Conference contributions

Posters

06/2023	11th uct Science Day, Marburg
02/2023	1st Joint MSNZ Symposium, Würzburg
08/2021	Mildred Scheel Career Center Meeting 2021, online

Oral Presentations

06/2023	34rd Annual Meeting of the Kind-Philipp-Fundation, Wilsede
06/2022	33rd Annual Meeting of the Kind-Philipp-Fundation, Wilsede

Curriculum Vitae